

Time Reversal Symmetry Breaking and *Fragile Magnetic Superconductors*

Warren E. Pickett¹

¹Department of Physics and Astronomy, University of California Davis, Davis CA 95616

(Dated: February 16, 2026)

Roughly twenty reports (as of 2025) of time-reversal-symmetry breaking (TRSB) states in low critical temperature (T_c) superconducting (SC), otherwise conventional Fermi liquid, metals have emerged primarily from muon spin relaxation (μ SR) data. The detected fields, inferred from the current interpretation of depolarization data, are similar in magnitude and not far above the lower limit of detection, corresponding to magnetizations of no more than $10^{-3} \mu_B/\text{atom}$. These materials comprise a new class of *fragile magnetic superconductors* modeled as triplet pairing. The measured SC state properties, excepting only the fields detected below T_c , are representative of low T_c singlet BCS SCs, not showing unusual coherence lengths or critical fields. While it is recognized that the muon does affect the sample by displacing nearby atoms and impacting magnetic interaction parameters, the measurement process, changing the system from sample \rightarrow sample+ μ^+ thereby breaking TRS, may deserve further scrutiny. This overview provides a survey of the environment of the muon, from the normal state to the superfluid state, where the induced supercurrent and Yu-Shiba-Rusinov gap states provide coupling of the muon moment to the superfluid. The unusual topological superconductor LaNiGa_2 , currently modeled as non-unitary triplet, is used as a case study. Supposing that the prevailing μ SR inference of a small spontaneous field within the bulk of the SC obtains, the current picture of (possibly non-unitary) triplet pairing is discussed and an attractive alternative for LaNiGa_2 is noted.

I. INTRODUCTION

A recent manuscript on *nanostructured superconductivity*¹ giving an overview of the various ways in which the superconducting state can be distorted when the bulk condensate is impeded by structural disruptions, begins with the sentence “the relevant length scales for superconductivity are of the order of nanometers.” This statement is appropriate for the emphasis of that paper. Practically all of the theoretical description and experimental interpretation of superconducting (SC) properties have been, and still are, done at the Ginzburg-Landau level of the coherence length (several to many nanometers) and the penetration depth (usually tens to hundreds of nanometers), or for the superfluid density at the London theory level.

An important development is that the materials-level theory of the singlet SC gap 2Δ and critical temperature T_c due to phonon exchange is formulated at the atomic level and is accurate to any realistic expectation^{2,3} for these properties for phonon-coupled bulk superconductors. While the study of unconventional superconductors has progressed considerably on the basis of symmetry requirements satisfying both theoretical constraints and experimental data, there are sub-nm electronic processes that may need clarification for exotic pairing and condensate formation, along with symmetry considerations.

This manuscript represents a collection of, then discussion of, several of the aspects necessary in evaluating the data and forming an evaluation of their implications for the superconducting phases, especially the order parameters, of a growing variety of superconducting Fermi liquid, low T_c , metals. These SCs have been assigned as time-reversal symmetry breaking (TRSB) largely by muon spin resonance (μ SR) data reflecting anomalous depolarization of the muon spin polarization within the

SC state. One focus here will be on exploring processes relating to the depolarization of the muon spin arising below T_c . Parts of the introductory paragraph or two of (sub)sections are pedagogical, as are some appendices, because many anticipated readers will not have a strong background on the broad picture considered here. Thus there is occasional repetition, mostly intentional, which might be useful when the paper is not read in a single sitting (which has a likelihood of measure zero). The various sections were borne as “notes to the author” (by the author), gathered over three years and shared in bits with a few colleagues, then organized into the current form.

Since this paper is about magnetic effects – *fragile magnetic superconductors* – a basic feature of magnetism in solids should be in the forefront. In the normal state, spin polarization is the dominant response to a magnetic field. Orbital polarization is minor, and for valence electrons, less straightforward to identify and study. The SC state reverses this relative importance. The spin (Pauli) susceptibility decreases and vanishes for singlet pairing. Orbital response to a magnetic field takes over, as displayed at the most basic level by the Meissner effect – repulsion or expulsion of a magnetic field by the SC condensate. Most of the language here is for singlet pairing, because that applies to the overwhelming majority of known low T_c Fermi liquid superconductors. Behavior of triplet pairing systems is model dependent. It is the magnetic character of the SC state that provides the fundamental issues, although several other probes enter the picture; the review of Sr_2RuO_4 by Mackenzie and Maeno⁴ already in 2003 presented many of the complications that can arise.

Before continuing, it should be noted that triplet pairing – dominant in ${}^3\text{He}$ – would, if clearly verified in standard Fermi liquid metals, be a large disruption in condensed matter physics. Overcoming the energy gain from

singlet Cooper pairing to produce spin-up and spin-down pairs could amount to a revolution in materials physics. Triplet pairing in such metals is a high priority possibility in materials physics that needs close scrutiny.

A. Roles of Symmetries

Superconductivity is one of a wide variety of phases of condensed matter that arises from broken symmetry, and for an overwhelming fraction of SC ones it is only unitary $U(1)$ – pairing and condensation – symmetry that is violated. *Exotic* superconductivity, *i.e.* pairing and condensation characterized by an order parameter (OP) violating a symmetry beyond $U(1)$, thus beyond a spin-singlet, crystal-symmetric OP, has been attracting avid interest in solids for some decades.⁵ There is an assortment of normal state symmetries that are available to be broken⁶ along with unitary (particle conserving) $U(1)$ symmetry, its breaking giving Cooper pairing of electrons that “disappear” into the superconducting condensate, as long as the symmetries can be coupled. Symmetries include point group symmetry of the electronic state and of the energy gap $\Delta(T)$ (viz. *s*-like, *d*-like, etc.), singlet spin pairing, spin rotation symmetry, space group, or translational symmetry, and perhaps more intricate types.^{4,7–16}

One of the more elusive phases of SCs is that of time reversal symmetry breaking (TRSB) which, while alarming in name, is in usual form the appearance of a magnetic field and therefore a magnetic component of the OP in an otherwise non-magnetic material. According to zero-field muon spin relaxation (μ SR) depolarization data (to be discussed), roughly 20 standard Fermi liquid type metals with low critical temperature T_c display spontaneous magnetic fields of 0.1-1 G ($10^{-5} - 10^{-4}$ T) appearing below T_c ; a list and references to original works are provided in Sec. VIII A. This topic of *superconductivity hosting fragile magnetism* raises several questions which are addressed here, including some that seem to have attracted little attention.

An opening question is ‘what broken symmetries?’,⁶ based on the reports of broken TRS. In the normal state the full symmetry group is something like $U(1) \otimes \mathcal{G} \otimes \mathcal{S} \otimes \mathcal{T}$ in terms of the space group \mathcal{G} comprised of translation and point group, giving equivalence of atoms on a given sublattice (often inversion is considered separately), spin rotation symmetry \mathcal{S} , and time reversal \mathcal{T} . Occasionally even atomic orbital equivalence on symmetry-related atoms – charge order – is suggested for violation of their symmetry; spontaneous orbital current possibilities have been suggested. At T_c , coherence of Cooper pairs breaks $U(1)$ symmetry. If the magnetization causing a spontaneous field is spin in origin, \mathcal{S} is broken. If it is orbital (currents) in nature, then crystal symmetry \mathcal{G} of the electronic system is also broken, such as unit cells suffering a reduced symmetry (orbital polarization). Both of these latter occurrences break TRS.

If the material involves open shell transition metal

atoms (especially in ionic materials), or $4f$ or $5f$ atoms, the appearance of some sort of magnetic order is not so unexpected, and there are a few examples, *viz.* in heavy fermion superconductors.¹⁷ There are several examples of proposed breaking of the space group symmetry, *viz.* *d*-wave character of the order parameter in some cuprates, and others with more enigmatic phase diagrams (*viz.* uranium compounds).

In the conventional *s-p-d* metals (standard non-magnetic Fermi liquids) considered here, spin polarization (TRS breaking) leading to an internal magnetic field, costs band (“kinetic”) energy which requires compensating gain in interaction (“potential”) energy, and it is unclear how to recover that energy cost from violation of singlet (Cooper) pairing to a rare (and higher energy) parallel spin (triplet) pairing. This change in pairing is commonly presumed to provide the magnetic signal as reported primarily from zero field μ SR experiments. Orbital polarization with its resulting magnetic field is a similarly-related possibility. However, experimental constraints are provided by the SC state properties: critical fields, coherence length, penetration depth, and several thermodynamic (*viz.* specific heat) or spectroscopic (*viz.* NMR) measurements.

An example that will be addressed late in this paper is LaNiGa₂, identified as a TRSB superconductor ($T_c=2$ K) by μ SR.^{18–20} Originally identified²¹ from powder samples to have non-centrosymmetric space group *Cmmm*, LaNiGa₂ has since been synthesized and characterized in single crystal form^{22–27} revealing a non-symmorphic space group (*Cmcm*) with important implications. The electronic structures in these two space groups are similar, *viz.* the Ni 3d bands are filled in both. However, the multisheeted Fermi surfaces are different, and the differing space groups lead to an essential distinction, as will be discussed. A prominent observation is that the SC parameters of single crystal LaNiGa₂ and all members of this class are analyzed and understood in terms of singlet pairing expressions. This case study compound is discussed in Sec. VII, with properties presented in Appendix XVI I. The proposition of considering all superconducting properties together is returned to in the Discussion.

B. Previous overviews, relevant background

A pedagogical, handbook-style monograph on muon spin rotation spectroscopy in solids was published by Schenck²⁸ in 1985, discussing several areas including the technique and applications of muons to metals. This introduction has been followed by a number of books, lecture notes, and reports on μ SR spectroscopy.^{29–35} The μ SR experiment and analysis has been described by several authors associated with one of the present four muon facilities. Representative discussions include a description by Blundell,³² contrasting the pictures of the muon as a heavy positron or alternatively as a light proton, a contemporary view of μ SR theory and data on selected

materials by Hillier *et al.*,³⁶ and a broad discussion provided in a recent monograph (an ‘Introduction,’ but for serious readers) by Blundell and co-authors.³⁵ For recent techniques, Blundell and Lancaster provided³⁷ a description of a ‘DFT+ μ ’ method (density functional theory treatment including the interstitial muon) for finding the muon stopping position(s) in a crystal. More information on the package and an easy-to-use interface ‘MuFinder’ for the researcher is described by Huddart *et al.*³⁸ Calculation of the muon anharmonicity and zero point positional uncertainty for solid N₂ has been described by Gomilsek *et al.*³⁹ using methods developed in recent years. Application of quantum muon position uncertainty methods^{40–43} has been extended and applied by Onuorah *et al.* to elemental and binary metals, obtaining improved values of hyperfine constants.⁴⁴

After discovery of heavy fermion SCs, Heffner reviewed in 1992 μ SR studies of this class of quantum materials, with emphasis on uranium superconductors.¹⁷ This class of highly unconventional materials, discovered in the early 1980s, have strongly renormalized properties in the normal state and are not the topic of this article. An extensive review of defect-induced properties in such materials, and in conventional superconductors, was provided by Balatsky, Vekhter, and Zhu in 2006.⁴⁵

Reviews on exotic order parameters more generally are relevant to discussions in this paper. Earlier work on isotropic superfluid ³He required adaptation to crystal systems. In 1991 Sigrist and Ueda⁸ provided a review and extension of the theory of unconventional SC states, extending from the generalization of BCS theory⁴⁷ to symmetry classification and its relation to Ginzburg-Landau theory,⁴⁸ to symmetry-breaking including the non-unitary possibility for triplet superconductors, to crystal symmetry lowering effects (structural transformations, consequences of surfaces and interfaces, and more). Sigrist has provided following reviews on broken time-reversal symmetry,⁴⁹ on unconventional SCs,¹² and on an extension specifically aimed at non-centrosymmetric SCs.¹³ Wysokinski provided in 2019 an overview¹⁴ of time-reversal symmetry breaking, with focus on Sr₂RuO₄.

An overview of the interplay between inhomogeneities and SC order parameters, especially TRSB ones, by Andersen, Kreisel, and Hirschfeld, addressed topics of relevance to μ SR experiments⁵⁰ and relevant to the description in this article. They provide a brief but informative description of the zero field μ SR experiment that has provided evidence of TRSB SC phases in several otherwise conventional intermetallic compounds. Among the situations they discuss is that defects in a TRSB SC can produce local magnetic fields from spin disruption and from orbital currents. The current article will provide discussion of effects of magnetic impurities, viz. the muon, in a generic Fermi liquid superconductor, leaving interaction of impurities with exotic OPs to specific treatments of such cases, cited above.

C. Motivation and Purpose

Electron pairing and related symmetries are fundamental to the formalism of the superconducting state and its excitations. OP character is intimately tied to the symmetry of the Cooper pair of fermions: the exchange of electron coordinates must lead to a π phase change of the pair wavefunction. A listing of the materials and (some) symmetries in the μ SR-identified TRSB materials are listed in Sec. VIII A. One can notice that TRSB is observed in a variety of space (and point) groups, in centrosymmetric, or not, materials, and in symmorphic, or non-symmorphic, crystal systems. One possibly unifying characteristic is that these Fermi liquid-based TRSB SCs are all low T_c and without significant electronic correlations. A viable presumption could be to suppose there is some universal nature of, or proclivity toward, TRSB at T_c, with certain attribute(s), yet unknown, that determine whether it happens or not. Since there are no outstanding similarities or distinctions among the group of *fragile magnetic superconductors*, allowable OP symmetries have been pursued case by case by theorists, sometimes complicated by somewhat conflicting data.

The purpose here is on surveying a broader picture of the multiscale behavior, identifying behavior that may either complicate analysis or, conversely, contribute to new information about possible microscopic mechanisms for coupling of an emergent magnetic moment to the pairing OP than can be found in the literature. It has been understood, and established by DFT studies⁵¹ that the μ^+ ion density disturbs the sample locally,^{38,52,53} see Sec. III.A. The current understanding is that this charge disturbance, without considering any magnetic character, is unlikely to influence conclusions about TRS.⁵¹

A 2021 overview by Ghosh *et al.* mentions microscopic complications of interest here⁵⁴ that are not easy to find elsewhere. Some of these arise from the realization that the muon is a significant local perturbation of the sample beyond charge effects. These authors mention⁵⁵ that (i) the inferred magnetization depends on the choice of presumed pairing symmetry (not often made explicit), (ii) “the muon does not measure μ_s [the magnetic moment per unit cell of the SC state] but the induced internal field $B_{int}(\vec{r})$ which depends, on an atomic scale, on the location \vec{r} of the muon within the unit cell,”⁵⁴ and (iii) the strong local perturbation changes the local crystal structure, alters the electronic structure, destroys the local symmetry, and influences the induced magnetization.

Late in this paper alternative possibilities to the present picture of this class as *fragile magnetic superconductors* are suggested. The present picture is that of a TRSB order parameter based on the detection of a magnetic depolarization onset below T_c, being characteristic of an unusually small magnetic field, just above the limit of detection. The other viewpoint – not specifically stated before, but indicating there may be some other explanation for this signal – is based on (1) recognition that deposition of the polarized muon induces a magnetization into the sample that already breaks TRS of the

coupled system in the normal state, and that (2) the superconducting properties such as coherence lengths, critical fields, etc. are characteristic of many low T_c singlet BCS superconductors,²⁷ whereas triplet SCs are expected to display significantly different properties. The purpose here is to review, and extend somewhat, this picture of the general behavior of a conventional metal with an implanted polarized muon.

II. ORGANIZATION OF THE PAPER

Normal state: Secs. III-VIII. Some background information on the muon's magnetic moment and resulting field are presented in Sec. III. Subsection III B specifically addresses aspects of a model homogeneous electron gas+ μ^+ (HEG+ μ) system in the normal state, discovering complexities, including anomalies in the theory (an infrared divergent integral in first approximation) that obviate precise quantification of the behavior in the vicinity of the muon. Magnetic field complications are introduced in Sec. IX B, with the objective being to begin to construct a picture of the local behavior near the muon resulting from its magnetic field.

Near-muon quantum effects – positional uncertainty, non-linear susceptibility, electron pair correlation – in Sec. V are suggested to regularize some difficulties of the quasi-quantum formalism, but leave some fundamental questions as highly numerical in nature (and perhaps not yet well posed), as a challenge arising from the divergent magnetic field near the muon. Another qualitative aspect – anisotropy (versus the isotropic HEG) – is material specific, and is addressed in Sec. VI. The unique case of the topological superconductor⁵⁶ LaNiGa₂ is the topic of Sec. VII.

Superconducting state: Secs. IX-XI. Passing into the SC state is the topic of Sec. VIII and beyond, with the strong magnetism-superconductivity conflict providing a complex picture of the system in the SC state. Sec. IX provides one of the key aspects of this paper. The supercurrent, circular like the vector potential if conventional theory holds, produces its magnetic field, which emerges upon entering the SC state.

Effects of possible Kondo screening or other magnetic effects of the muon moment are addressed in Sec. X. Study of a magnetic impurity in a SC initially by Yu, Shiba, and Rusinov (YSR), and more recently using density functional methods for specific superconductors, reveal that bound states within the SC gap form upon entering the SC state, and their character may provide clues to the coupling of the muon moment to the SC order parameter.

Specific aspects of pairing follow. Issues concerning pairing symmetry form the focus of Sec. XI, where possible OPs are contrasted with the current model for LaNiGa₂. Having left several details to Appendices A-N to make the main text more readable, the Discussion and Summary ares given in Sec. XIII.

Appendices. A number of relevant discussions or nu-

merical data are relegated to appendices. The full microscopic non-relativistic Hamiltonian of the muon+sample is laid out in Appendix XV A, but manipulations of this Hamiltonian in this paper are few. The setup of the μ SR experiment is given in overview in Appendix XV B, including some discussion of the analysis of data. The full analysis is no doubt more involved. The simple but important-to-understand symmetry of the dipolar field is presented in Appendix XV C. Appendix XV D delves into a central question: the muon-generated magnetic field at the muon site in the normal state, arising from the electronic spin polarization due to the muon's field. Appendix XV D provides the expression for the induced field. An operator formalism is presented in Appendix XV D 2 to reaffirm the conclusion.

Following an introduction in Sec. V C, Appendix XV E provides additional discussion of quantum effects, specifically the quantum position uncertainty of the muon in the crystal, full spin polarization near the muon, and pair correlation consequences of the fully polarized valence electrons, these becoming involved in the near field of the muon. The coupling of the muon to conduction electrons is the topic of XV G, discussing a possible Kondo screening, or not, of the moment. The long studied Yu-Shiba-Rusinov states appearing within the superconducting gap, pinned to the muon's magnetic moment, is the subject of Appendix XV H. Appendix XVI introduces the reader to several of the properties and relevant energies of the case study material LaNiGa₂.

Considerations of possible superconducting order parameters form the discussions in Appendix XV J, with application to LaNiGa₂ in Sec. XII B: (possible) singlet versus triplet, unitary versus non-unitarity, and the currently proposed model of triplet pairing, and the special role that LaNiGa₂ might play.

III. THE MUON DIPOLAR MAGNETIC FIELD

For purposes here the effect on the normal state of the muon moment need not be described. Briefly, the muon moment (denoted $\vec{\mu}$ throughout this paper), has a dipolar magnetic field⁵⁷ that extends to interatomic distances, polarizing the electron gas in its neighborhood as it diverges as r^{-3} approaching the site of the muon. The characterization of the origin of point particle moments by Jackson⁵⁸ was

“Usually the books are a little vague about the nature of these intrinsic magnetic moments, letting the word ‘intrinsic’ imply that it is beyond the realms of present knowledge or none of your business, or both.”

He went on in his CERN document to describe the theoretical description of intrinsic magnetic dipole moments, and that point (particle) dipoles must be regarded as the limit of a current loop with area going to zero rather than as north and south monopoles coalescing, consistent with experimental data from elementary particle studies. The conclusion is included below.

A. The muon quantum spin

The conventional dipole vector potential and magnetic intensity for an isolated muon moment μ is (some expressions following will incorporate $\vec{\mu} = \mu(0, 0, 1)$ defining the z -direction)

$$\begin{aligned}\vec{A}^\mu(\vec{r}) &= \nabla \times \frac{\vec{\mu}}{r} = \frac{\vec{\mu} \times \hat{r}}{r^2} = \frac{\mu}{r^3}(-y, x, 0) \\ \vec{B}_{tot}^\mu(\vec{r}) &= \nabla \times \vec{A}^\mu(\vec{r}) = \frac{3\hat{r}(\hat{r} \cdot \vec{\mu}) - \vec{\mu}}{r^3} + \frac{8\pi}{3}\mu\delta(\vec{r}) \\ &= \vec{B}_{dip}^\mu + \vec{B}_{con}^\mu\end{aligned}\quad (1)$$

with dipole and contact terms. The divergenceless gauge is used for the vector potential.⁴⁶ This form of magnetic field has amplitude μ/r^3 times an angular term of order unity, and $\vec{A} \sim \mu/r^2$. Throughout this paper *cgs – gaussian* units will be used, for which the magnetic susceptibility is unitless.

The purpose of this subsection is to remind of the direction of a spin-half. The symmetry treatment above is that of a classical moment. Neglecting for now the moment strength μ , a spin-half moment in spin space has a magnitude

$$|\vec{\sigma}| = (\sigma_x^2 + \sigma_y^2 + \sigma_z^2)^{1/2} = \frac{\sqrt{3}}{2}. \quad (2)$$

With full polarization $\sigma_z = 1/2$, this leaves the quantum spin with a perpendicular component according to $\sigma_x^2 + \sigma_y^2 = 1/2$. Thus the direction of the polarized quantum spin is off the \hat{z} direction as

$$\vec{\sigma} = \frac{1}{\sqrt{2}}(\cos \phi, \sin \phi, \frac{1}{2}) \quad (3)$$

with polar angle ϕ indeterminant within $[0, 2\pi)$. Given that the emission of the positron in muon decay is along the direction of the moment (not along the direction of polarization), its direction is $\frac{1}{2}$ in the \hat{z} direction with a large statistical component in the x - y plane. Standard analysis accepts that the positron is emitted preferentially (sometimes ‘predominantly’) along the polarized z -component of the muon spin at the time of decay. Further description of the quantum conditions is provided in Appendix XV B, with a graphical figure indicating the statistical distribution of the positron emission direction, which is dependent on the positron kinetic energy.

Back to the classical description: the field lines are pictured in scale independent form in Fig. 1, and more about its algebraic form and symmetry elements are provided in Appendix XV C. Since only non-magnetic metals are discussed here, the choice of H (field strength) versus B (flux density) will be primarily conventional.

It is conventional that in the midst of a electronic system, the contact term in Eq. 1 will give rise to an interaction term

$$H^{\mu-el} = -\frac{8\pi}{3}\vec{\mu} \cdot \vec{m}(0) \quad (4)$$

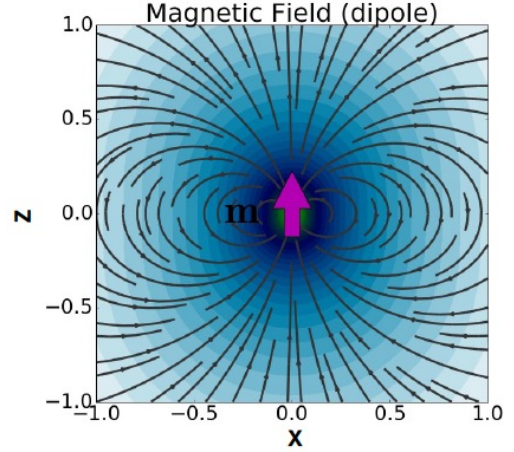


FIG. 1. Plot of constant magnetic field lines of a point dipole oriented along the \hat{z} direction of this plot, plotted in the x - z plane; distances along the axes are in arbitrary units relative to the magnitude of the point dipole at the origin. The large arrow indicates the direction of the dipole. The lines with arrows indicate the direction of the field at that point. The darker blue shading indicates larger magnitudes of the \vec{B} field. The radial modulation as $1/r^3$ is evident.

in terms of the electronic magnetization density $\vec{m}(\vec{r})$. Although it may be an interesting question how this contact term is affected by the onset of SC pairing and gap opening, this point is beyond the scope of this article. Relevant complications of the near-muon region are addressed in Sec. V.

The factor $8\pi/3$ can be found, confusingly, in some literature to be replaced by $-4\pi/3$. Jackson described⁵⁸ how the correct $8\pi/3$ factor for the muon (and any elementary particle now known) is consistent with experimental information that concludes that the point magnetic moment must be considered as the limit of a tiny circulating current. A $-4\pi/3$ factor instead arises if the dipole results from the limit of a bound pair of north-south monopoles (as could conceivably occur in an elementary particle, but in the Standard Model does not).

Throughout this paper m will denote the electron mass, m_μ the muon mass, m^* an effective mass. Electron magnetization will be denoted by $\vec{m}(\vec{r})$, which by the context should not be confused as a mass.

The polarization of the electron density will in turn produce an additional magnetic field in the region arising from the dipolar vector potentials of the partially aligned electrons; see Sec. IX B and Appendix XV D.

B. Charge effects, broadly

The immediate local environment of the muon is that of a positive charge in a slowly varying electron gas, where it attracts one unit of electron density to its vicinity from the valence density. A first approximation is that of the constant electron density (jellium) plus the attracted density into an effective electron $1s$ orbital, centered at the muon's site and spherically symmetric, given approximately by $n(r) = n_o + n_{1s}^\mu(r)$, where n_o is the value of the uniform jellium density and n_{1s} is an effective $1s$ orbital density of the μ^+ attracted from the conduction electron reservoir (*i.e.* the $H\ 1s$ orbital). Neutrality apart from decaying Friedel oscillations will be achieved within a few times the Thomas-Fermi screening length.

At interstitial densities of densely packed intermetallic compounds characteristic of most SCs, hybridization of the muon $1s$ orbital with itinerant electronic states will ensure that the muon "atomic density" will not be spin polarized due to electron gas exchange effects. (Some DFT studies indicate a muon bound state below the bottom of the conduction band,⁵¹ in which case single occupation (Hubbard U) and hence magnetic polarization effects might arise.)

Within a crystal, this effect is not as simple as for the proton, because the minima of the muon's potential in the solid must be augmented by study of the quantum uncertainty of the spatial position of the light mass muon, which expands the region over which the simple Hartree potential is sampled. This effect is structure- and material-dependent. The region of interest will first be considered to be a spherically symmetric system responding to the axial muon magnetic moment. At this level the discussion is that of a proton in a HEG,⁵⁹ except that the proton's vector potential is smaller.

C. Magnetic polarization

Spin polarization. Away from the short range (diverging) field region near the muon considered in Sec. V, the induced magnetization at position \vec{r} is given from linear response as

$$\vec{M}^{ind}(\vec{r}) = \mu_B [n_\uparrow(\vec{r}) - n_\downarrow(\vec{r})] \rightarrow \chi_{sp}[n(r)] \vec{B}^\mu(\vec{r}). \quad (5)$$

The last expression includes the Pauli spin susceptibility χ_{sp} , with this linear response result remaining realistic to multi-tesla-scale fields. [Recall that $\mu_B B$ at one tesla is 0.7 K in temperature units, which will be a factor of 207 smaller for the muon moment.] In this HEG approximation, which is formalized by density functional theory,^{60,61} \vec{M}^{ind} is parallel to \vec{B}^μ at each point, hence it and the entire system satisfies the same cylindrical and reflection symmetries given for \vec{B}^μ in Appendix XVC. In a HEG the induced field at the muon $\vec{B}^{ind}(0)$ will, by symmetry, align with the muon moment. It will then not provide any torque on the muon moment, hence be undetectable by depolarization studies. That the muon lies

at a low symmetry position is relevant and is discussed later.

Orbital polarization. The muon-induced electron currents will produce a local orbital polarization and related susceptibility χ_{orb} . For the HEG and a uniform magnetic field the value of this (Landau diamagnetic) susceptibility is $\chi_{orb} = -(1/3)\chi_{sp}$. In the following discussion a net paramagnetic susceptibility $\chi_p = \chi_{sp} + \chi_{orb}$ in the normal state will be accounted for. Nonlinear effects (in the high field region) will be discussed separately. In normal density Fermi liquid metals χ_p is of the order of $10^{-3} - 10^{-4}$, in *cgs-gaussian* units. This small polarization may be relevant because the inferred spontaneous field reported in these metals is unusually small.

For the muon's strongly non-uniform near-field, the orbital effect will require new formulation. Conventional quasi-classical transport theory is used for uniform or slowly varying electric and magnetic fields, and thermal gradients. This approximation enables the application of a distribution function $f(\vec{k}, \vec{r})$ and its derivatives, describing the response of thermally excited electrons on the Fermi surface (see for example Ref. [62]). For regions of sharply varying magnetic field such as near the muon, a quantum formulation will be required. Qualitatively, there will still be a circulating current surrounding the muon, with scattering processes in the normal state leading to the steady state. A reason for mentioning these spin and orbital processes is that the resulting local magnetism possibly could bias a metal approaching and crossing T_c toward a SC OP that has a magnetic component, *i.e.* triplet pairing.

IV. THE INDUCED MAGNETIC FIELD

Each electron carries a magnetic moment of one μ_B , thus each volume element of induced magnetization $\vec{M}^{ind}(\vec{r}) \Delta V$ will produce the same form of magnetic field intensity from the incremental moment $\vec{M}^{ind} \Delta V$ as given by the dipole expression in Appendix XV A Eq. (32), except that the initial origin $\vec{0}$ will be assumed by \vec{r} (the position of ΔV) and the position of a given field point will be \vec{r} . Some details are presented in Appendix XV D.

The net result of the polarization is the magnetic flux density in the region (in *cgs-gaussian* units)

$$\begin{aligned} \vec{B}^{tot}(\vec{r}) &= \vec{B}^\mu(\vec{r}) + \vec{B}^{ind}(\vec{r}) \\ &= \vec{B}^\mu(\vec{r}) + 4\pi\chi_p \vec{B}^\mu(\vec{r}) \\ &= [1 + 4\pi\chi_p(\vec{r})] \vec{B}^\mu(\vec{r}), \end{aligned} \quad (6)$$

The result is a textbook-like result, reminding again that this local linear response enhancement is good except within a small volume surrounding the muon, to be addressed in the next section. The polarization response is comparatively small, however, small magnetic fields are the topic of this paper.

Integrating the effect of the induced moment over all space, the magnetic field created by aligned vector potentials of the electrons corresponding to $\vec{M}^{ind}(\vec{r}')$ will

be

$$\vec{B}^{ind}(\vec{r}') = \int d^3r \frac{3\hat{R}[\vec{M}^{ind}(\vec{r}) \cdot \hat{R}] - \vec{M}^{ind}(\vec{R})}{|R|^3}. \quad (7)$$

where $\vec{R} \equiv \vec{r}' - \vec{r}$. Simplification occurs because we are only interested in the field at the muon site, *i.e.* at $\vec{r}' \rightarrow 0$, so $\hat{R} \rightarrow -\hat{r}$, and that the source is a point (the muon). Due to the symmetry of any dipolar field $\vec{B}(-\vec{r}) = \vec{B}(\vec{r})$ the induced magnetization gives, in the quasiclassical expression of Eq. 7 arising from linear response, a divergent result at the muon site, which is discussed in Appendix IX B. Quantum corrections are necessary to give regular results, see Refs. [63–65] and Sec. V. Necessity for quantum corrections to the supercurrent-generated magnetic field will arise in Sec. IX.

V. QUANTUM EFFECTS NEAR THE MUON

The infrared divergence of the integral for $B_z^{ind}(0)$ in Eq. 7, with detail presented in Appendix XV D, is daunting and obviously unphysical. Additional factors must be entering the physics. Three quantum factors may serve to regularize the integral.

A. Quantum positional uncertainty

This quantum positional uncertainty (QPU), commonly and imprecisely referred to as zero point motion, contains information on how a confined quantum particle samples a region around the classical position. In its ground state the muon will sample a region around a minimum of the Coulomb potential, the minimum being the classical ground state position. Theoretical description and implementation of anharmonicity and QPU has undergone recent substantial progress.^{41–43} For an ideal harmonic oscillator the shape of the region of the ground state wavefunction would be an ellipsoid. This uncertainty is sometimes important for interstitial protons,⁶⁶ but the effect will be larger for a muon with its factor of nine smaller mass. With a lower symmetry environment the shape of the potential well will be less regular in shape,⁵¹ and may even involve a quantum oscillation between two classically-preferred sites.³⁸

Until recently, this QPU of the muon position had not become a mainstay of μ SR analysis. The first step, finding the classical muon position, has been made more efficient through a user-friendly platform, since the advent of the μ SR analysis application MuFinder.³⁸ With only the underlying crystal structure as input, the algorithm chooses likely sites for the muon, calculates from DFT the energy of the system including relaxation (structural and electronic) of nearby atoms, and with calculated forces iterates to the minimum energy structure. The results can be used in the analysis of μ SR data, especially for nuclear magnetic fields and for magnetic solids. QPU

of the muon has now been realized as important for the interpretation of μ SR data.

In the second step, the factor of 207 difference in muon and electron masses allows one to invoke an adiabatic approach as first approximation: for each point \vec{R} within the muon ground state normalized wavefunction $\Psi(\vec{R})$, the electron density $n(\vec{r}; \vec{R})$ and polarization (magnetization) $M^{ind}(\vec{r}; \vec{R})$ can be evaluated, and from it the magnetic flux density $B^{ind}(\vec{r}; \vec{R})$. The resulting (“smeared”) induced magnetic field is given by the expectation value

$$\vec{B}^{ind}(\vec{r}) = \int d^3R \Psi^*(\vec{R}) \vec{B}^{ind}(\vec{r}; \vec{R}) \Psi(\vec{R}). \quad (8)$$

Here \vec{r} is measured from the classical muon position \vec{R}_o . This field is then evaluated at the muon minimum energy position. Onuorah *et al.* have formalized this expression using their ‘double Born-Oppenheimer approximation’ approach,⁴⁴ and applied it to various elemental transition metals and binaries at an ensemble of ‘classical positions’ of the muon to provide the above integral. It was demonstrated that this quantum correction improved resulting values of hyperfine field. Moving back to the current issues, it can be observed that the muon samples regions where the integrand in the induced field is less divergent, so the divergence at the muon site may be somewhat ameliorated. The effect may be to introduce into the magnetic field integral something like an $r^2 dr$ factor in the integrand that reduces the divergence by two powers of r . Additional discussion is provided in Appendix X E.

B. Region of full polarization

The diverging magnetic field at the muon site will completely spin polarize the nearby conduction electrons along the lines of its dipolar field, modulo quantum restrictions. Specifically, inside some small radius the spin polarization will be 100% along the local direction of the field. This situation suggests an analog of the study by Ortiz, Jones, and Ceperley⁶⁷ of the H_2 molecule in superstrong applied magnetic field. They applied quantum Monte Carlo (fixed phase and variational) methods and determined, among other things, that the ground state is a TRS-breaking electronic triplet, additionally having angular momentum $L_z = -1$ (the field was applied along the H_2 axis). The protons were treated classically and their vector potentials (quite small compared to the 10^5 – 10^8 T fields considered) were not treated, but their study provides probable methods to study the muon problem at radii where non-linear magnetism develops.

When the polarization (here \uparrow, \downarrow indicates the direction with respect to the the local magnetic field), following the magnetic field shown in Fig. 1,

$$P(\vec{r}) = \frac{n_\uparrow(\vec{r}) - n_\downarrow(\vec{r})}{n_\uparrow(\vec{r}) + n_\downarrow(\vec{r})} \quad (9)$$

approaches unity, the analog of the Ortiz *et al.* condition of triplet alignment may apply.⁶⁷ Any additional longitudinal field will produce no extra polarization. Specifically,

$$\chi_p(n(r)) \rightarrow \chi_p(n(r), m(r)) \rightarrow \chi(n(r), +1) \rightarrow 0, \quad (10)$$

because the fully polarized region $P(\vec{r}) \rightarrow 1$ no longer can be further polarized, *i.e.* the longitudinal magnetic susceptibility goes to zero as some power of the distance r from the muon site. This saturation of the polarization, hence vanishing of the susceptibility, will result in a reduction of the divergence, by (perhaps) another factor of r^{-2} .

C. Electronic pair correlation

From variational^{59,68,69} and quantum⁷⁰ Monte Carlo calculations on correlated wave functions (Gutzwiller-Slater determinants) at full polarization, the probability of parallel spin electrons (all electrons in this limit) being at the same point vanishes (Pauli repulsion). The pair correlation function in three dimensions increases from zero quadratically. This many-body consideration of the system thus further reduces the divergence of the integral by canceling a factor of r^{-2} , producing a convergent result. The magnitude of the final induced field $\vec{B}^{ind}(0)$ seems not to be amenable to any simple estimate.

VI. EFFECTS OF ANISOTROPY

The muon comes to rest in an interstitial site between two or a handful of atoms, at a local minimum in the Coulomb potential at a site with no symmetry, especially considering the relaxation of local atoms. Considering the crystal symmetry, for a space group with N operations and a site without symmetry, there will be N symmetry related sites in the unit cell but with different orientations of the local environment with respect to the fixed muon polarization, hence different projections of a muon-induced field along the muon polarization axis.

In the preceding discussion we have taken the vicinity of the muon, before considering magnetic fields and crystallinity, as isotropic. This is a beginning point but a simplification, as the actual symmetry experienced by the muon will be low^{38,52,53}, as mentioned above. Moreover, DFT studies have shown that the muon's quantum zero-point uncertainty is not only substantially larger than that of a proton but more anisotropic as well,^{38,51,52} and large anharmonicity and quantum uncertainty are correlated by motion during the muon's relatively long lifetime.

It follows that the induced magnetization and its magnetic field will no longer have the symmetry of the point dipole field, thus the field at the muon site at a given time will not align with the muon spin and will produce a torque on the muon moment, with different torques for the symmetry-equivalent muon sites. This effect of

anisotropy holds for either induced spin polarization or orbital currents. The effective field at the muon site may become amenable to DFT+ studies,⁷³ (+ indicates manybody or quantum corrections, see Sec. V and Appendix XV E).

It may be premature to speculate further. What seems clear is that it is necessary for quantitative studies to (i) determine the classical site of the muon, (ii) calculate the quantum uncertainty of the muon position, which may adjust the muon's most probable position, (iii) account for the motion of the muon during its lifetime, then (iv) determine the resulting effective field near and at the muon site taking into account these various effects.

VII. A CASE STUDY: LANIGA₂

A. Background on singlet versus triplet

The fully gapped superconducting state of LaNiGa₂, with critical fields²³ $H_{c2}(0)=0.27, 0.09, 0.24$ T for uniform applied fields along the three (a, b, c) crystal axes (Appendix XVI), typical of low T_c singlet SCs, must accommodate the 'external' magnetic field from the muon via superconducting magnetic shielding currents, analogous to the simpler case of the Meissner effect at a surface. LaNiGa₂ is Type II,²³ – anisotropic Abrikosov indices $\kappa=3.38, 28.9, 4.00$ along the three crystal axes – like several other orthorhombic fragile magnetic superconductors, listed in Sec. VIII A.

Standard Meissner expulsion of magnetic fields applies to singlet pairing, where only the supercurrent density is involved. Triplet OPs respond to magnetic fields very differently than do singlets, as shown from time-dependent Ginzburg-Landau simulations by Pechenik *et al.*⁷⁴ They found that breaking of spin-rotation symmetry requires less energy than for singlet states, which implies a paramagnetic contribution to susceptibility as opposed to the purely diamagnetic response of singlet pairing, which would enhance critical fields. Rosenstein *et al.* described that longitudinal and transverse (to the direction of the OP) penetration depths and coherence lengths can be very different⁷⁵ for an isotropic 3D model, which would be significantly complicated for a crystal of orthorhombic symmetry.

All materials parameters of LaNiGa₂, though crystal axis dependent, are in line with singlet pairing,²³ with the exception of indications of additional depolarization from μ SR studies (see Sec. VIII A). In a triplet SC, it can be expected that a magnetic field will (i) tend to rotate and align triplet pairs relative to the spontaneous SC magnetization, increasing magnetization into the applied field direction (increasing $|\uparrow\uparrow\rangle$ pairs versus $|\downarrow\downarrow\rangle$ pairs), engendering a susceptibility process not available to singlet pairing, and more general supercurrents may arise. Each of these effects, and more, may depend on the type of OP.⁷⁵

To quantify the energy cost of converting spin-down pairs to spin-up pairs would require a specific Hamiltonian

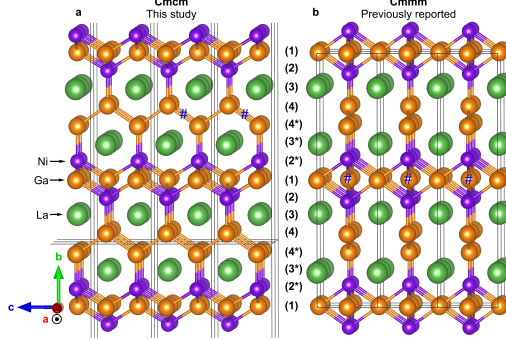


FIG. 2. (a) The structure of LaNiGa_2 from Badger *et al.*, determined from single crystal XRD. (b) The structure obtained in 1982 by Yarmolyuk and Grin²¹ from powder XRD. The difference lies in (i) the Ni-Ga layer in the center (and top and bottom) layer of this plot, with Ni repositioning, and (ii) repositioning of Ga between the La layers, together resulting in a non-symmorphic operation and the $Cmcm$ space group.

nian. Studies of quantified properties of triplet phases are at an early stage. One suggestion⁷⁵ is that coherence lengths can depend strongly on the choice of triplet OP. Unusual properties are not observed in LaNiGa_2 .

B. Non-symmorphic symmetry of LaNiGa_2

Recent studies of single crystals of LaNiGa_2 revealed^{22–24} its space group to be $Cmcm$, with a non-symmorphic crystal symmetry, versus the 1982 assignment of symmorphic $Cmmm$ space group based on powder x-ray data.²¹ The structural similarity and differences are displayed in Fig. 2. The non-symmorphic space group operation results in a double degeneracy (beyond spin symmetry) across an entire face of the Brillouin zone, a well known non-symmorphic symmetry consequence, but a full planar degeneracy is an unusual occurrence in an exotic SC, with points on the Fermi surface with topological index thus characterizing it as an exotic topological superconductor.

It is useful to clarify the topological aspect. Upon including spin-orbit coupling (SOC), this planar degeneracy is lifted throughout the zone *except* along a single symmetry line (the Z - T line).^{23,24} Any pair of bands cutting the Fermi energy along this line thus has a Dirac point degeneracy in the normal state at that point. The Dirac point will lie *on the Fermi surface, independent of doping, strain, etc.*, i.e. independent of the position of E_F – $Cmcm$ symmetry demands that the degeneracy. The Dirac point simply moves along the Z - T line, only vanishing if the Fermi surfaces no longer cross the symmetry line. It is highly unusual – almost an improbability – to have *diabolical points that remain pinned* to the Fermi surface as it varies due to external influences – doping, strain, pressure, etc. – remaining on the Fermi surface as long as the structural symmetry is retained. This symmetry-related pair of points has four-fold degeneracy and the topological character of anisotropic 3D

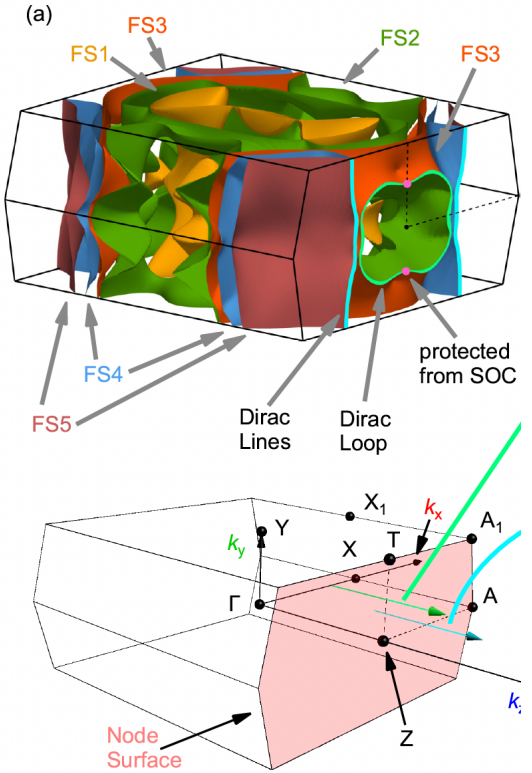


FIG. 3. Top panel: the five Fermi surfaces of $Cmcm$ LaNiGa_2 , illustrating the degeneracies on the node surface (the pink plane in the lower panel). The green and red Fermi surfaces (FS2 and FS3) merge together on the light green loop, while the blue and brown Fermi surfaces (FS4 and FS5) merge on the vertical blue line. The red dots, denoted by “protected from SOC,” pinpoint where the loop of degeneracies cross the Z - T lines, leading to 3D Dirac point character at those dots. Bottom panel: symmetry labels of $Cmcm$ Brillouin zone, with the node surface shown in pink.

Dirac points. The Fermi surfaces, symmetry point labelings, and Z - T line are shown in Fig. 3.

This topological degeneracy is only lifted by the opening of the SC gap.²³ Assuming a triplet OP, the bands that are involved open with two bandgaps, given by the expression (see Appendix XVJ, Eq. (52) for the BdG quasiparticle bands). This point degeneracy of a quartet of bands (including spin and SOC) at a pair of Dirac points, finally split only by pairing, form a basis with precise degeneracy for the discussion of a two-component system in k space. Previously, approximate symmetries based on bands or Fermi surfaces have been suggested to allow for triplet pairing. Ghosh *et al.* proposed Hund’s coupling within Ni $3d$ orbitals to account for triplet pairing,²⁰ invoking symmetry-breaking of one of the $3d$ orbitals. However, the density of states $N(E)$ indicates that the Ni d bands are rather narrow and fully occupied, lying in the -3 eV to -1.5 eV range and contributing only mildly at E_F through mixing with Ga s - p orbitals.²⁴

VIII. μ SR REPORTS OF TRSB

A. Reported TRSB below T_c

The following near comprehensive list (as of this writing) includes a variety of materials types, space groups, and degree of anisotropy, each followed by the reported spontaneous field, or by NA if the field was not available.

- skutterudite $\text{Pr}(\text{Os},\text{Ru})_4\text{Sb}_{12}$ (0.6 G)^{54,76}
- non-centrosymmetric $I43m$ Re_6Zr (0.6 G, 1.2 G)^{54,77}
- non-centrosymmetric $Amm2$ LaNiC_2 (0.1 G)⁷⁸, (NA)⁷⁹⁻⁸¹
- Dirac silicides (Nb,Ta) OsSi (0.83 G, 0.17 G)⁸²
- quasi-skutterudite $\text{Lu}_3\text{Os}_4\text{Ge}_{13}$ (1.1 G),⁸⁴
- putative frustrated superconductor Re_2Hf (1.2 G),⁸⁵
- non-centrosymmetric intermetallic La_7Pd_3 (NA)⁸⁶
- rocksalt structure monosilicide ScS (NA)⁸⁷
- centrosymmetric $Cmcm$ LaNiGa_2 (NA)¹⁹, (0.2 G).⁵⁴
- cubic $\text{Re}_6(\text{Zr},\text{Hf},\text{Ti})$ (0.2 G)⁵⁴
- unusual $I4/mmm$ tetragonal SC Sr_2RuO_4 (0.5 G)⁵⁴
- tetragonal Fe-based $\text{Ba}_{1-x}\text{K}_x\text{Fe}_2\text{As}_2$ (0.1 G)⁵⁴
- non-centrosymmetric hexagonal SrPtAs (0.07 G)⁵⁴
- non-centrosymmetric tetragonal CaPtAs (0.8 G)⁵⁴
- cubic (bcc) $\text{Re}_{0.82}\text{Nb}_{0.18}$ (0.4 G)⁵⁴
- hexagonal $P6_3/mmc$ Re (0.2 G)⁵⁴
- non-centrosymmetric hexagonal $\text{La}_7(\text{Ir},\text{Rh})_3$ (0.1 G)⁵⁴
- tetragonal $I\bar{4}2m$ Zr_3Ir (0.08 G)⁵⁴
- tetragonal $I4_1/acd$ ($\text{Lu},\text{Y},\text{Sc}$) $\text{Rh}_6\text{Sn}_{18}$ (0.6 G)⁵⁴

Although this paper concerns primarily μ SR experiments, separate indications of TRSB signals have appeared. Of the examples provided above, Sr_2RuO_4 ⁸⁸ and $\text{PrOs}_4\text{Sb}_{12}$ ⁸⁹ have been proposed as TRSB by observation of Kerr polar effect rotation angles of 0.06 μrad and 0.25 μrad respectively, and for LaNiC_2 by direct magnetization measurement, reporting a field of 0.01 G. (See Sec. XIII for more discussion of Sr_2RuO_4 .) Ghosh *et al.*⁵⁴ provide references to the original papers for the field values they provide. In a few cases, such as Re_6Zr , analysis shows enhanced depolarization below T_c when analyzed with Lorentzian relaxation but not with Gaussian relaxation, or vice versa. Table 2 of the Ghosh *et al.* paper⁵⁴ provides a list of correlated electron materials that have been probed with ZF- μ SR or polar Kerr rotation, some showing a TRSB signal and some not. Section XIII provides further discussion of sample dependence in some of these metals.

An overview of depolarization analysis expressions are given in Appendix XV B 2. The signal of depolarization as $T \rightarrow 0$ is a few to several percent of the normal state value, sometimes with an anticipated T -dependence (qualitatively like the gap) but sometimes appearing somewhat below T_c and sometimes with unclear T -dependence (due to uncertainty in data). As an example, for Re_6Zr ⁵⁴ with $T_c=6.8$ K (much the highest T_c in the above list of SCs), the maximum signal at $T \rightarrow 0$ is 3%

above the normal state value, with the associated spontaneous field value having been provided as either 0.6 G or 1.2 G. For LaNiGa_2 , the sample case we have chosen for this article, with $T_c=2$ K, the increase is 6% above the normal state value as $T \rightarrow 0$ and is representative of that of a secondary OP.¹⁹ See Sec. XIII for some discussion of sample dependence.

B. Comments on the order parameter

The SC state is addressed in the following sections, with discussion of the order parameter in Sec. XI. As an indication of the issues given the experimental indication of TRSB, why does the proposed exotic state of, say, LaNiGa_2 require a combination of (i) breaking of $U(1)$ symmetry [a given], (ii) avoidance of isotropic singlet spin pairing [uncommon], (iii) change of magnetic symmetry (TRSB) [uncommon], (iv) broken orbital/band symmetries at T_c [uncommon], and in LaNiGa_2 should do so in (v) a nonunitary manner [uncommon]? One ‘given’ and four ‘uncommons’ multiply to a ‘highly uncommon’ occurrence – a rare sighting. The topological band character of LaNiGa_2 , due to two Dirac points on the Fermi surface, does give a distinction from the other cases listed in Sec. VIII A, but several of the above questions extend to other members of this class of *fragile magnetic superconductors*.

A primary question, addressed by several superconductor theory groups more widely is: what type of order parameter is consistent with the measured constraints, and precisely what are the constraints? It has been understood since not long after BCS theory appeared that a magnetic impurity diminishes a singlet order parameter locally and degrades SC properties, that is, a magnetic moment has a detrimental effect on singlet superconductivity locally. The muon is a magnetic impurity. A triplet OP will respond differently from a singlet state, in ways that depend on the form of the triplet OP.⁷⁵ The following sections deal with the electronic behavior underlying these questions, then addressing them to some extent.

IX. SUPERCURRENT AND ITS EFFECT

A. Supercurrent versus vector potential

In identification of a bulk superconducting state, more convincing than zero measured resistance is the magnetic susceptibility, reflecting the transition from paramagnetic to dielectric character. The magnitude of the diamagnetic susceptibility below T_c provides, among more detailed inferences, the superconducting fraction of the sample. A fundamental property is the response of the SC material to the imposition of a magnetic field, *i.e.* spin-antiparallel Cooper pairing versus spin-parallel alignment of spins with the magnetic field. The triplet case should provide low energy pair spin flips without depairing, hence a paramagnetic susceptibility, versus the

large diamagnetic susceptibility of singlet SCs.

The theory of the origin of the supercurrent has gone through progression as the theory of SC has been fleshed out. A very brief accounting of the various expressions^{46–48} relating the vector potential to the magnetic field is given in Appendix XV F, with more discussion in Ref. [71]. Each gives a result in the London form,⁴⁶ a staple of superconductivity theory,

$$\vec{J}^s(\vec{r}, T) = -\frac{1}{\Lambda(T)} \vec{A}^\mu(\vec{r}), \quad (11)$$

where Λ incorporates the linear (and local) response of the superconductor. The three expressions differ, especially the latter (BCS), but do not affect the discussion in this paper.

The point of interest here is more general: a magnetic field in a superconductor interacts with the charge directly through the vector potential \vec{A} , not through the magnetic field $\nabla \times \vec{A}$. While this is a fundamental precept of SC theory and phenomena, the interaction of the moment with the SC order parameter has never, to the knowledge of this author, been theorized on the small distance scale of the muon vector potential. Given Eq. 11, \vec{A}^μ creates a supercurrent proportional⁷² to \vec{A}^μ , as required by the Meissner effect. However, in a region where the muon field exceeds the experimental critical field, superconductivity will be quenched and there are other considerations. Gor'kov's Greens function theory,⁹¹ which verified the Ginzburg-Landau theory below and near T_c , may be generalizable to address short length scale behavior.

The scale on which this happens – varying by orders of magnitude over a few Angstroms – is less than the penetration depth or coherence length. This length scale is not addressed by the theoretical progression mentioned above. The Usadel Green's function approach,⁹² in which the SC gap $\Delta(\vec{r})$ becomes position dependent due to disorder, a magnetic field, or proximity to a boundary, may be adaptable to the case of a position dependent, short range vector potential such as that provided by the muon.

B. Field at the muon site

The supercurrent density J^s with circular form from \vec{A}^μ produces a magnetic field $\vec{B}^{sc}(\vec{r})$. Each z level (a circular sheet of current loops) produces a contribution to $\vec{B}^{sc}(\vec{r})$ without any cancellation. The muon experiences the combined field (not its own)

$$\vec{B}^{tot}(0) = \vec{B}^{ind}(0) + \vec{B}^{sc}(0), \quad (12)$$

the last field from the supercurrent arising only below T_c .

We focus on the vector potential \vec{A}^μ , which leads to a field arising from the induced spin magnetization \vec{B}^{ind} and to the field arising from the supercurrent $\vec{B}^{sc} \propto \vec{A}^\mu$. Theory of a superfluid region at this sub-nanoscale is unavailable, so applying the conventional theory is what is

available. From magnetostatics, the field due to a (super)current, and its value at the muon site, is (keeping only \vec{B}^{sc} as the strongest field)

$$\begin{aligned} \vec{B}^{sc}(\vec{r}) &= \frac{1}{c} \int \vec{J}^s(\vec{r}') \times \frac{\vec{r} - \vec{r}'}{|\vec{r} - \vec{r}'|^3} \\ \vec{B}^{sc}(0) &\propto \int \vec{A}^\mu(\vec{r}') \times \frac{\vec{r}'}{|\vec{r}'|^3} d^3 r' \\ &\propto \mu \hat{z} \int \frac{\rho^2}{(\rho^2 + z^2)^3} d^3 r \end{aligned} \quad (13)$$

where cylindrical coordinates ρ, ϕ, z have been introduced, and using $\vec{A}^\mu = (\vec{\mu} \times \vec{r})/r^3$, $\vec{\mu} = (0, 0, \mu)$.

The integral for the x and y components vanishes, consistent with the symmetry for a homogeneous environment allowing only a z component. (For an anisotropic environment these components will not vanish.) The integral over ϕ gives 2π , leaving the integrals

$$\begin{aligned} B_z^{sc}(0) &= -\frac{4\pi c\mu}{\lambda_L^2} \int_0^\infty \rho d\rho \int_{-\infty}^\infty dz \frac{\rho^2}{(\rho^2 + z^2)^3} \\ &= -\frac{2\pi c\mu}{\lambda_L^2} \int_{-\infty}^\infty dz \int_0^\infty \frac{w dw}{(w + z^2)^3}. \end{aligned} \quad (14)$$

The dw integral ($w = \rho^2$) from Gradshteyn and Ryzhik⁹⁵ is lengthy and unhelpful, but irrelevant for now because there remains an infrared divergence $\int z^{-3} dz$ (reminiscent of the infrared divergence of the integral for the self-induced field at the muon site in the normal state), reflecting the already encountered need for including quantum treatment and high field physics in the muon near-field region (see Sec. V). Evidently the field must be finite, and the quantum effects near the muon that regularize the integral are discussed in Sec. V.

This result returns one to the same (an)isotropy discussion as for the normal state. For the homogeneous electron gas with cylindrical symmetry of the system, the field at the muon site will align with the muon moment, thereby providing no torque and no depolarization. Again, the low symmetry of the muon site will cause the field to deviate from the z direction, thereby providing torque on the muon moment and possibly a mechanism of depolarization.

X. KONDO PHYSICS; YSR STATES

A. Magnetic moment coupled to pairing

The Kondo picture of a magnetic impurity in an electron gas addresses the coupling of the spin degree of freedom of a magnetic impurity coupled to itinerant electrons through an on-site interaction $J_K \sum_j \vec{S} \cdot \vec{s}_j$ in terms of an on-site Kondo exchange parameter J_K and the impurity and electron (j) spin operators \vec{S}, \vec{s}_j , respectively. As Cooper pairing initiates, an itinerant electron in the area is frustrated between anti-aligning with another electron

(for singlet pairing), or with anti-aligning with the impurity spin, causing fluctuation. Kondo coupling is anti-alignment in sign, which without pairing leads to a collective singlet forming between the impurity and the electron gas, and to a heavy fermion metal for a periodic lattice of spins \vec{S} . This interaction only for an isolated moment is discussed here. A magnetic impurity imposes a vector potential, an orbital coupling in addition to the electronic exchange spin coupling that couples differently to the conduction electrons – a magnetic field over a region versus an effective δ -function on-site exchange coupling.

Early work addressed data on superconducting samples containing a collection, perhaps a sublattice, of magnetic particles,^{96,97} and effects that arise due to anisotropy and a Type-II state.⁹⁸ A related emphasis was the interaction between a dipole and the superconducting surface.⁹⁹ Küster and collaborators⁷³ have studied how to probe this question for the case of magnetic atoms on surfaces. However, some superconductors with dense lattices of rare earth ions with large moments show little coupling to itinerant electrons, *i.e.* potential Cooper pairs. High T_c cuprates, *viz.* $\mathcal{R}\text{Ba}_2\text{Cu}_3\text{O}_{7-\delta}$, \mathcal{R} =rare earth (except for Pr), with $T_c \sim 80\text{-}100$ K, display little evidence of coupling, with the $4f$ moments finally ordering antiferromagnetically only at a few kelvin with negligible effect. The rare earth \mathcal{R} class $\mathcal{R}\text{Ni}_2\text{B}_2\text{C}$, on the other hand, displays a rich competition between SC and antiferromagnetic order in the 10-20 K range, even showing coexisting superconductivity and magnetic order in the H-T phase diagram.¹⁰⁰

Another issue arises from the $3\mu/r^3$ scaling of the muon magnetic field. When this field exceeds the upper critical field, the order parameter vanishes. For the critical field of LaNiGa_2 , this distance is 1.3\AA . The muon then will always exist in a small normal state region. This change from bulk order parameter to a normal region occurs on a smaller length scale than ξ (the small length scale in Type II SCs, determined from singlet pairing considerations), which brings up the (possibly) unexplored question of how this crossover occurs on the \AA scale. For comparison, scanning tunneling microscopy spectra and S-I-S tunneling characteristics demonstrate that a bulk gap extends to very near, if not at, a surface or interface, where there is a very rapid change from full amplitude order parameter to vanishing OP, seemingly less than 0.5 nm. How the increasingly large near-field might affect a muon's detection of relaxation-inducing fields, and indeed the reaction of the OP to such a rapidly varying field, are areas yet to be clarified, as discussed in Sec. IX B. Miyake and Tsuruta explored the effect of the muon's magnetic field in a p -wave superconductor (without accounting for the degenerate Fermi liquid aspect of superconductors), resulting in ~ 1 G fields as an estimation of the consequences.¹⁰¹

1. Kondo singlet versus Cooper singlet

An early approach to this coupled local moment-pairing order parameter issue is embodied in the 1970 results of Zittartz and Müller-Hartman,¹⁰² (ZMH) who extended earlier works at the model Hamiltonian level that had been influential in understanding the normal state Kondo effect. One viewpoint was that the opening of the SC gap interrupts the essential low energy Kondo physics, and the quantum aspects of the spin (perhaps the vector potential) could be treated less explicitly. What is known is that Kondo lattice materials – crystals with a sublattice of magnetic moments – can enter the now well studied Kondo heavy Fermi liquid (“heavy fermion”) and sometimes superconducting phase.

Appending the Kondo Hamiltonian with a BCS ‘pairing potential’ term, ZMH established within this model that as the gap opens, bound states involving the local moment appear within the gap but near the gap edges – the YSR states, as foreseen by the YSR authors. The character of these states should include strong local moment character, and more recent studies have clarified both their energetic and orbital character. The next two subsections discuss these states.

According to this level of theory, a single muon impurity couples to the electron cloud that is beginning to pair into Cooper singlets but also is encouraged to form competing Kondo singlets. The outcome becomes, besides other spectral changes, a pair of magnetic moment-derived localized bound states within the gap, at energies near the gap edges at $\pm\Delta(T)$. This connection provides a mechanism of coupling of the SC order parameter to an impurity spin. As derived in Sec. IX B (not considering Kondo coupling), the μ^+ moment creates a spin polarized region around the muon that is changing direction with polar angle θ , with near-field greater than the critical field. This electronic magnetization near the muon, having strong polarization (varying with direction) acts to obviate singlet SC pairing in that region (not necessarily encouraging triplet pairing), thereby reducing the gap magnitude, to the extent that any OP can be treated on the Angström scale. The magnetic ion's (muon's) field at some point dominates, providing a moment-quasiparticle coupling of as yet unstudied character. Study of the SC-Kondo model has since that time been addressed by more recent many-body techniques, see for example Sykora and Meng's calculation of the interplay between the Kondo singlet state and the induced YSR states.¹⁰³ Some results of the study by Choi and Muzikar¹⁰⁴ of a Kondo impurity in an exotic superconductor are discussed in Appendix XV G.

2. Yu-Shiba-Rusinov states

As mentioned, a magnetic impurity in a gapped singlet SC interferes with the OP, leading to bound YSR (Yu-Shiba-Rusinov¹⁰⁵⁻¹⁰⁸) states within the SC gap 2Δ but, according to early model studies, near the gap edges at

$\pm\Delta$. Such states are analogous to shallow donor and acceptor states in semiconductors, and might someday play a similar role in SC electronics. After the Kondo effect was elucidated, one viewpoint was that the SC gap inhibited low energy processes (which dominate the Kondo effect) as being frozen out, and the moment could be considered as classical. As theoretical interest and experimental capabilities have progressed, quantum behavior of the impurity spin has become a topic of more detailed study, while the internal structure of the state raises interest. This area of study should be regarded as ongoing, with relevance to this article to be determined. The status of impurity-induced states in superconductors as of 2006 was reviewed by Balatsky, Vekhter, and Zhu.⁴⁵

Previous studies treated the impurity moment-electron coupling, implicitly (point contact coupling) in early work but increasingly explicitly in more recent studies, as interatomic electronic exchange akin to (but more broadly than) the rules of Goodenough,¹⁰⁹ Kanamori,¹¹⁰ and Anderson¹¹¹ between the impurity orbital mixing with orbitals of itinerant states. This direction of study neglected the smaller effect of the orbital behavior near the dipolar field of the moment. In studying the muonic impurity at the atomic level, both effects may become relevant. The environment in μ SR studies provides a direct coupling between the muon vector potential (orbital effects) and the SC condensate as well as creation of μ YSR states. Coupling of the muon is of a distinct character due to the fact that the coupling is through the vector potential which reduces the gap plus polarization of the 1s electron orbital off the muon, rather than through (say, 3d) atomic orbitals. Hydrogen interstitials should introduce similar formal considerations, but with a smaller effect.

3. μ YSR states

As noted earlier, the implanted muon is a close cousin of interstitial hydrogen. Given a more-or-less singly occupied 1s orbital of the muon, typically lying within the valence bands of the host, there is no anticipation of an electronic (spin) moment (density functional theory reports rarely consider magnetic activity) and a 1s orbital has no orbital moment. Regarding this point: it seems that DFT studies of proton and muon interstitials^{37,39,51–53} have rarely searched for spin polarized activity of the muon. Interest in an “ultra-deep donor” state in ultra-pure semiconductors received a boost from a simple type of correlated electron calculation applied to the H 1s orbital in Ge, which identified such a spin-polarized state a few eV (note: not a few meV) below the gap in Ge.¹¹² Screening in metals alters the physics of such states. Back to the main topic: the muon vector potential field will interact with the OP and it can be expected to give rise to defect states within the gap, which will here be denoted μ YSR states. A study of persistent YSR resonances in an exotic SC state was presented by Senkpiel *et al.*¹¹³

The study of YSR states has progressed to DFT studies of 3d ions with selected symmetries. Fe, with its large moment, has been the preferred magnetic atom, within or on the surface, of conventional SCs such as Pb¹¹⁴ and Nb,¹¹⁵ revealing a great amount of detail that can occur in such cases. Some cases are addressed in Appendix XVH. In-gap states due to a muon, with only the moment’s vector potential and with the unpolarized 1s orbital not involved, have yet to be studied, although a few groups may soon have the capability (see App. XVH).

XI. IMPLICATIONS FOR PAIRING SYMMETRY

Construction of plausible exotic order parameters relies on the guiding principles of antisymmetry of the Cooper pair and the BCS form of the nonlinear gap equation, which becomes linear at T_c . For elements and intermetallic compounds that display conventional Fermi liquid behavior without any unusual magnetic tendencies, superconductivity is initially assumed and then (frequently) verified to be due to phonon-induced pairing of electrons – singlet *s*-wave pairing. When properties, in the normal or SC state, are unexpected, an exotic (i.e. non-BCS) OP is anticipated. For this paper we include the scenario of TRSB without accepting it as a strict limitation on concepts.

The two subclasses of OP are (spin) singlet pairing and (spin) triplet pairing, while each is subject to orbital (real space, k space) effects including symmetry reduction. The singlet versus triplet distinctions provide the first line of attack in constructing possible OPs, with TRSB signals providing the dominant triplet viewpoint. Beyond that, symmetry in momentum space (‘orbital symmetry’ of the gap Δ_k beyond *s*-wave) provides the second consideration. Accepting TRSB, spin (or orbital) magnetization becomes the issue, arising from an accompanying symmetry breaking. This section provides an overview of the progression of theory. More extensive reviews cited in the Introduction should be consulted for a more complete picture.

A. The spin singlet issue

Occam’s razor¹¹⁶ encourages one to shave away unduly involved models while continuing to connect with observations. This maxim is of course not such a straightforward and easy guideline to apply when faced with unusual data. Singlet pairing due to phonon glue should be considered first, as it provides the presumption underlying experimental identification of materials properties that lie within familiar ranges for weak coupling Fermi liquid superconductors. Cooper’s demonstration that the Fermi surface is unstable to formation of bound *singlet* pairs of zero total momentum is the underpinning of the theory of superconductivity, subject only to the necessity

of a net-attractive effective interaction. The BCS choice was exchange of a boson but more specifically a phonon, because phonons are always present and the isotope effect was known. Phonons are known to strongly favor zero momentum singlet pairing, subject to interruptions from other pairing mechanisms that are usually negligible in conventional Fermi liquids. Spin triplet scenarios have not relied significantly on the question of energy loss versus gain of the spin pairing choices.

1. Ubiquitous electron-phonon coupling

Electron-phonon coupling (EPC) is distinctive given that it (i) is always in play, and (ii) is always attractive for *s*-wave pairing (the kernel in the gap equation does not change sign), with coupling strength λ moderated by a retarded Coulomb repulsion μ^* , typically falling in the 0.10-0.16 range.^{117,118} For low T_c 's, say below 5K, it has been difficult but is recently becoming possible due to extended methods, to verify theoretically^{2,119} that SC derives from EPC.

The difficulty is that calculating low T_c requires *precise* knowledge of both λ and μ^* , especially the latter of which is normally unavailable. An added complication is that the fundamental Coulomb repulsion is μ , which is very involved to calculate precisely; almost all calculations of μ involve (possibly reasonable) approximations, but as EPC becomes weak, the precision of μ becomes important. μ^* , used in the majority of solutions of the Eliashberg equations to date, and in existing T_c equations, is a renormalization that depends on subjective energy scales and a frequency cutoff used in solving the Eliashberg equations.¹²⁰

Taken together (they are each always present), the combination $\lambda_k - \mu^*$ contains some richness, based on the k -dependence of λ_k and the near-independence of μ^* on wavevector (it involves higher energy virtual processes that serve to average out the dependence on k across the Brillouin zone). If λ_k is strongly anisotropic and μ^* is unusually large, the net interaction $\lambda_k - \mu^*$ can change sign on the Fermi surface, and non-*s*-wave orbital behaviors may become favored.¹²¹ For a weak but anisotropic λ_k , a change in sign of $\lambda_k - \mu^*$ in the kernel introduces the possibility of a exotic gap symmetry, denoted *p*-wave, *d*-wave, or even more involved combinations of symmetries, such as *s+id*. While a few *p*-wave and *d*-wave SCs have been suggested for quantum materials, some with several types of support, none has been established in the weakly-correlated Fermi liquid metals that are the topic of this article. Simple Fermi liquid SCs, with conventional μ^* and low T_c are commonly and successfully interpreted to arise from EPC, due to the isotope effect on T_c when available, partly due to other experimental information on λ , and partly simply due to the ubiquity of the phonon mechanism.

A pairing strength $\lambda=0.45\text{-}0.6$ in an *s-p* electron compound can account for a T_c up to 5K or so (but is still sensitive to μ^*), a range including all TRSB SCs in the class

of *fragile magnetic superconductors*. Given the seemingly necessary exotic order parameter, an additional channel for symmetry-breaking is anticipated. While weak for EPC, this value of coupling may be strong compared to additional candidates, hence alternatives should be complementary to, rather than competitive with, EPC. More visually expressed, they might be simply additional to EPC. Possible phonon coupling to additional degrees of freedom should not be discounted.

2. Eliashberg calculations

Subedi and Singh¹²² calculated the phonon spectrum, the Eliashberg spectral function $\alpha^2 F(\omega)$, and T_c for LaNiC₂, a sister compound to LaNiGa₂ with closely related composition, filled 3d bands, an orthorhombic space group, and similar value of $T_c=2.7\text{K}$. It has a different point group, but one that also has only 1D irreducible representations, *i.e.* no degenerate crystal symmetry to be lifted. The μ SR identification as TRSB is based on extraction from analysis of a spontaneous field as small as 0.1 G, a value frequently stated as the lower limit of detectability. The calculated coupling strength is $\lambda=0.52$, and using a standard value of the retarded Coulomb repulsion $\mu^*=0.12$, $T_c=3\text{K}$ was obtained. This value is consistent with experiment, and provides the strength of electron-phonon coupling that must be confronted by competing pairing mechanisms.

Related calculations on LaNiGa₂ were reported by Tütüncü and Srivastava.¹²³ They assumed the *Cmmm* space group²¹ understood at the time to determine the structure, rather than the more recently discovered *Cmcm* structure from single crystal XRD.^{22,23} The electronic structure is similar to the *Cmcm* result, for example the Ni 3d states are filled and lie in the same energy range, and given the similarities of the crystal structures the phonon spectrum should be similar. The Fermi surfaces for both are large and multisheeted, but different. Based on a limited *Q*-mesh for the phonons, they obtained $\lambda\approx0.7$, and choosing $\mu^*=0.17$ for their estimate, their calculated T_c was close to the 2 K experimental value. Calculations using the more recently determined *Cmcm* space group have not been reported.

Calculated values of T_c , when small, are sensitive to (i) the choice of the parameter μ^* , introduced for computational simplicity but reflecting the retarded nature of the Coulomb interaction, (ii) accurate calculation of phonon frequencies and electron-phonon matrix elements, and (ii) a well converged calculation of λ . In any case, the modest values of λ indicate weak coupling and low but non-zero T_c when augmented with μ^* . These results for two TRSB superconductors provide a strong indication that the pairing is BCS (spin singlet, phonon mediated, weak coupling), and that other origins of the spontaneous magnetic field should be sought. In this scenario, the reported spontaneous magnetic fields from μ SR spectroscopy could be attributed to the field generated by the supercurrents that onset at T_c , involving modifications of

the OP. Suggestions of such changes in the OP are discussed in later sections.

B. *p*-wave versus *s*-wave

The near (possibly complete) absence of anisotropic pairing states in conventional Fermi liquid metals raises questions about why they seem to be so disfavored. For example, the antisymmetric *p*-wave state should gain energy due to the two members of the Cooper pair having a reduced short-range Coulomb repulsion. Foulkes and Györffy¹²¹ looked at the scattering vertex function Γ , given schematically by $\Gamma = I - IGG\Gamma$, where I is the irreducible scattering vertex and G is the single particle Green's function. Assuming that I does not depend on relative spin orientations, they compared the coupling strength λ_0 for an *s*-wave kernel to its *p*-wave counterpart λ_1 . A key point is that for *p*-wave, μ and therefore μ^* will be much reduced, perhaps to near negligible, so the effective couplings $\lambda_0 - \mu^*$ and λ_1 may be the quantities that should be compared.

Foulkes and Györffy took into consideration the accepted lore that anisotropic pairs are strongly affected by impurity scattering, requiring very clean metals. Reducing $T_{c,1}$ (*p*-wave pairing) proportional to the transport broadening \hbar/τ , an accepted approximation, they suggested that *p*-wave pairing might occur in Pd, W, or Rh samples, but requiring residual resistivity ratios between 10^3 to 10^5 , representative of *extremely* pure crystals. This work provided at least the plausibility of *p*-wave pairing in conventional metals. Other works have suggested that phonon pairing in conjunction with other interactions can generate odd-pairing for certain choices of parameters.^{124,125}

C. Spin triplet pairing

As mentioned above, the superconducting properties of this class of *fragile magnetic superconductors*, barring the emergent magnetic field, have been analyzed in terms of singlet pairing, with results similar to related singlet superconductors with similar low T_c . Nevertheless, triplet pairing has become the favored direction of study for the order parameter in this class. Ferromagnetic spin fluctuations have long been considered as the likely source of triplet pairing,¹²⁶ although triplet models based on anti-ferromagnetic fluctuations have been constructed.¹²⁷

In the formalism reviewed earlier, the symmetries have been triplet S (even), L symmetric and even (full space group symmetry), and the additional broken symmetry, call it G , odd. The triplet S space provides coupling to the magnetic field, and receives the attention. The developers of the INT model, Weng *et al.*¹⁸ and Ghosh *et al.*,²⁰ posit this type of spin-triplet order parameter. Their G degree of freedom relied on breaking of band, Fermi surface, or orbital (near) symmetry, which allowed the even triplet-spin symmetry to provide what was nec-

essary to account for a spontaneous magnetic field. This model has evolved and deserves an overview.

1. The INT model

TRSB is conventionally associated with triplet, *i.e.* solely equal spin, pairing; orbital possibilities are discussed in the next section. In their 2010 study of the symmetry restrictions in LaNiC_2 , Quintanilla *et al.*⁷⁹ arrived at an initial proposal for the observation of TRSB. Specific properties they addressed were (i) the non-centrosymmetric space group, (ii) the point group (C_{2v}) with only non-degenerate irreducible representations, (iii) necessity of considering spin-orbit coupling (SOC), (iv) the restriction that the effect of SOC must be small, in spite of their observation that SOC splitting of bands around the Fermi level is more than an order of magnitude larger than the SC gap. Satisfying these conditions, the only allowed order parameter was distinctive: primarily singlet with a small admixture of triplet, *i.e.* most Cooper pairs are (conventional) singlet, while a few are equal-spin paired. There was however the possibility that an additional symmetry of the normal state, not considered by them, if broken would lead to additional considerations.

Possibly concluding that the singlet+triplet state was unlikely, Weng *et al.* constructed¹⁸, and Ghosh *et al.* refined²⁰ an Internally (antisymmetric) Nonunitary Triplet pairing (INT) spin-triplet picture for LaNiC_2 and LaNiGa_2 in which there is parallel-spin pairing (the $S_z=0$ channel is a symmetric combination of singlet pairs and would lie at higher energy). For the magnetization, $|\uparrow\uparrow\rangle$ ($S_z = +1$) occupation exceeds (slightly) that of $|\downarrow\downarrow\rangle$ ($S_z = -1$). Without going into further details (see Appendix XV J), this one-parameter model is based on some electronic (quasi)degeneracy – nearly degenerate bands or Fermi surfaces, or alternatively that of an active atomic orbital on symmetry-related atoms – any might account for the necessary additional symmetry to be broken. From some structure in the penetration depth $\lambda_L(T)$ and specific heat $c_v(T)$ they argued that a “two gap” (or “two band”) character might be responsible. Data for $c_v(T)$ obtained on single crystals of LaNiGa_2 since these papers were published may be consistent with a single anisotropic gap.²³

D. Challenges to triplet pairing

Based on the assignment of triplet $S=1$ pairing in the class of materials under discussion here, such exotic pairing was initially considered as a possibility only in correlated materials. A more detailed understanding of the interaction and present interpretation, based on TRSB of weak coupling Fermi liquid metals, of triplet pairing appears to confront several common expectations and challenges:

- that low T_c , weak coupling SCs commonly conform

to Cooper's (BCS) singlet $S=0$, zero momentum pairing instability based on the ever-present electron-phonon coupling, in terms of ξ , λ , H_{c1} , and H_{c2} that are understood on that basis

- triplet correlations will need to dominate singlet correlations to break TRS, implying at least a moderately strong triplet coupling (of unclear origin in an uncorrelated metal),
- magnetic impurities diminish singlet (Cooper) pairing moderately; triplet states are predicted to be highly sensitive to defects, or even non-magnetic defects,^{45,50} while in some of the listed materials, T_c values are consistent across sample quality,
- there are open questions relating to the superconducting state coexisting with an intrinsic magnetic field,⁷⁵
- only a select group of intermetallic compounds of seemingly similar non-magnetic Fermi liquid character but across compositions and space groups, are identified as breaking TRS, and all are low T_c materials,
- triplet pairing appears to require a wholesale reconstruction of the pairing interaction, most of which (to repeat) are currently analyzed successfully in terms of singlet pairing phenomena.

This class of *fragile magnetic superconductors* may be analogous to the situation in EPC, where a small uncertainty in a weak-coupling λ can account for the difference between low T_c or none. A smaller than detectable spontaneous field will lead to assignment to the conventional class, while a larger, just detectable, will lead to TRSB behavior. According to muon effects discussed here, all implanted muons should experience an emergent field and perhaps additional depolarization below T_c , but with some the field is smaller enough that it lies below detectability and thus is not included in the class of *fragile magnetic superconductors*.

Triplet $S=1$ pairing in this class has the sole, but crucial, justification that it justifies the observation of additional muon spin depolarization, or polar Kerr rotation, or (in one study) magnetization, below T_c . The conclusion has been that the order parameter must couple to a magnetic field. For triplet pairing, equal $S_z=\pm 1$ occupations provide a degeneracy from which symmetry can be broken by some small interaction. As mentioned, other properties of this class seem not to be consistent with triplet pairing. It is also a challenge, for the future, to identify a microscopic mechanism favoring equal spin pairing in this class, one that overrides Cooper's strong favoring of both singlet pairing and symmetric zero momentum pairs. These challenges are being addressed by theorists material by material. Some generalities of triplet OPs, of which the INT model^{18,20} discussed below is one, are provided in Appendix XV J.

XII. EXOTIC SINGLET MODELS

Signals of TRSB have been proposed to be possible with singlet OPs, which would however need to include some additional 'exotic' components. This section pro-

vides a brief description of one, and mentions a second, different approach.

A. Orbital magnetism scenario

Spontaneous orbital magnetism in crystalline solids is generally expected to be much smaller than conventional spin magnetization. However, given the reported small field μ SR values of 0.1-1 G, orbital magnetization would only need to be the same as the spin magnetization discussed earlier, of the order of $10^{-3} - 10^{-4} \mu_B$ per active unit in a cell.¹²⁸ Orbital currents have been discussed originally in the context of strongly correlated materials,^{129,130} and not yet verified. Independent searches in the layered cuprates have placed upper limits on the magnitude of such currents,¹³¹ however they remain of theoretical interest.

In such an event, the orbital current (on a [sub]nm radius scale) would need to couple to the $U(1)$ order parameter (pairing). As discussed in Sec. IX, an orbital supercurrent is driven by the muon moment that produces a local field, and which in a susceptible system might trigger an orbital current state more broadly.

The orbital loop current picture of Ghosh, Annent, and Quintanilla¹²⁸ provides a mechanism – an OP satisfying the requirements – in a proposed model. Based on the idea of a Josephson current flowing between equivalent atoms in the primitive cell, they constructed a Ginzburg-Landau-like expression for the condensation energy involving right and left oriented current loops. The requirements were that the OP satisfied the appropriate symmetries and that the free energy was real.

The phase diagram in terms of the free energy constants α and $\{\beta\}$ could be examined, finding regimes where the condensation energy was positive (SC would occur). Their model carried their stated requirements for such orbital order parameter: (i) there is on-site intra-orbital *singlet pairing*, (ii) more than two distinct but symmetry related sites within the unit cell are required to host the orbital current loop, (iii) there must be a degenerate irrep in the point group, and (iv) the free energy parameters require tuning. The only k -dependence arises from electronic form factors, and nodal lines might occur across the Fermi surface but are not required by symmetry. This model was proposed as a possibility for the compounds in the $\text{Re}_6(\text{Ti},\text{Zr},\text{Hf})$ system. With its somewhat larger value of T_c than others in this class, they explored for a maximum of the magnetization and obtained a maximum field of the order of 1 G. The stated criteria for this orbital current do not seem to correspond to most of the class of *fragile magnetic superconductors*, including LaNiGa_2 .

B. A different singlet scenario for LaNiGa_2

This compound has a unique characteristic: the pair of Dirac points pinned to the Fermi surface, discovered by

Quan *et al.*²⁴ and confirmed by ARPES data.²² These points are the remaining degeneracies after SOC splits the rest of a degenerate loop on the BZ face, as discussed in Sec. VII B. This pair is analogous to the Dirac points (DPs) in graphene,¹³² but in an orthorhombic 3D crystal. They provide a weak $N(E)$ non-analyticity $\Delta N(\varepsilon) \propto |\varepsilon|^3/v^4$ at the Fermi energy (v is roughly the geometric mean of the velocities along the principal axes) but in the background density of states $N(0)$. These Dirac points provide a precise valley degeneracy that may be susceptible to instability by spontaneous symmetry breaking, as discussed extensively for graphene.

While the scale of SOC band splitting, 30-40 meV in LaNiGa_2 , is typically regarded as small, it is (i) the crucial point in having DPs rather than a loop of degeneracies, and (ii) it is large compared to $2\Delta, k_B T_c$, the SC condensation energy, and the energy associated with the small inferred magnetic field. Categorizing the possible order parameters when (schematically) $\mathcal{J} = L + S$ defines the symmetries of the normal state, rather than L and S separately, will be left for further study. (Here L characterizes the symmetry in real space, or in the BZ, and SOC couples it to S .) A possibility can be suggested.

Suppose that the Cooper pair entities couple to a standard (odd) singlet. The two-dimensional space of the pair of DPs can be represented by Pauli matrices $\vec{\tau}$ analogous to conventional spin. Of the DP singlet $\tau = 0$ or triplet $\tau = 1, \tau_z = \pm 1$ ($|u, d\rangle + |d, u\rangle\sqrt{2}$) possibilities, the triplet provides the even member of the order parameter to satisfy the antisymmetry of the Cooper pair. u, d are the projections onto the quantization axis in $\vec{\tau}$ space. Its part of the order parameter would have the familiar form $\vec{t} \cdot \vec{\tau} i\tau_y$, where (in general complex) \vec{t} would describe the ‘direction’ in τ -space analogous to the \vec{d} vector in spin triplet OPs, and $i\tau_y$ provides coupling to $U(1)$.

This scenario would account for the singlet-like SC properties²³ of LaNiGa_2 . But what about the observed muon depolarization, inferring a spontaneous magnetic field in the SC state? Here again spin-orbit coupling is essential. Each BdG band carries, as does the normal state electron band, a mixture of spin and orbital character. When pairing opens the gap, its coupling breaks the τ degeneracy, with $|u, d\rangle$ and $|d, u\rangle$ being displaced oppositely in τ space, giving different band fillings for the two ‘directions’ of bands. Due to SOC that gives spin (and orbital) character to each quasiparticle state, the two directions of spin (and orbital) character will no longer cancel, resulting in a non-zero magnetization, *i.e.* TRSB. The magnetization, and hence TRSB, becomes a parasitic (secondary) effect of the primary valley symmetry breaking. Mechanisms for inversion (valley) symmetry breaking can be named, *viz.* either inversion symmetry breaking or a low symmetry strain that would break the Dirac point symmetry.

Although this scenario shares some mathematical similarity to the INT model, it is completely different physically, both in the symmetry breaking and in the importance of SOC, in how the magnetization arises. This picture has another similarity to the INT model: it does not

transfer easily, if at all, to other members of the *fragile magnetic superconductors*.

XIII. DISCUSSION AND SUMMARY

A synopsis of this paper is this: primarily μ SR studies, but also polar Kerr rotation, and direct magnetization, have provided evidence of a spontaneous magnetization appearing below T_c in a set of around 20 superconductors, being conventional weak coupling Fermi liquid metals in the normal state and with low critical temperature. This group, referred to here as *fragile magnetic superconductors*, have been the focus of this article. When reported, the magnitude of the inferred magnetic field from μ SR experiments is 10^{-5} - 10^{-4} T, not far from the limit of detection. This signal is interpreted as evidence of time-reversal symmetry breaking accompanying, or near, the onset of pairing.

The signal, providing a time reversal symmetry breaking origin, in the case of μ SR originates from the region sampled by the muon moment, obtained from decay of the muon. The muon sits in a non-symmetric position of the crystal, with consequences that have not been studied fully: circulating supercurrents due to the muon vector potential, which would give rise to a magnetic field in the region. Another result would be localized Yu-Shiba-Rusinov states lying within the SC gap, which would provide coupling of magnetic character to the order parameter but may be challenging to observe.

Sample type (polycrystal or single crystal) and quality have been found to be relevant in several cases (see the following subsection), emphasizing the possibility that the muon will find stopping points near defects, or regions of magnetization, that are not representative of the ideal crystal. The questions raised are (i) whether the depolarization signal can be due to some effect other than a TRSB order parameter, and (ii) does it supersede in importance other SC properties that are typical of singlet superconductors. Sample dependence is discussed next.

A. Sample type and quality

New materials are often synthesized as polycrystalline powders or intentionally pulverized for experimental reasons. In polycrystals μ SR data will average over directions of the muon spin relative to any spontaneous magnetic field fixed to a sample orientation, and polarization direction will not be important. In single crystal samples, a spontaneous field will be oriented at various angles with respect to the symmetry-related sites of the implanted muon.

In low symmetry, un-oriented samples, the measurement will average over anisotropic responses, with the impact (loss of detailed information) increasing with the degree of anisotropy of the crystalline and electronic structure. Samples will differ in imperfections – point impurities or vacancies, linear and planar crystal defects,

grain boundaries – each of which may affect each measurement in its own way and complicate reproduction of results. Muons may be attracted to regions of defects, where more open spaces would enable them to increase their distances from the positive ion cores. Such questions have been coming to the fore in discussions of μ SR and Kerr rotation data, of which we list some cases.

- UPt_3 . An early case was this hexagonal heavy fermion SC, with two SC transitions observed at 0.50 K and 0.45 K, as well as other signatures of exotic SC phases. Luke and collaborators¹³³ observed muon spin depolarization (only) below 0.45 K, pointing to a spontaneous magnetic field origin, thus suggesting a TRSB field (of 0.1G) only for this lower temperature phase.^{133,134} Schemm *et al.* later reported a polar Kerr effect also in the low T_c phase of a crystal,¹³⁵ without reporting a value of field. However, further work on single crystals by Dalmas de Réotier *et al.* found¹³⁶ no additional depolarization below T_c for muon spin oriented either in-plane or along the *c*-axis, and with their analysis concluded that any spontaneous field could be no larger¹³⁶ than 3 μT . Sample quality was suggested to be the difference from earlier work. Higemoto *et al.*¹³⁷ extended μ SR study of UPt_3 on a single crystal cylinder down to 20.8 mK, without finding indication of spontaneous depolarization.

- $(\text{U,Th})\text{Be}_{13}$. The well-studied heavy fermion SC system $\text{U}_{1-x}\text{Th}_x\text{Be}_{13}$, with huge effective mass, reported also from μ SR an increased depolarization^{90,133} with onset below 0.4 K for $x = 0.019 - 0.035$ (where other experiments had indicated two SC transitions, the upper one sometimes around $T_c=0.55-0.65$ K), but did not report a value for the inferred TRSB field. Some evidence indicated that the lower transition might involve a spin density wave transition, providing its own local field. A neutron scattering study by Hiess *et al.*,¹³⁸ with somewhat less resolution in magnetic field, found no evidence of a field in an $x=0.035$ single crystal, but did find evidence of spin fluctuations (a likely mediator of triplet superconductivity). Further references can be found in the review of Stewart,¹³⁹ which seems to leave the issue for this system undecided, while the overview of Ghosh *et al.*⁵⁴ addresses this system for $x=0.02-0.04$ as TRSB.

- UTe_2 . After the discovery of unusual phases of UTe_2 , there were reports of evidence (2019-2023) supporting TRSB from three NMR studies¹⁴¹⁻¹⁴³ and two reports of a nonzero polar Kerr effect signal.^{144,145} Sample type and quality was reported and discussed in these papers, even noting that positive or neutral signals could be observed in various regions of single crystals.

μ SR measurements on molten flux-grown single crystal samples in 2023 by Azari *et al.*¹⁴⁷ reported no observable μ SR signal, while describing a helpful discussion of how counts from the sample holder and sample moments (atomic and nuclear) are taken into account in analysis of data. Sample quality, possibly involving U vacancy complexes that could become magnetic, was suggested to be a source of the earlier experimental indications. Further polar Kerr rotation studies by Wei *et al.*¹⁴⁵ and Ajeesh *et al.*¹⁴⁶ found no evidence of a TRSB signal.

- Sr_2RuO_4 . This extensively studied transition metal oxide, a Fermi liquid with low T_c (1.5K) but with enhanced susceptibility and heat capacity with respect to band structure values, exhibited μ SR depolarization reported by Luke *et al.* in 1998,¹⁴⁸ followed by a 2009 polar Kerr rotation study¹⁴⁹ supporting TRSB. The angular rotation signals of a fraction of a μrad were, as in μ SR studies of several members of this class, not far from the limit of resolution.

A review⁴ by Mackenzie and Maeno in 2003 of considerable experimental data on Sr_2RuO_4 and potential order parameters concluded that triplet pairing remained a likely possibility. Although this compound is included in the list in Sec.VIIIA because it is a low T_c Fermi liquid metal, it is different in that the normal state susceptibility and electron effective mass show factors of five or more enhancement above band values, reflecting noteworthy spin fluctuation enhancements. The 2019 overview by Wysokinski presented accumulating evidence supporting triplet pairing.¹⁴ Grinenko *et al.* in 2021 reported increased μ SR depolarization below T_c under pressure in Sr_2RuO_4 single crystals.¹⁵⁰ A related group reported supporting results, with additional peculiarities, under strain.¹⁵¹ Miyake provided a theory¹⁵² built on an energy-dependent density of states, viz. near a van Hove singularity, with correspondingly different spin-up and spin-down pairing gaps. Using parameters from Sr_2RuO_4 led to a spontaneous TRSB field of the order 10^{-2} G. From this period proposals of singlet pairing with exotic real space order parameters appeared¹⁵³⁻¹⁵⁷ as new samples¹⁵⁸ and more data accumulated.

A 2024 review by Mackenzie and Maeno emphasized that the issue of TRSB in Sr_2RuO_4 was not settled.¹⁶⁰ A following 2024 survey by Maeno, Yonezawa, and Ramires¹⁵⁹ stated "...a new development overturned past experimental results, and spin-singlet-like behavior became conclusive." The comment by Mazin also refers to this reversal of consensus in the field.¹⁶¹ Singlet pairing in this compound had already been entertained by theorists, for example by Schnell *et al.*¹²⁴ Singlet pairing does not exclude a field of orbital origin, although it requires tuning of parameters or an exotic form of real-space character, viz. chiral *d*-wave. Holmvall and Black-Schaffer referenced more than twenty suggestions¹⁴⁰ of chiral *d*-wave order parameters that will host TRSB, including some in the list in Sec. VIII A. The procession of numerous experiments and evolving evaluations reflects how delicate the determination of exotic order parameters can be, and has been.

- LaNiC_2 . μ SR observation of a depolarization increase near and below T_c on a polycrystalline sample was reported in 2012 by Hillier *et al.*⁷⁸ for LaNiGa_2 , with a field value given by Ghosh *et al.*⁵⁴ as 0.1 G. A 2015 report by Sumiyama *et al.*⁸⁰ from magnetization measurement detected a field at the 0.01 mG (μT) level, and only for *c*-axis orientation. Their observed signal onset occurred *above* $T_c=2.7$ K, in the 2.7-3.0K temperature region. Sumiyama *et al.* noted that inferred fields in LaNiC_2 are sample dependent. A μ SR study by Sundar

*et al.*⁸¹ on a single crystal showed only a weak depolarization well below T_c .

These variations over samples and techniques emphasize that TRSB signals first, are small and sample dependent, and involve very small inferred fields, and second, TRSB signals need to be weighed against other data. As of this writing, the experimental reports on most of the *fragile magnetic superconductors* listed in Sec. VIII A stand, even while other SC properties are consistent with singlet pairing.

Polar Kerr rotation studies¹⁴⁹ obtained an observable but very small polar Kerr rotation angle for the actinide- and lanthanide-based materials UPT_3 , URu_2Si_2 , UTe_2 , and $\text{Pr}(\text{Os},\text{Ru})_4\text{Sb}_{12}$, suggesting small magnetic fields that might reasonably be expected to reflect *f*-electron contributions, albeit very small ones especially for heavy fermion metals. See Ref. [54] for further references. As described above, the original reports on UTe_2 and Sr_2RuO_4 apparently have been superseded as providing no reproducible TRSB signal.

Three of the above cases are for strongly correlated, heavy fermion SCs, with reported TRSB signals having been questioned by subsequent data. Considering other correlated systems, measurements on two cuprates, where there have been theoretical suggestions¹²⁹ of orbital loop derived magnetic fields, have put upper limits on such a field, which has not been detected. For the cuprate high temperature SCs (80-93 K) $\text{YBa}_2\text{Cu}_3\text{O}_7$ and $\text{Bi}_2\text{Sr}_2\text{CaCu}_2\text{O}_8$, no additional depolarization was detected below T_c .⁸³ It is emphasized however that this paper focuses on weak coupling *fragile magnetic superconductors*, where strong coupling complications and exotic normal state properties are not a factor. The discussions in this section involving strongly correlated electronic systems are included only to point out the sample type and quality dependence of TRSB signals.

B. Summary

This paper has focused on a class of normal Fermi liquid, low T_c , metals that have been identified (primarily) by μSR depolarization data as time-reversal symmetry breaking SCs, against a few others giving negative results. This class has been denoted *fragile magnetic superconductors*, because the inferred magnetization is no more than $10^{-3}\mu_B$ per atom.

A few points can summarize the content.

- Superconducting properties – critical fields, coherence lengths, penetration depth, TRSB signals – should be considered *in toto*¹⁶¹ in contemplating the relevant order parameter. All SCs are initially analyzed as such, and the weakly coupled SCs discussed here have typical singlet SC properties.
- In μSR studies, time reversal symmetry is broken, strictly speaking, when the muon is implanted, with magnetic effect most strongly so near the muon site where the measurement (muon decay) originates.

- Conventional theory, giving a circulating supercurrent around the muon proportional to the muon vector potential, will give rise to a magnetic field in the region of the muon in any superconductor. Quantum theory of the short-range supercurrent remains to be elucidated.

- The spontaneous field, detected primarily by zero-field μSR studies, appears at T_c (occasionally below or above T_c), with a value not far above the limit of detection, and one that seems challenging to estimate theoretically, or to support with known mechanisms.

- With TRSB signals near the lower limit of detection, it is normal that some superconductors with weaker field at the muon will give no detectable signal and thus be classified as conventional, while those with somewhat stronger fields that extend above the detectability limit are designated as TRSB.

- Several systems have shown differences due to sample quality, with some signals disappearing in better quality single crystal samples.

- Calculated T_c of singlet, phonon-pairing SC, in two of the *fragile magnetic superconductors*, LaNiC_2 and LaNiGa_2 , indicate that phonon coupling is sufficient to account for singlet pairing and low T_c .

XIV. ACKNOWLEDGMENTS

I acknowledge important continuing interactions with V. Taufour, N. J. Curro, I. Vishik, and R. R. P. Singh, and helpful references to the literature from J. Autschbach, D. M. Ceperley, and J. Terning.

XV. APPENDICES

A. The fundamental Hamiltonian

1. Electrons and a muon in a lattice

With the muon producing a vector potential \vec{A}^μ in an electron gas, and allowing for a spontaneous vector field \vec{A}^{spn} appearing below T_c , the non-relativistic Hamiltonian for the muon and the conduction electrons is (leav-

ing the subscript e off electron operators)

$$\begin{aligned}
H^{orb} &= \frac{[p_\mu + \frac{e}{c}\vec{A}^{spont}(\vec{r}_\mu)]^2}{2m_\mu} + \sum_{j,s} \frac{[p_{j,s} - \frac{e}{c}\vec{A}(\vec{r}_{j,s})]^2}{2m} \\
&\quad - \sum_{j,s} \frac{e^2}{|\vec{r}_{j,s} - \vec{r}_\mu|} + V^{e-ion} + V^{e-e} \\
&\quad + H^{\mu-ion} + T^{ion} + V^{ion-ion} \\
\vec{A}(\vec{r}) &= \vec{A}^\mu(\vec{r}) + \vec{A}^{spont}(\vec{r}) \\
\vec{A}^\mu(\vec{r}) &= \nabla \times \frac{\vec{\mu}}{r} = \frac{\vec{\mu} \times \vec{r}}{r^3}.
\end{aligned} \tag{15}$$

Several terms are abbreviated with self-evident notation. In an applied field the corresponding vector potential \vec{A}^{ext} would be included in each vector potential term. The electronic terms are to be treated with DFT methods, and the ion kinetic energy T^{ion} vanishes for static atoms. Treating the vector potential accurately in density functional terms requires current density functional theory,¹⁶² which has not been implemented in current codes. Nuclear vector potentials are not displayed here, nor are those of the itinerant electrons which without polarization are presumed to average out, randomly or statistically. Each vector potential field is evaluated at the position of the respective moment. The first term is for the muon, the second is the kinetic energy for all electrons. The muon does not experience its own field. The curl operators provide the magnetic fields that couple to the charges and moments.

Moving to Dirac's relativistic treatment of the kinetic energy operator results in expressions that involve the particle (muon and electrons) spin moments that couple to magnetic fields (other than their own), external or from other particles. The spin-related terms are

$$\begin{aligned}
H^{spin} &= -\mu_B \sum_j \vec{\sigma}_j \cdot \nabla \times (\vec{A}^\mu + \vec{A}^{ind} + \vec{A}^{spont}) \\
&\quad + \vec{\mu} \cdot \nabla \times (\vec{A}^{ind} + \vec{A}^{spont}),
\end{aligned} \tag{16}$$

where $\vec{\sigma}_j$ is the Pauli spin matrix of the j -th electron.

The quadratic term (in \vec{A}^μ) in the kinetic energy operator has the form

$$\begin{aligned}
H^{(2)} &= \frac{e^2}{2mc^2} \vec{A}^2 = \frac{\mu_B^2 \mu^2}{\hbar^2} \frac{(x^2 + y^2)}{r^6} \\
&= \frac{\mu_B \mu^2}{\hbar^2} \left[\frac{\rho^2}{(\rho^2 + z^2)^3} \right].
\end{aligned} \tag{17}$$

The last expression is written in the natural cylindrical coordinates ρ and z , with absence of the polar angle ϕ reflecting the circular symmetry. This term falls off as r^{-4} ; on the other hand, it diverges with a power as r approaches the muon position, becoming worse as z approaches zero; there is however an extra factor of μ . Final effects are apparently negligible and are not addressed in this paper.

The electronic system is first treated, as in Sec. III B, in the jellium picture of constant density: electron-electron

repulsion is compensated by attraction to a smoothed version of the positive ion cores. Extension to band electrons is no problem for our considerations except for complicating equations and subsequent calculations (not done in this paper). The electronic part of this Hamiltonian can be transformed to occupation of states k, s within the Fermi surface, since we deal with systems very near the electronic ground state. The muon, located at the origin of coordinates in most equations, breaks translational invariance.

2. The muon magnetic operator

The linear-in-field term involving the muon in the Hamiltonian simplifies readily. For each electron j, s , and dropping this subscript for simplicity, (\vec{A}^μ is evaluated at $\vec{r}_{j,s}$; $\vec{p} = -i\hbar\nabla$)

$$\begin{aligned}
H_B^\mu &= -\frac{e/c}{2m} [\vec{p} \cdot \vec{A}_\mu + \vec{A}_\mu \cdot \vec{p}] \\
&= \frac{2\mu_B}{\hbar} \vec{A}_\mu \cdot \vec{p},
\end{aligned} \tag{18}$$

using the definition of the Bohr magneton $\mu_B = e\hbar/(2mc)$ and noting that in the divergenceless gauge $[\vec{p} \cdot \vec{A}^\mu]$ vanishes identically. Then the magnetic part of the Hamiltonian becomes (for each electron)

$$\begin{aligned}
H_B^\mu &= \frac{2\mu_B}{\hbar} \vec{A}^\mu \cdot \vec{p} \\
&= \frac{2\mu_B}{\hbar} (-i\hbar) \frac{\mu}{r_3} (-y, x, 0) \cdot (\partial_x, \partial_y, \partial_z) \\
&= -\frac{i\mu_B \mu}{r^3} (-y\partial_x + x\partial_y) \\
&= \frac{\mu}{r^3} \mu_B \frac{L_z}{\hbar} \rightarrow \frac{\mu \mu_B}{\hbar} \left\langle \frac{L_z}{r^3} \right\rangle.
\end{aligned} \tag{19}$$

This expression contains the μ/r^3 factor of \vec{B}^μ (Sec. III) leading to a troublesome radial integral to quantify the perturbation. \vec{L} is the electronic orbital angular momentum operator relative to the muon at the origin. The Hamiltonian thus favors the development of an electronic angular momentum with respect to the muon position. This may produce an orbital magnetic moment, allowed by the broken TRS due to the muon magnetic moment.

The vector potential accompanying the μ^+ magnetic moment, which does not affect the muon that creates it, is conventionally treated, again in the Coulomb gauge $\vec{\nabla} \cdot \vec{A} = 0$, as

$$\vec{A}_\mu(\vec{r}) = \nabla \times \frac{\vec{\mu}}{r} = \frac{\vec{\mu} \times \hat{r}}{r^2} = \frac{\mu}{r^3} (-y, x, 0), \tag{20}$$

a toroidal potential field with a divergence that displays a singularity at the muon site. One first considers the ground state: the muon sits in a stable quadratic potential in its harmonic oscillator ground state with its spin along the z -axis, and the electrons are in, or very near, their ground state.

The dipole magnetic field, from above, is (neglecting the Fermi contact δ -function term⁶⁵)

$$\begin{aligned}\vec{B}_\mu(\vec{r}) &= \nabla \times \vec{A}(\vec{r}) \\ &= \frac{3\hat{r}(\hat{r} \cdot \vec{\mu}) - \vec{\mu}}{r^3} \\ &= \mu \frac{3\hat{r}(z/r) - \hat{z}}{r^3} \\ &= \mu \left(\frac{xz}{r^2}, \frac{yz}{r^2}, \frac{z^2}{r^2} - 1 \right).\end{aligned}\quad (21)$$

Treated as a perturbation, the first order change in energy of an electron in state $\eta_{n\ell m_\ell}(\vec{r})$ in a spherical potential is

$$\begin{aligned}\Delta E &= \langle \eta_{n\ell m_\ell} | \frac{\mu}{r^3} \mu_B \frac{L_z}{\hbar} | \eta_{n\ell m_\ell} \rangle \\ &= \mu \mu_B m_\ell \langle n\ell m_\ell | \frac{1}{r^3} | n\ell m_\ell \rangle \langle \ell m | L_z | \ell m \rangle.\end{aligned}\quad (22)$$

This expression as written is indeterminate for s orbitals: the orbital is finite at the origin so the integral is $\int r^2 dr/r^3$, thus logarithmically divergent if the dr integral is done first. The $m_\ell = 0$ for s orbitals would give a zero result if the angular integral were to be done first and the environment has circular symmetry. For higher ℓ states p, d, f, \dots , the wavefunction is proportional to r^ℓ , thus giving an extra $r^{2\ell}$ factor in the integrand near the origin and a finite integral. Since hyperfine quantities are the topic here, one can note that a similar question arises in a relativistic treatment (Dirac equation), where the $p_{1/2}$ orbital is non-zero at the origin.

A successful treatment of this indeterminate integral was given by Abragam and Bleaney.⁶⁴ Reverting to the relativistic Dirac equation, the integrand for the matrix element (evaluated with the large component of the wavefunction $\gamma(\vec{r})$) was manipulated using the expression $\vec{A} = \nabla \times (\vec{\mu}/r)$. The perturbation term is

$$\frac{\beta}{\hbar} \vec{\sigma} \cdot \langle \gamma | [\vec{A} \times \vec{p} + \vec{p} \times \vec{A}] | \gamma \rangle \quad (23)$$

where β is the 4×4 Dirac β -matrix. The gradient operator operates on the function γ , and $\gamma^* \nabla \gamma$ is one half of the density gradient $\nabla \gamma^* \gamma$. Thus the derivative operator that had non-relativistically resulted in a r^{-3} factor in the denominator has been transferred to the gradient of the (large component) spin current

$$\vec{J}_{\text{spin}} = \nabla \times |\gamma(\vec{r})|^2 \vec{\sigma}, \quad (24)$$

leaving only a r^{-2} factor in the denominator of the integrand, which is regularized by the $r^2 dr$ volume factor. A key factor is the replacement the usual expression of the vector potential by the differential form $\vec{A} = \nabla \times \frac{\vec{\mu}}{r}$. The ground state orbital (above denoted by γ) is asymmetric for a general non-symmetric position of the muon, and will include p, d, \dots symmetry contributions in a spherical expansion. The $s_{1/2}$ - $p_{1/2}$ contribution to the gradient of the spin density will be regularized in the same manner as the diagonal s treated just above, and higher- ℓ contributions will approach zero in a way that the integrals are straightforward and finite.

B. The μ SR experiment

1. The setup: μ^+ + sample

Overviews and reviews of the experiment and analysis were referenced in Sec. I. A synopsis is given here. The μ^+ ion, an elementary particle, decays after production with a half-life of $\tau_\mu = 2.2 \mu\text{s}$, producing a positron (conserving charge) and two neutrinos (one anti-electron type, one muon type, conserving lepton number). Positron emission occurs symmetrically around the direction of the muon spin, but with the variation in angular distribution changing with the energy of the positron. The mass of the muon provides ~ 100 MeV of energy for the decay products, of which the positron carries away 25-50 MeV kinetic energy (its rest mass of 0.5 MeV can be neglected). At the lower end of emission energy, 25 MeV, emission is practically isotropic – at any angle with respect to the muon spin. Toward the higher range of energy ~ 50 MeV, the angular dispersion of emission becomes weighted toward the forward direction (the direction of the μ^+ spin at the time of decay), although with little variation within a cone of $\pm 40^\circ$ of forward. These two distributions are pictured in Fig. 4.

The spin-half moment has the largest quantum uncertainty of its direction (a mathematical concept, if not a physical one, since only s_z is specified). Thus for full polarization $s_z = +1/2$, \vec{s} varies off-vertical by $\sin^{-1}(s_z/|\vec{s}|) = \sin^{-1}(1/\sqrt{3}) \approx 35^\circ$ with random polar angle, a variation that must contribute to the distribution that varies little within the $\sim \pm 40^\circ$ forward cone and increases as depolarization occurs. It is difficult to find this quantum uncertainty of spin direction addressed in the descriptions of analysis.

The direction of emission of the positron, described as predominantly forward (muon s_z direction) at the time of decay, is useful to understand. Decay of the positron along the muon spin direction must take into account quantum spin “direction” mentioned above, and that the emission direction is strongly dependent on the positron kinetic energy E_p . Defining the energy parameter $\zeta = E_p/m_\mu c^2$, denoting the fractional polarization at time of decay as P_μ , and using θ as the angle between spin at decay relative to the initial polarization, the decay distribution from the quantum field theory of particles according to Bayes is¹⁶³

$$\begin{aligned}\frac{d^2\Gamma}{d\zeta d\cos\theta} &\propto \zeta^2 \left[(3 - 3\zeta) + \frac{2}{3} \rho (4\zeta - 3) + 3\eta \zeta_o \frac{1 - \zeta}{\zeta} \right. \\ &\quad \left. + P_\mu \xi \cos\theta [(1 - \zeta) + \frac{2}{3} \delta (4\zeta - 3)] \right].\end{aligned}\quad (25)$$

The constants are Standard Model parameters, calculated by Michel^{164,165} to be $\rho = \delta = \frac{3}{4}$, $\xi = 1$, $\eta = 0$. There is no reason here to try to fully comprehend this distribution, the point is that it is a necessary Standard Model result and there has not yet been any known violation of the SM. These calculated values have been verified experimentally¹⁶⁶ within very tight uncertainties, and considerably simplify the expression.

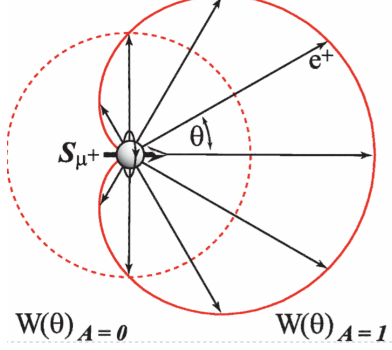


FIG. 4. Angular distribution of the direction of emission of the positron upon muon decay into a positron and two neutrinos, given by $W(\theta) \propto 1 + A \cos \theta$. The factor A depends on the energy of the emitted positron. Two positron energies are pictured: dashed line, 25 MeV near minimum, $A \approx 0$; full red line, 50 MeV near maximum, $A \approx 1$. The arrow denotes the muon polarization direction upon decay. For reference: the rest mass of the muon is 207×0.511 MeV ~ 100 MeV, which is what is available for the decay products. See text for further discussion.

Measurements of counts and angles by an array of detectors enables collection of counts versus time that contains the information on depolarization. Typical solid state processes are orders of magnitude quicker than the μ^+ lifetime, thus allowing accumulation of data representative of the muon within an electronic system in its thermodynamic state at temperature T and time t after deposition.

The direction of the muon polarization defines our z direction. The muon's spin is associated with a point magnetic dipole μ at the muon site, in a favorable interstitial stopping site, away from positive atomic cores, and in metals not pictured as being bonded with an atom.

The muon is like the much studied proton interstitial, but with smaller mass and larger moment. Takada, Maezono, Yoshizawa¹⁷⁰ have studied, with density functional methods supplemented by diffusion Monte Carlo calculations, the case of a proton in an electron gas from high density, where the system becomes that of a proton mixing with and screened by electrons, to the low density regime where the proton attracts an extra electron to become an H^- ion favored by the filling of the $1s$ shell. The intermediate regime includes the Kondo effect. Takada *et al.* did not consider explicitly the vector potential of the proton. The discussion in this paper is confined to intermetallic metals with typical metallic densities; semimetals and insulators require their own treatment.

2. The data and analysis

Typically presented from zero-field studies is the rate of depolarization $\sigma(T)$. Above T_c there is a normal state temperature independent depolarization from small quasi-static nuclear moment fields and from larger fluctuating magnetic fields at a continuum of distances and

with random directions of moments. These are observed to average to some constant rate above T_c . Below T_c in materials identified with TRSB, the rate increases with decreasing temperature to a value as $T \rightarrow 0$ that is $\sim 3\text{--}10\%$ above the normal state value. $\sigma(T = 0) - \sigma(T)$ is interpreted in terms of depolarization arising from a field at the muon site, with the simplest interpretation being that it arises from a spontaneously appearing uniform magnetic field.

The key result in zero-field experiments is the time development (relaxation) of the muon moment polarization, followed by the process of muon decay. Distinctions may be required for the two types of muon beams: continuous wave (CW), at the Paul Scherrer Institute (Switzerland) and TRIUMF (Canada), and pulsed, at ISIS (U.K.) and KEK (Japan),³² but these distinctions will not be of interest here.

Theories of the depolarization process have been presented at a few levels over time, of which three are mentioned here. Very often the 1967 Kubo-Toyabe functional form,¹⁷¹ which takes into account a stochastic depolarization field and anisotropy, is adopted as a first step in the process to fit the depolarization data and extract materials properties. The Kubo-Toyabe form gives the polarization distribution G^{KT} versus time as

$$\begin{aligned} A(t) &= A_0 G_z^{KT}(t) e^{\lambda_{ZF} t}, \\ G_z^{KT}(t) &= \frac{1}{3} + \frac{2}{3} (-\sigma^2 t^2) e^{-\sigma^2 t^2/2}, \end{aligned} \quad (26)$$

where $\sigma = \gamma \Delta$ in terms of an isotropic Gaussian distribution width Δ and the muon gyromagnetic ratio $\gamma = 2\pi \times 13.55$ kHz/G. This form is used to fit data in many μ SR papers. The asymmetry data is provided by

$$A^{expt}(t) = \frac{N_F(t) - \alpha N_B(t)}{N_F(t) + \alpha N_B(t)}, \quad (27)$$

where N_F and N_B are the time histograms of the temporal dependence of the decay positron count rate in the forward and backward detectors and α is an apparatus dependent calibration constant. Schematic illustrations of $F(t)$ and $B(t)$ were provided by Blundell.³²

Another expression for analysis was included in the Topical Review of Ghosh *et al.*⁵⁴ The polarization function is given by a generalized Lorentzian and Gaussian Kubo-Toyabe form used for fit to data is

$$A(t) = \frac{1}{3} A_0 + \frac{2}{3} (1 - \sigma_{ZF}^2 t^2 - \lambda_{ZF}) e^{-\frac{\sigma_{ZF}^2 t^2}{2} - \lambda_{ZF} t} \quad (28)$$

where A_0 is the initial asymmetry and ZF indicates a zero field value.

The cases of LaNiGa_2 ($T_c=2\text{K}$) and LaNiC_2 ($T_c=2.7\text{K}$) provide interesting insight into analysis. According to Ghosh *et al.*⁵⁴ evidence for TRSB occurs due to increase in σ below T_c , but sometimes appears as a change of λ_{ZF} below T_c . For LaNiGa_2 the change occurred in σ whereas for LaNiC_2 the change appeared in

λ_{ZF} . Both have been included in the list of TRSB superconductors. TRSB was also indicated by direct magnetization measurement on single crystal LaNiC₂, where a field was detected but only at the 0.01 mG (10^{-9} T) level, and oriented along the c axis.⁸⁰ The field onset occurred above $T_c=2.7$ K, in the 2.7-3.0K temperature region.

Kornilov and Pomjakushin¹⁷² in 1991 extended the theory to include randomly-directed field with δ -function strength H_o (possibly modeling a polycrystalline sample) as well as the Gaussian distribution. The analytic expression they obtained was

$$G_z^{KP}(t) = \frac{1}{3} + \frac{2}{3} \left[1 + \frac{\sigma^2 t^2}{\omega} \right] e^{-\sigma^2 t^2/2} \times \left[\cos \omega t + \tan^{-1} \frac{\sigma^2 t}{\omega} \right]. \quad (29)$$

This formula introduces a frequency $\omega = \gamma H_o$, and plots of the difference from G_z^{KT} versus σt were presented.

A recent (2020) description has been given by Takahashi and Tanimura¹⁷³ that is said to consist of a more fully quantum derivation, and includes the thermal bath of vibrations and spins, hence giving a T-dependent expression resulting from their hierarchical equation of motion method. The result requires numerical solution and fitting of several parameters, hence the identification of a specific field value from experimental data is less direct.

An aside from the Standard Model. The direction of emission of the positron, described as primarily forward along the muon polarization direction at the time of decay, is more interesting, being dependent on the positron kinetic energy E_p . Defining the energy parameter $\zeta = E_p/m_\mu c^2$, denoting the fractional polarization at time of decay as P_μ , and using θ as the angle between spin at decay relative to the initial polarization, Bayes provided the decay distribution from the quantum field theory of particles as¹⁶³

$$\frac{d^2\Gamma}{d\zeta d\cos\theta} \propto \zeta^2 \left[(3 - 3\zeta) + \frac{2}{3}\rho(4\zeta - 3) + 3\eta\zeta_o \frac{1 - \zeta}{\zeta} + P_\mu \xi \cos\theta [(1 - \zeta) + \frac{2}{3}\delta(4\zeta - 3)] \right]. \quad (30)$$

The constants are Standard Model parameters, calculated by Michel^{164,165} to be $\rho = \delta = \frac{3}{4}$, $\xi = 1$, $\eta = 0$. There is no reason here to try to understand this distribution, the point is that it is a necessary Standard Model result and there has not yet been any known violation of the SM. These calculated values have been verified experimentally,¹⁶⁶ and considerably simplify the expression.

C. Symmetry of the dipolar field

The point dipole of the muon corresponds to an axial vector potential, given here in the divergenceless gauge,

and corresponding magnetic field, for $\vec{\mu}=\mu\hat{z}$,

$$\begin{aligned} \vec{A}^\mu(\vec{r}) &= \frac{\vec{\mu} \times \hat{r}}{r^2} = \frac{\mu}{r^3} (-y, x, 0) \\ \vec{B}_{tot}^\mu(\vec{r}) &= \nabla \times \vec{A}_\mu(\vec{r}) = \frac{3\hat{r}(\hat{r} \cdot \vec{\mu}) - \vec{\mu}}{r^3} + \frac{8\pi}{3} \mu \delta(\vec{r}) \\ &= \vec{B}_{dip}^\mu + \vec{B}_{con}^\mu \end{aligned} \quad (31)$$

with dipole and contact terms.

The gauge independent magnetic field $\vec{B}^\mu(\vec{r}) = \nabla \times \vec{A}_\mu(\vec{r})$ is given by the textbook expression with the moment taken as the \hat{z} direction, and with the result given in various useful coordinates,

$$\begin{aligned} \vec{B}^\mu(\vec{r}) &= \frac{3\hat{r}(\hat{r} \cdot \vec{\mu}) - \vec{\mu}}{r^3} \\ &= \mu \frac{3\hat{r}(z/r) - \hat{z}}{r^3} \\ &= \frac{\mu}{r^3} \left(3\frac{xz}{r^2}, 3\frac{yz}{r^2}, 3\frac{z^2}{r^2} - 1 \right) \\ &= \frac{3\mu}{r^3} \left(\sin\theta \cos\theta \cos\phi, \sin\theta \cos\theta \sin\phi, \right. \\ &\quad \left. \cos^2\theta - \frac{1}{3} \right) \\ &= \frac{3\mu}{r^3} \left[\frac{2}{3} \cos\theta \hat{r} + \frac{1}{3} \sin\theta \hat{\theta} \right] \\ &\equiv \frac{3\mu}{r^3} f(\theta, \phi), \end{aligned} \quad (32)$$

where $|f(\theta, \phi)| \leq 1$ is the angular variation. The δ -function term (Fermi contact term) of the dipole field $(8\pi/3)\mu\hat{z}\delta(\vec{r})$ is, with relativistic extensions, finite but with small expectation value for low nuclear charge.⁶⁵ These different forms of the common point dipole expression, including the one in polar coordinates, are useful for following symmetry considerations. Units are cgs-gaussian as used in Jackson's classic textbook on classical electrodynamics.¹⁶⁷

The system symmetry of the dipolar magnetic field $\vec{B}(x, y, z)$ includes the following:

- for $x \rightarrow -x$ the x -component changes sign, and analogously for the y -component (cylindrical symmetry),
- the cylindrical symmetry gives

$$\sqrt{B_x^{\mu 2} + B_y^{\mu 2}} = 3\mu |\sin\theta \cos\theta|/r^3 \quad (33)$$

independent of ϕ . Only the z -component is non-zero along the axis and in the x - y plane

- the z -component is invariant under z -reflection, the x and y components reverse under z -reflection
- there is inversion symmetry: $B^\mu(-\vec{r}) = B^\mu(\vec{r})$. A consequence is that the HEG+ μ^+ system, introduced in Sec. III B, has this same axial symmetry.

D. Field at μ^+ site arising from magnetic polarization

1. Classical treatment

Magnetic polarization to an applied (“external”) field is usually treated in the quasiclassical approximation of spin up versus spin down. However, each electron has its own vector potential arising from its Bohr magneton magnetic moment, which in the electron gas is commonly averaged out. The effect can be modeled as follows. Each volume element of electron moment $\vec{M}^{ind}(\vec{r})\Delta V$ will produce from its magnetic moment the same form of dipole field $\vec{B}^\mu(\vec{r}')\Delta V$ from the magnetization from \vec{r}' via $\chi_p \vec{B}^\mu(\vec{r}')$ as given by the dipole expression, except that the original origin $\vec{0}$ will be assumed by \vec{r} and the position of a given field point will be \vec{r}' .

Then

$$\vec{B}(\vec{r}') = \int d^3r \frac{3(\widehat{r'-r})\vec{M}^{ind}(\vec{r}) \cdot (\widehat{r'-r}) - \vec{M}^{ind}(\vec{r}' - \vec{r})}{|r'-r|^3}.$$

Simplification occurs because we are only interested in the field at the muon site, *i.e.* at $\vec{r}' \rightarrow 0$, so $\widehat{r'-r} \rightarrow -\hat{r}$. Note: $\hat{z} = (0, 0, 1)$ is a direction and remains unchanged. Then by change of coordinates

$$\begin{aligned} \vec{B}(0) &= \int d^3r \frac{3(-\hat{r})\vec{M}^{ind}(\vec{r}) \cdot (-\hat{r}) - \vec{M}^{ind}(\vec{r})}{r^3} \\ &= \int d^3r \frac{3\hat{r}\vec{M}^{ind}(\vec{r}) \cdot \hat{r} - \vec{M}^{ind}(\vec{r})}{r^3}. \end{aligned} \quad (34)$$

By cylindrical symmetry (of the assumed HEG) only need the z -component of the field is non-zero. The dot product in Eq. 34

$$\begin{aligned} \vec{M}^{ind}(\vec{r}) \cdot \hat{r} &= \chi_p(r) \vec{B}_\mu(\vec{r}) \cdot \hat{r} \\ &= \chi_p(r) \frac{\mu}{r^3} (3\frac{xz}{r^2}, 3\frac{yz}{r^2}, 3\frac{z^2}{r^2} - 1) \cdot (x, y, z)/r \\ &= \chi_p(r) \frac{\mu}{r^3} \left[(3\frac{x^2}{r^2} + 3\frac{y^2}{r^2}) + (3\frac{z^2}{r^2} - 1) \right] \frac{z}{r} \\ &= \chi_p(r) \frac{2\mu z}{r^3} = \chi_p(r) \frac{2\mu \cos \theta}{r^3}. \\ \frac{3}{r} \frac{z}{r} [\vec{M}^{ind}(\vec{r}) \cdot \hat{r}] &= \frac{\mu}{r^3} \chi_p(r) = \mu \frac{6z^2}{r^2}. \end{aligned} \quad (35)$$

This result is non-negative, positive along the \hat{z} -axis and vanishing in the x - y plane. It is worthy of note that the x and y dependence has dropped out of the dot product of two vectors depending (apparently) independently on \vec{r} , again an effect of symmetry.

After subtracting off the $M_z^{ind}(\vec{r})$ term in the dipolar field that is large along the \hat{z} -axis, negative in the x - y plane, the z -component of $\vec{B}(0)$ involves some cancellation: the ‘incoming’ dipolar field from the muon is interfered with by the ‘outgoing’ dipolar fields from each

point \vec{r} . The result becomes

$$\begin{aligned} B_z(0) &= \int d^3r \chi_p(r) \left[\frac{3z}{r} \left(\frac{2\mu z}{r^3} \right) - \frac{\mu}{r^3} (3\frac{z^2}{r^2} - 1) \right] / r^3 \\ &= \mu \int d^3r \chi_p(r) \left[6\frac{z^2}{r^2} - (3\frac{z^2}{r^2} - 1) \right] / r^6 \\ &= \mu \int r^2 dr d\nu d\phi \chi_p(r) \left[3\frac{z^2}{r^2} + 1 \right] / r^6 \\ &= 8\pi\mu \int \chi_p(r) \frac{dr}{r^4}, \end{aligned} \quad (36)$$

leaving, at this level of discussion, a divergent field at the muon site. The strong small- r divergence is startling, but at small r non-linear response (substituting for χ_p) and quantum effects require reconsideration. Discussion of the resolution of this unphysical result is given in Sec. V.

2. Operator representation for induced B -field

The magnetic field of the muon, with magnetization $\vec{M}^\mu(\vec{r}) = \vec{\mu}_\mu \delta(\vec{r})$, gives rise to the well known dipolar magnetic field in Appendix XV C. The linear relationship suggests the definition of an integral “dipolar operator” $\mathcal{D}(\vec{r} - \vec{r}')$ by

$$\begin{aligned} \vec{B}(\vec{r}) &= \int d\vec{r}' \mathcal{D}(\vec{r}, \vec{r}') \vec{M}(\vec{r}') \\ &= \int d\vec{r}' \frac{3 \widehat{\vec{r} - \vec{r}'} [\widehat{\vec{r} - \vec{r}'} \cdot \vec{M}(\vec{r}')] - \vec{M}(\vec{r}')} {|\vec{r} - \vec{r}'|^3}, \end{aligned} \quad (37)$$

which gives the magnetic field $\vec{B}(\vec{r}')$ due to any magnetization field $\vec{M}(\vec{r}')$. Applying this to the z -oriented μ^+ point magnetic moment gives Eq. 32 and is visualized in Fig. 1.

The field

$$\vec{B}^\mu(\vec{r}) = \int d\vec{r}' \mathcal{D}(\vec{r}, \vec{r}') \vec{\mu} \delta(\vec{r}'); \quad \vec{B}^\mu = \mathcal{D} \vec{M}^\mu, \quad (38)$$

polarizes the electron density according to the susceptibility χ_p , $\vec{M}^{ind}(\vec{r}) = \chi_p(n(\vec{r})) \vec{B}_\mu(\vec{r})$ [in operator notation $M^{ind} = \chi_p B^\mu$]. This electronic magnetization (excess of \uparrow moments over \downarrow) gives rise to its own magnetic field which becomes, in terms of the dipole operator

$$\begin{aligned} \vec{B}^{ind} &= \mathcal{D} \vec{M}^{ind} = \mathcal{D} \chi_p \vec{B}^\mu = \mathcal{D} \chi_p \mathcal{D} \vec{M}^\mu; \\ \vec{B}^{ind}(\vec{r}) &= \int d^3r' \int d^3r'' \mathcal{D}(\vec{r}, \vec{r}') \\ &\quad \times \chi_p(n(\vec{r}')) \mathcal{D}(\vec{r}', \vec{r}'') \vec{M}^\mu(\vec{r}'') \\ \vec{B}^{ind} &= \mathcal{D} \chi_p \mathcal{D} \vec{M}^\mu. \end{aligned} \quad (39)$$

There are two important simplifications. First, for connecting to μ SR data we want only the on-site $\vec{r} = 0$ field. Second, the original field arose from the point muon $\vec{r}' = 0$, which removes the second integral. In addition,

$n(\vec{r})$ varies smoothly by a factor of two or less in an interstitial site in a metallic compound, and $\chi_p(n)$ is a regular and moderately varying function of n ,⁶⁰ so we pull a representative value $\bar{\chi}_p$ out of the integral. This leaves

$$\vec{B}^{ind}(0) \approx \bar{\chi}_p \int d^3r' \mathcal{D}(0, \vec{r}') \mathcal{D}(\vec{r}', 0) \vec{\mu}. \quad (40)$$

This integral has the look of $\bar{\chi}_p < \mathcal{D}^2 > \vec{\mu}$, and indeed $\mathcal{D}(-\vec{r}) = \mathcal{D}(\vec{r})$ bears out this positive integrand.

The magnetization $M^{ind}(\vec{r})$ operated on by the dipolar operator $\mathcal{D}(0, \vec{r}')$ gives the induced magnetic field. Simplifying the integration variable to cylindrical coordinates with z -component of $\hat{r} = z/r$:

$$\begin{aligned} \vec{B}^{ind}(0) &= \bar{\chi}_p \int d^3r \frac{1}{r^3} [3\hat{r} \cdot \left(\frac{3\hat{r}(\hat{r} \cdot (\vec{\mu}) - \vec{\mu})}{r^3} \right) \\ &\quad - \frac{3\hat{r}(\hat{r} \cdot \vec{\mu}) - \vec{\mu}}{r^3}] \\ &= \mu \bar{\chi}_p \int \frac{d^3r}{r^6} 3\hat{r} \left[3\frac{z}{r} - \frac{z}{r} \right] - [3\hat{r} \frac{z}{r} - 1]. \end{aligned} \quad (41)$$

The z -component is

$$\begin{aligned} B_z^{ind}(0) &= \mu \bar{\chi}_p \int \frac{d^3r}{r^6} \left[9\frac{z^2}{r^2} - 3\frac{z^2}{r^2} \right] - [3\frac{z^2}{r^2} - 1] \\ &= \mu \bar{\chi}_p \int_0^\infty \frac{2\pi r^2 dr}{r^6} \int_{-1}^{+1} d\nu (3\nu^2 + 1), \end{aligned} \quad (42)$$

using cylindrical coordinates ($\nu = \cos\theta$). This procedure reproduces the more direct result of Appendix XVD, a divergent integral that must be regularized by quantum or relativistic near-field effects. All of this is complicated by the zero point uncertainty of the muon position, discussed in the next section.

E. Quantum uncertainty of the muon

The infrared divergence of the integral Eq. 42 for the self-induced field at the muon site is daunting and unphysical. Additional factors must be entering the physics. An obvious one is zero-point uncertainty (ZPU) of the muon position, commonly and inaccurately called zero-point motion. While the harmonic oscillator ground state (harmonic phonon) already contains an uncertainty, interstitial protons in crystals are known to encounter larger ZPU and anharmonicity, and the factor of nine lighter muon will be even more anharmonic with larger ZPU. This effect has been calculated to impact the ground state interstitial position of the muon.⁵² Obviously this effect cannot be treated in a HEG model, and various levels of treatment have been applied.

Classical treatment of the muon. The first step in determination of its equilibrium position is to treat the muon as a classical particle. DFT codes can readily calculate the energy of a muon in an interstitial position in the lattice, requiring the relaxation of a few shells of atoms for each position of the muon. The muon is

simply an additional (small mass) nucleus, experiencing the Hartree potential of the surrounding atoms and electrons. After calculating a set of energies (for chosen positions), they can be fit to a smooth function to accelerate zeroing-in to the equilibrium muon position, which is at the bottom of the locally quadratic potential function. Finding the correct muon site has been found to affect some properties that are measured by other μ SR experiments.^{37,38,52} The displacement of neighboring atoms by the muon can be up to several tenths of \AA . With the positions given, one can obtain the magnetization resulting from the muon's magnetic field, modulo the quantum and high field effects discussed in Sec. V that require more effort.

Quantum nature of the muon. Anharmonicity and ZPU are known to be substantial – even crucial, as in the inverse isotope shift of the superconducting critical temperature⁴⁰ in PdH – and with the lighter mass of the muon by a factor of nine, anharmonic and ZPU effects can be expected to be roughly a factor of three larger (square root of the mass) than for an interstitial proton. Both of these effects relate to the large displacement, or range of uncertainty, so they are often studied effectively together. The range of ZPU from the potential minimum, plus the behavior of the potential function around the minimum, give a measure of the importance of both effects.

There are various ways to address these effects, of which we mention two, ultimately at two different levels of treatment. The stochastic self-consistent harmonic approximation (SSCHA) addresses both anharmonicity and ZPU of the light atom, with classical treatment of the host lattice⁴¹ (this latter approximation makes it more straightforward to obtain ‘effective’ harmonic frequencies and eigenvectors). Beginning with the static lattice and its derivatives (giving forces) with fixed pressure and obtained from DFT, the derived free energy is minimized with respect of all the position coordinates, thermal fluctuations, and quantum uncertainty. Optimization of the functional leads not only to the target free energy but produces renormalized (effective harmonic or quasi-harmonic) phonons that can be used in transport (viz. superconducting properties) and spectroscopic calculations.

This method has been applied to the near-room-temperature superconductor LaH_{10} , finding several quantitative, and sometimes qualitative, corrections⁴² to the standard (classical muon) DFT and harmonic Eliashberg theory results, including quantum stabilization of the cubic structure to lower temperature in agreement with experiment, and generally extending the range of crystal stability of materials predicted to be unstable due to their very strong electron-phonon coupling.^{42,43} For SH_3 , quantum effects similarly stabilize the high symmetry structure and corrects its pressure-temperature phase diagram substantially, and provides the large isotope shifts observed experimentally.⁴³ With the electronic density now depending on a (using semiclassical language) ‘diffuse muon charge’ rather than the usual

classical point charge, there is still a piece of the full loop to be filled in, where this change is taken into account.

Quantum nuclei of the crystal lattice. A different approach was used by Gomilsek *et al.*³⁹, combining DFT and path integral molecular dynamics (DFT+PIMD). The application was to a muon in the N₂ crystal, with emphasis on quadrupolar resonance frequencies and parameters rather than electron-phonon coupling and vibrational properties. The method incorporates quantum nitrogen nuclei, and DFT+PIMD obtains some degree of muon-N quantum entanglement, *i.e.* there is zero-point correlation between their positions. Energies are provided by DFT for each position of muon and nitrogen nuclei within a supercell to guide the Monte Carlo path integral. As in other methods, electrons are treated in Born-Oppenheimer approximation. It could be an opportune time to address how the ZPU of the muon effects the magnetic field experienced by the electrons (not treated in this method).

Relative to the equilibrium position of the muon, the ground state wavefunction at small r is of the form of an (anisotropic) harmonic oscillator (HO) orbital, falling off roughly as $\Psi(r) = C \exp(-\alpha r^2/2)$, where α is an inverse mean square displacement and C is a normalization constant, then decreasing more slowly over longer range. The expectation of the magnetic field at the muon site in this state includes a small r integrand of the form

$$\int d^3r \Psi(\vec{r}) \vec{B}^\mu(\vec{r}) \Psi(\vec{r}) \sim G\mu \int_0 r^2 \frac{e^{-\alpha r^2}}{r^3} dr \sim \int_0 \frac{dr}{r}, \quad (43)$$

where G is a factor from angular integration and the small r form has been given in the last expression. The divergence is reduced by the small phase space at small r , making the integral more mildly infrared divergent. Anisotropy of the HO potential will not reduce this remaining infrared divergence, which will be regularized by a many-body treatment of the high field region and quantum corrections in the near-field, as discussed in Sec. V.

F. Supercurrent: three theories

There has been a progression of theory of the supercurrent, each providing a linear relation between \vec{J}^s and an applied vector potential \vec{A} , necessary to account for the Meissner effect. They differ substantially following progress in condensed matter theory. Only the final expressions will be given here, the first two are textbook material, the third follows from BCS theory. Each assumes a properly gauged vector potential. a somewhat more expanded discussion is provided in Ref. [71].

London theory. For an inhomogeneous magnetic field, the London brothers obtained the relation⁴⁶

$$\vec{J}^s(\vec{r}, T) = -\frac{4\pi}{\lambda_L^2(T)} \vec{A}(\vec{r}), \quad (44)$$

$$\frac{c^2}{\lambda_L^2} = 4\pi e^2 \frac{n_s}{m}, \quad (45)$$

where a superelectron density n_s and mass m were unspecified properties (and were later put into electronic structure expressions¹⁶⁸). This is a simple, local and temperature dependent, proportionality. This expression arises from (in addition to characteristics of a SC) screening by a charged plasma, with material-dependent London penetration depth $\lambda_L(T)$. Supposing m is of the order of the free electron value, and choosing Nb as an example – it is a borderline Type I - Type II SC, with bcc lattice constant of 3.3 Å and the accepted penetration depth of $\lambda^{Nb} \approx 47\text{nm}$ – its London superfluid density is $\lambda_L^{Nb} \sim 5 \times 10^{-7}$ electron/atom. Type II SCs have penetration depths 1-2 orders of magnitude larger, and $n_s \propto \lambda^{-2}$ will give even smaller values of superfluid densities (see Ref. (71) for further investigation of this question). Nevertheless, the London expression remains in the minds and the publications of many researchers.

Ginzburg-Landau theory. Following from a Landau free energy functional involving a complex order parameter Ψ , (not to be confused with a manybody wavefunction) later established to be proportional to the SC gap. The Ginzburg-Landau result⁴⁸ was

$$\begin{aligned} \vec{J}_{GL}^s(\vec{r}, T) = & \frac{-ie^*\hbar}{2m^*} \text{Re}[\Psi^*(\vec{r}, T) \nabla \Psi(\vec{r}, T)] \\ & - \frac{(e^*)^2}{m^* c} |\Psi(\vec{r}, T)|^2 \vec{A}(\vec{r}). \end{aligned} \quad (46)$$

Later developments identified $e^* = 2e$ as the charge of a Cooper pair, $|\Psi|^2$ related to the density of Cooper pairs, and m^* being the Cooper pair mass. The last term is a London-like expression of a material dependent quantity times $\vec{A}(\vec{r})$, however this generalized “penetration depth” is position as well as temperature dependent. There is in addition a new term involving the gradient of the order parameter, which easily simplifies⁹³ to the gradient of the phase of Ψ . This equation must be solved self-consistently with one for Ψ and typically involves boundary conditions. Within Ginzburg-Landau theory, Ashcroft and Krusch found⁷² that for a δ -function magnetic impurity in a Type II SC and within a range of model parameters, a localized *magnetic* impurity behaves similarly to a magnetic vortex, the two being related by a gauge transformation in their model.

BCS theory. This revolutionary theory established that SC is a low energy property of a fermionic system, with transport and thermodynamic phenomena involving only dynamically available carriers within $\sim \pm k_B T$ of the Fermi surface in the normal state, or within a few times the gap 2Δ in the SC state. F. London had earlier discarded his phenomenological parameters n_s and m , instead incorporating the language of Fermi surfaces and velocities into the theory of the penetration depth.¹⁶⁸ Chandrasekhar and Einzel¹⁶⁹ derived the corresponding relation from BCS theory,⁴⁷ obtaining a tensor with diagonal terms for orthorhombic and higher symmetry struc-

tures (j is a Cartesian index)

$$\begin{aligned}\vec{J}_{BCS,j}^s(\vec{r}, T) &= -\frac{e^2}{c} \sum_k \left[-\frac{\partial n_k}{\partial \varepsilon_k} + \frac{\partial f(E_k)}{\partial E_k} \right] \vec{v}_{k,j}^2 \vec{A}_j(\vec{r}) \\ &\rightarrow -\frac{e^2}{c} N(0) v_{F,j}^2 \\ &\times \left[1 - 2 \int_{\Delta}^{\infty} \left[-\frac{\partial f(E)}{\partial E} \right] \frac{E dE}{(E^2 - \Delta^2)^{1/2}} \right] \vec{A}_j, \\ \vec{J}_{BCS}(\vec{r}, T) &= -\frac{4\pi}{\lambda_{BCS}^2(T)} \vec{A}_j(\vec{r}).\end{aligned}\quad (47)$$

where the last expressions are for an isotropic gap $\Delta(T)$ (obtained from BCS theory) and applies to orthorhombic or higher symmetry crystals. In this expression $E_k = \sqrt{\varepsilon_k^2 + \Delta(T)^2}$ is the energy of an excited quasiparticle in state k , ε_k is the normal state electron energy, $f(E)$ is the Fermi distribution, and n_k is the single particle state occupancy. This expression gives a substantially different picture of the response to \vec{A} : the first term is a T-independent diamagnetic current similar in form to the London counterpart, and the second term is a paramagnetic current from the excited quasiparticles, which is zero at $T=0$ and grows to cancel the diamagnetic current at T_c .

This expression also differs by involving definitions of the constants in terms of materials properties: the Fermi level density of states $N(0)$ (the measure of available dynamic electrons) and the Fermi velocity v_F (the speed of response). The T-dependence arises from that of the gap $2\Delta(T)$, also given by BCS theory. This BCS expression holds for the uniform bulk, thus with no \vec{r} dependence. Usadel theory^{92,93} based on averaged Gor'kov Green's functions provides a generalization of SC theory to cases where the gap $2\Delta(\vec{r}, T)$ is position dependent due to disorder, fields, or boundaries. A general introspection into supercurrents in SCs was provided by Koizumi and Ishikawa.⁹⁴ While the aspect of a background degenerate fermion system was not taken into account, this work gives vivid impression of the complexity of the supercurrent problem, and should be useful for further considerations.

G. Kondo impurity in an exotic superconductor

This appendix follows from Sec. X, providing an example of a Kondo impurity within an exotic order parameter state in a spherical model. The question of impurity-induced magnetic fields in unconventional SCs was addressed by Choi and Muzikar,¹⁰⁴ taking an OP of the 3He A -phase as an example: $\Delta(\hat{k}) = (\hat{k}_x + i\hat{k}_y)\Delta_o$, with orbital angular momentum character of $+\hbar$. This order parameter describes an internal orbital momentum of the pair characterized by symmetry as ‘ferromagnetic,’ and the resulting supercurrents produce a magnetic field at the impurity site. Taking parameters thought at that early time to be characteristic of $YBa_2Cu_3O_7$, but with sizable uncertainty, they estimated the emergent field.

The Choi-Muzikar approximation in general form for the on-site impurity magnetic field was

$$B(0) = -\hat{z}\beta(T)(ek_F^2) \left(\frac{T_c}{T_F} \right)^2 \frac{v_F}{c} (\sigma k_F^2). \quad (48)$$

This result is expressed in nearly-free electron language, hence involving generic parameters. Here $\beta(T)$ is a numerical factor that varies between zero and unity, ek_F^2 is a field value expected to be of order 10^2 T,¹⁰⁴ T_F is the Fermi temperature of the order of 5×10^4 K for a large multisheeted Fermi surface metal ($E_F \sim 4 - 5$ eV), $v_F \sim c/300$ for good metals, and σ is the impurity cross-section for which σk_F^2 is expected to be of the order of unity. For this set of parameters they estimated the field as roughly 10^{-3} G.

H. YSR states in real materials

Computational developments in treating defects (large unit cells in DFT) and in modeling the Bogoliubov-de Gennes (BdG) band structure of real superconductors has substantially extended the understanding of the spectra and energetics of YSR states in actual materials. Extending scanning tunneling methods to the study of magnetic atoms or molecules on superconductor surfaces has provided direct evidence of the behavior caused by YSR states.⁷³

The extension of the multiple scattering method (KKR: Korringa, Kohn, Rostoker) to handle very large unit cells opened up the study of truly isolated impurities. Similar extensions of band theory to the superconducting state – the gap, BdG quasiparticle spectrum – for actual materials has played an important role in furthering understanding.¹¹⁵ These methods have enabled the study of YSR states, with real atomic moments in (or on the surface of) materials being studied in labs. The chosen SCs include the second discovered SC (Pb, $T_c=7$ K) and the best elemental SC (Nb, $T_c=9.2$ K) and a possibly unconventional SC, NbSe. Fe, with its large and very well studied moment, provides the preferred magnetic atom. Rare earth atoms, with their larger but more local moments, also invite attention. At present, applications incorporate phenomenological attractive pair potentials to simulate the SC state of the host.

DFT methods and applications to the nominally non-magnetic N impurity in Nb have been described by Saunderson *et al.*,¹¹⁵ who studied the effect on the gap and the excitation spectrum above the gap. Park *et al.*¹⁷⁴ studied the spectrum, including a zero bias peak, for a magnetic impurity (Mn, Fe, Co) in the *s*-wave SC Pb ($T_c=7$ K). The atomic 3d series embedded in Pb was studied by Ruessmann *et al.*¹⁷⁵, who obtained strong magnetic-SC coupling and orbital splitting of a number of gap states (or resonances), sometimes extending across most of the gap. Spin-orbit coupling was shown to have a strong effect on the spectrum, as spin-orbit splittings are much larger than the gap of ~ 2.5 meV. For the Fe impurity the gap is essentially closed, *i.e.* SC order is effectively

quenched in the vicinity of the impurity. Topological SC was brought into study by Chiu and Wang,¹⁷⁶ who analyzed the system Fe on Fe(Te,Se) with their topological Z_2 bands. Their study indicated that the topological character of the bulk becomes reflected in new behavior of the surface YSR states.

Several groups have reported spectroscopic studies, including YSR states, on SC surfaces decorated with magnetic entities.¹⁷⁷⁻¹⁸⁰ The orbital structure of YSR states resulting from Cr atoms on SC Pb(111) was reported by Choi *et al.*¹⁷⁷, who found that the Cr-derived YSR resonances extended across much of the gap but left a pseudogap of low DOS around mid-gap ($\Delta = 2.7$ meV). Xia *et al.*¹⁷⁹ studied YSR states of a Kondo molecular magnet Tb₂Pc₃ layer on the Pb(111) surface.

I. LaNiGa₂ material parameters, energy scales

The choice here is a representative case: the topological superconductor LaNiGa₂ (orthorhombic, *Cmcm*), $a = 4.29\text{\AA}$, $b = 17.83\text{\AA}$, $c = 4.27\text{\AA}$ with the characteristic measured quantities given below taken from the Supplemental Information of Badger *et al.*²³, giving values for single crystal samples. The analysis assumes convention BCS singlet pairing. This list is followed by several calculated or estimated energies mostly from Quan *et al.*²⁴ When three numbers are given, they refer to the a, b, c lattice direction anisotropic values, and T=0 values are given for the T-dependent properties. KWR is the Kadawaki-Woods ratio.

- $T_c=2$ K; $k_B T_c=0.17$ meV, a relevant energy scale
- $\lambda_{GL}=174, 509, 189$ nm
- $\xi_{GL}=51.5, 17.6, 47.3$ nm
- $\kappa=3.38, 28.9, 4.00$
- $\gamma=14.1$ mJ/mole-K² (specific heat constant)
- $\Delta C(T_c)/\gamma T_c=1.33$; BCS value is 1.43
- $\rho_o=5.2$ $\mu\Omega$ cm, residual resistance; clean limit
- $H_p(0)=3.66$ T, the (extrapolated) Pauli limiting field
- $H_{c2}=0.275, 0.094, 0.253$ T, Helfand-Werthamer
- $H_c=23$ mT, thermodynamic critical field
- KWR: $A/\gamma_n^2=1.28$ ($[\mu\Omega \text{ cm}/\text{K}^2]/[\text{mJ/mol K}^2]^2$)

The a - c near isotropy of the superconducting parameters is evident, while the long b -axis values are quite different. Sometimes useful is averaging over the orthorhombic directions (viz. for making estimates or comparing with cubic materials): $\xi_{GL}\sim 35$ nm, $\lambda_{GL}\sim 300$ nm, $\kappa\sim 4.29$ (a moderately to strongly Type II superconductor, depending on direction), $H_{c2}\sim 0.2$ mT. These values compare favorably with powder values¹⁹ $\lambda_{GL}^{ave}=350$ nm, $H_{c2}^{ave}=0.4$ T, $\xi_{GL}^{ave}=38$ nm.

The following list gives material properties and representative energies for LaNiGa₂, using conventional notation. The notation $\delta\mathcal{E}$ is the energy difference (gain due to ordering) between normal and SC or magnetic phases.

- $N(0)=3.25$ states/eV-f.u.-both spins, the DFT value
- $N_{BCS}(0)=1.63$ states/eV per spin
- $\gamma_o=7.66$ mJ/mole-K²
- el-ph $\lambda = \frac{\gamma}{\gamma_o} - 1 = 0.84$
- $\Delta_o \approx 1.5$ kT_c=0.25 meV; $2\Delta_o=0.5$ meV
- $\Delta\mathcal{E}_{SC} = \frac{1}{2}N_{BCS}(0)\Delta_o^2=5.1 \times 10^{-8}$ eV
- $B^{spont}=0.2$ G from μ SR data
- $\mu_B B^{spont} \approx 8 \times 10^{-9}$ eV [μ SR]
- $m^{spont}=0.012 \mu_B/\text{f.u.}=3 \times 10^{-3} \mu_B/\text{atom}$ [μ SR]
- $\frac{m}{N_\uparrow(0)} \approx 4$ meV, exchange splitting of bands [μ SR]
- $\Delta\mathcal{E}_{mag}=\frac{1}{4}I_{st}m^2=6 \mu\text{eV}$ [μ SR] (Stoner $I_{st} \approx 0.5$ eV)

Note: the BCS paper uses the Fermi level DOS/spin, $N_{BCS}(0)$. The last energy in the list is the cost, in conventional theory, of producing a magnetization m^{spont} in a non-magnetic material. The disparity in the various energy scales is apparent, however the energy related to the chosen spontaneous field B^{spont} is comparable to the BCS condensation energy $\Delta\mathcal{E}_{SC}$. The value of λ from this theory/experiment heat capacity is somewhat larger than expected for a 2K superconductor.

J. The triplet order parameter

TRSB order parameters, *i.e.* emergence of magnetic polarizations, are conventionally represented by a spin-triplet SC OP of the form⁸

$$\Delta_k = \vec{d}_k \cdot \vec{\sigma} i\sigma_y, \quad (49)$$

where \vec{d} is a complex triplet magnetization 3-vector whose k - and band n -dependence is neglected until required by data, and $\vec{\sigma}$ is the vector of Pauli matrices for spin. $i\sigma_y$ accounts for TRSB. In terms of triplet spin notation this is^{8,9}

$$\begin{aligned} \Delta_{\uparrow\uparrow} &= -d_x + id_y, \\ \Delta_{\downarrow\downarrow} &= d_x + id_y \\ \Delta_{\uparrow\downarrow} &= d_z = \Delta_{\downarrow\uparrow}. \end{aligned} \quad (50)$$

(The vector \vec{d}_k has nothing to do with a singlet d -wave order parameter symmetry.)

This straightforward extension to triplet order parameter, with spin-pairing being even with respect to the Cooper pair that must be odd (antisymmetric) in total leaves an additional odd symmetry order parameter to be included. The point groups of LaNiGa₂ (also for LaNiC₂, with its symmorphic but noncentrosymmetric space group) have only one-dimensional irreducible representations in the universe of possible symmetries to be broken, hence providing no crystal symmetry to be broken. This deficiency was addressed by including an additional electronic degree of freedom, with the choice being a similarity of two Fermi surfaces or a pair of bands. Neither of these provides an exact underlying symmetry.

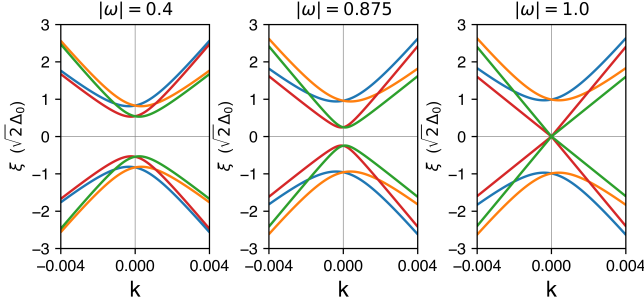


FIG. 5. Sketch of the quasiparticle (Bogoliubov-de Gennes) band structure along one dispersive band direction of the triplet, topological superconductivity model for LaNiGa₂.²⁴ Graphs for three values of the “triplet strength” ω are displayed. For $\omega=1$, the non-symmorphic band sticking at the zone boundary, hence two nodes, persists into the then gapless superconducting state. In the nonunitary regime $\omega < 1$ the degeneracy is broken, giving a gap to quasiparticle excitation.

The choice of a pair of atomic orbitals on (exactly) symmetry related Ni sites was also proposed. This proposition confronts the observations that the Ni 3d bands are filled, lying below -1 eV, with little opportunity for polarization, charge order, or other types of symmetry breaking.

The language of bands was used initially, later Fermi surfaces were thought to be more appropriate for LaNiGa₂ due to similarities of some Fermi surfaces, the mathematics is the same. Whatever the source might be, the two-dimensional orbital/band symmetry to be broken below T_c , is denoted by Pauli matrices $\vec{\sigma}$ in that space, for which some interaction might provide quantum mechanical coupling. The INT order parameter^{18,82} was

$$\Delta_k = \vec{d}_k \cdot \vec{\sigma} i\sigma_y \otimes i\tau_y, \quad (51)$$

where $\vec{\sigma}$ incorporates the two level band, Fermi surface, or orbital (near)degeneracy. This form is the one currently in use for LaNiGa₂.

Once included in the BdG quasiparticle Hamiltonian, the eigenvalue dispersions E_k are⁸

$$\begin{aligned} E_k &= \pm \sqrt{\varepsilon_k^2 + \vec{d} \cdot \vec{d}^* \pm |\vec{d} \times \vec{d}^*|} \\ &= \pm \sqrt{\sum_{j=1}^3 v_{k,j}^2 \delta k_j^2 + \vec{d} \cdot \vec{d}^* \pm |\vec{d} \times \vec{d}^*|}, \end{aligned} \quad (52)$$

where ε_k is the normal state band energy expanded in δk_j around the Fermi energy. The cross product is imaginary or zero, a non-zero value requiring an intrinsically complex \vec{d} . A nonzero value of $|\vec{d} \times \vec{d}^*|$ results in a *non-unitary* state for which there are eight BdG quasiparticle bands. A zero value of the cross product corresponds to a *unitary* state. An instructive example is $\vec{d} = \Delta_o(\cos \eta, i \sin \eta, 0)$ for the usual range of phases η .

Specialization to LaNiGa₂. The non-unitary state corresponds to quasiparticles with two dispersion curves

(split degeneracies), hence two separate energy gaps, prompting this peculiar feature at the Dirac points to be one focus of LaNiGa₂. Unitary states have an interpretation, generalized from singlet pairing, to amplitudes of $|\uparrow\uparrow\rangle$ and $|\downarrow\downarrow\rangle$ equal spin pairing, while the non-unitary state has unequal pairing hence magnetic polarization.

Figure 5 provides a schematic close-up view for LaNiGa₂ of the the quasiparticle bands around the gap along one axis, for three values of the nonunitarity quantity $\omega = |\vec{d} \times \vec{d}^*|$ in terms of normalized polarization vector \vec{d} and linear normal state dispersion $\varepsilon_k = v|\vec{k}|$ for Dirac points. Non-unitarity is discussed in the next Appendix.

Thus (non)unitarity is associated with the *phase difference between different components of \vec{d}* , which may be a delicate property. In the formulation of Ramires and coauthors, their time-reversal operator is defined by

$$\vec{q}_{tro} = 2i \vec{d}_k \times \vec{d}_k^*. \quad (53)$$

If nonunitary, TRS has been broken. Additional information, related to spin-orbit coupling (with or without), and effects of distinct point groups, are available from Ramires’ paper.¹⁵

Nonunitarity more generally. The symmetry classification and properties of triplet OPs, generalized from the spherically symmetric case of ³He to crystal symmetry, was presented by Blount in 1985.¹⁶ For nonunitary consequences of crystal symmetry, an overview appeared by Ramires,¹⁵ after extensions of the theory and some proposed examples from experiment. Sigrist and Euda⁸ expressed the general criterion for unitarity as

$$\Delta_k \Delta_k^\dagger \propto \sigma_o. \quad (54)$$

That is, if the generalized magnitude of Δ_k is proportional to the identity matrix, the state is a unitary one. Here this means that if $i\vec{d}_k^* \times \vec{d}_k$ is non-zero (*i.e.* they are ‘non-parallel’ in their complex vector space), then the OP is non-unitary. This property results in a non-vanishing average of the magnetic moment $\Delta_k^\dagger \vec{\sigma} \Delta_k$.⁸ A related OP couples to an external magnetic field in the Ginzburg-Landau free energy functional.¹⁸³

1. The INT model: more detail

The present picture for LaNiGa₂ has arisen from a progression from Hillier *et al.*¹⁹, to that of Weng *et al.*¹⁸, then to the more ‘quantitative theory’ of Ghosh *et al.*²⁰. These groups were not yet aware that the space group is *Cmcm*, so they built on the earlier reported²¹ non-centrosymmetric *Cmmm* structure. For the form of the required TRSB order parameter, point groups of both *Cmmm* and *Cmcm* have only one-dimensional (non-degenerate) irreducible representations, hence no degeneracy to be split⁴⁹ (symmetry to be broken). The non-symmorphic space group of *Cmcm* does however provide an unusual new degeneracy that is discussed below.

Hillier *et al.* reported TRSB initially and suggested that non-unitarity appeared to be required by symmetry. They provided no modeling of the order parameter, but reported the necessary form of the Ginzburg-Landau free energy functional that is required for TRS breaking (a triplet OP coupled to the magnetization). Weng *et al.* reported more data (penetration depth, specific heat, H_{c2}),¹⁸ noting the nodeless gap, and suggested that the additional broken symmetry that seemed necessary might be due to the degeneracy of orbitals on two symmetry-related atoms in the unit cell, viz. charge ordering, whose symmetry is also broken at T_c . They described a triplet picture in which the $S_{\uparrow\uparrow}$ occupation differs slightly from that of $S_{\downarrow\downarrow}$, based partly on a picture of active Ni atomic orbitals, with further discussion below. From small structure in $\lambda_L(T)$ and $c_v(T)$ they argued that a ‘two gap’ (or ‘two band’, or ‘two orbital’) character might be responsible.

The SC order parameter, which was constructed in the simplest form that would account for TRSB-related data available at that time, is given in the 4×4 space of Eq. 51 with the vector \vec{t}_k neglected as unnecessary,

$$\Delta_k = \vec{d}_k \cdot \vec{\sigma} (i\sigma_y) \otimes (i\tau_y). \quad (55)$$

Triplet (even) pairing would first suggest that the k dependence of \vec{d} must be odd, however symmetry imposed that all four possible choices of \vec{d}_k lie in the $(1, i, 0)$ direction,¹⁸ so $\vec{d} \cdot \vec{\sigma} = \sigma_x + i\sigma_y$. However, odd in k , viz. $\sin k_x$, has nodes, whereas LaNiGa₂ is fully gapped. Thus the k -dependence of \vec{d} must be fully symmetric, and taking it as k -independent was the simplest choice. The observation of broken TRS necessitated another degenerate degree of freedom, most readily available from the electronic or atomic structure.

Not long after, Ghosh *et al.* suggested that, because the (then expected) *Cmmm* Fermi surface displays a region where two sheets that are roughly parallel, certain bands or even atomic orbitals might lie at the root of (approximate) broken symmetry. They chose to focus on the Ni d_{z^2} and d_{xy} orbitals. Supposing a Hund’s-like attractive interaction encouraging parallel spins on the Ni atoms, they treated a parallel-spin-pairing OP model that involved incorporation of a full DFT calculation including all of the Fermi surfaces of LaNiGa₂. Adjusting the attractive interaction parameter to reproduce $T_c=2$ K, their model predicted a small magnetization and resulting spontaneous field of 0.3 G, effectively the same as experiment. The interested person should consult the original three papers discussed here for the many details that are addressed.

Regarding Ghosh *et al.*’s supposition²⁰ of Hund’s rule coupling in this compound: without the μ SR results the standard interpretation of the band structure of LaNiGa₂ would be that the $3d$ bands of Ni are narrow and confined between -2.5 eV and -1 eV below the Fermi level – they are filled and inert. There is some $3d$ character at E_F , but it is due to minor mixing with neighbor atom p orbitals, or the tails of such orbitals that leak into the Ni volume and are expanded in $L = 2$ symmetry. In either

case, any atomic Ni $3d$ character is minor and ambiguous. The key evaluation (of this author) is that the $3d$ bands are fully occupied, with no propensity toward moment formation. The small spin polarization calculated in their DFT+Hund’s $3d$ interaction must be sensitive to the amount of $3d$ character, which as noted above will be subjective.

K. Comments about magnetic superconductors

A charged fermionic superfluid, due to orbital effects, is conspicuous in its insistence on expelling a magnetic field (Type I), or confining it to vortices (Type II). In the singlet case the SC order parameter is depressed and vanishes at the vortex center, for triplet the behavior can become modified.⁷⁵ For triplet SCs there is the issue of their own self-magnetic field due to spin imbalance, which presumably survives (remains frozen in) in the steady state description of triplet SC properties. The behavior of a triplet SC in its own field, even more so in an applied field, seems to be little studied theoretically – apparently depending on the specific type of triplet OP – and not yet resolved by experiments.

This puzzle is most prominent in strongly ferromagnetic (FM) SCs such as UGe₂, where FM magnetic order results from large moments (up to $0.9\mu_B$) on the U atoms, whose magnetic origin is evidently of conventional electronic exchange interactions and whose ground state electronic structure is described reasonably (but probably not conclusively) in the bulk by correlated DFT methods, see for example Refs. [181,182]. The appropriate description of $5f$ electrons (localized versus itinerant, treatment of spin-orbit coupling [$\vec{L} \cdot \vec{S}$ versus $\vec{J} \cdot \vec{J}$, or more detailed correlations] seems to depend on band filling (*i. e.* the progression along the row of actinides), pressure, doping, and several other material characteristics. Orbital moment scenarios are mentioned briefly in Sec. XII A but are not appropriate for large magnetic moment SC states.

Inhomogeneities complicate this already uncertain picture. Relevant inhomogeneities include surfaces and interfaces, domain boundaries, and planar, line, and – in particular – point defects, with interstitial muons being the most studied type of point magnetic defect. Magnetic regions in nominally nonmagnetic actinide-based materials have been discussed as a material complication. These disruptions likely lead to local supercurrents that produce a magnetic field in the region, in a magnetically susceptible metal. Local magnetic regions have been suggested as the origin of polar Kerr rotation observed in U-based SCs. TRSB fields, when observed, by μ SR, by polar Kerr effect, or by magnetization, are not far from the threshold of detectability. Magnetization in LaNiC₂,⁸⁰ reported as resulting from a field of 0.01 G, is the most noticeable case.

The Meissner effect might have some theoretical commonality for singlet and triplet pairing, as it involves only an orbital (charge) component. The formulation of a mi-

croscopic theory of orbital currents, which possess a local angular momentum and provide a local moment, in a periodic solid has not been a straightforward theoretical question. Robbins *et al.*¹⁸⁴ have applied developments in the theory of polarization in crystals to address this challenge for the normal state, then extended the theory of the orbital moment in a superconductor to the formulation and application of a modern DFT-based band structure code (viz. BdG formulation for a SC) to explore such effects in real materials.

This work of Robbins *et al.* required a modern formulation of orbital momentum because in the usual angular

momentum operator $\vec{L} = \vec{r} \times \vec{p}$, the position operator \vec{r} is tricky to handle in an extended, periodic system, while the orbital moment will be a local or periodic quantity. Assuming a chiral, p -wave OP for the correlation-enhanced and enigmatic compound Sr_2RuO_4 , the model of Robbins *et al.* led to a predicted orbital moment of $3 \times 10^{-4} \mu_B$ per f.u., which they suggest accounts for a field of 0.3 G, near to the detection limit of zero-field μSR studies. The formalism they develop can be expected to be important in modeling and understanding orbital moments in superconductors. This topic of orbital currents is discussed in Sec. XII A, including the specific proposal by Ghosh *et al.*¹²⁸ of TRSB loop supercurrent order.

¹ W. Lang, Inhomogeneous superconductors, *Encyclopedia of Condens. Matt. Phys.* **3**, 368 (2024); arXiv:2310.18232.

² W. E. Pickett, Room Temperature Superconductivity: the Roles of Theory and Materials Design, *Rev. Mod. Phys.* **95**, 021001 (2023).

³ E. Kogler, D. Spath, R. Lucrezi, H. Mori, Z. Zhu, Z. Li, E. R. Margine, and C. Heil, IsoME: Streamlining High-Precision Eliashberg Calculations. *Comp. Phys. Commun.* **315**, 109720 (2025).

⁴ A. P. Mackenzie and Y. Maeno, The superconductivity of Sr_2RuO_4 and the physics of spin-triplet pairing, *Rev. Mod. Phys.* **75**, 657 (2003).

⁵ G. R. Stewart, Heavy Fermion Systems, *Rev. Mod. Phys.* **56**, 755 (1984).

⁶ R. E. Rudd and W. E. Pickett, Single Spin Superconductivity: Formulation and Ginzburg-Landau Theory, *Phys. Rev. B* **57**, 557 (1998).

⁷ J. F. Annett, Symmetry of the order parameter for high-temperature superconductivity, *Adv. Phys.* **39**, 83 (1990).

⁸ M. Sigrist and K. Ueda, Phenomenological theory of unconventional superconductivity, *Rev. Mod. Phys.* **63**, 239 (1991).

⁹ J. F. Annett, Unconventional superconductivity, *Contemp. Phys.* **36**, 423 (1995).

¹⁰ T. Tsuneto, *Superconductivity and Superfluidity*, (Cambridge University, Cambridge, U.K., 1998).

¹¹ V. P. Mineev and K. V. Samokhin, *Introduction to Unconventional Superconductivity* (Gordon and Breach, Amsterdam, 1999).

¹² M. Sigrist, Introduction to unconventional superconductivity, *AIP Conf. Proc.* **789**, 165 (2005).

¹³ M. Sigrist, Introduction to unconventional superconductivity in non-centrosymmetric metals, *AIP Conf. Proc.* **1162**, 55 (2009).

¹⁴ K. I. Wysokinski, Time Reversal Symmetry Breaking Superconductors: Sr_2RuO_4 and Beyond, *Condens. Matter* **4**, 47 (2019).

¹⁵ A. Ramires, Nonunitary superconductivity in complex quantum materials, *J. Phys.: Condens. Matt.* **34**, 304001 (2022).

¹⁶ E. I. Blount, Symmetry properties of triplet superconductors, *Phys. Rev. B* **32**, 2935 (1985).

¹⁷ R. H. Heffner, Muon studies of heavy fermions, *J. Magn. Magn. Compds.* **108**, 23 (1992).

¹⁸ Z. F. Weng *et al.*, Two-Gap Superconductivity in LaNiGa_2 with Nonunitary Triplet Pairing and Even Parity Gap Symmetry, *Phys. Rev. Lett.* **117**, 027001 (2016).

¹⁹ A. D. Hillier, J. Quintanilla, B. Mazidian, J. F. Annett, and R. Cywinski, Nonunitary triplet coupling in the centrosymmetric superconductor LaNiGa_2 , *Phys. Rev. Lett.* **109**, 097001 (2012).

²⁰ S. K. Ghosh, G. Csire, P. Whittlesea, J. F. Annett, M. Gradhand, B. Üjfalussy, and J. Quintanilla, Quantitative theory of triplet pairing in the unconventional superconductor LaNiGa_2 , *Phys. Rev. B* **101**, 100506(R) (2020).

²¹ Y. Yarmolyuk and Y. Grin, Crystal structure of the RNiGa_2 compounds (R=La, Ce, Pr, Nd, Sm, Gd), *Dopovidi Akademii nauk Ukrainskoi RSR, Seriya A: Fiziko-Matematichni ta Tekhnichni Nauki* **44**, 71 (1982).

²² M. Staab, R. Prater, S. Sreedhar, J. Byland, E. Mann, D. Zackaria, Y. Shi, H. J. Bowman, A. L. Stephens, M.-C. Jung, A. Botana, W. E. Pickett, V. Taufour, and I. Vishik, Symmetry Enforced Fermi Surface Degeneracies Observed in the Purported Time-Reversal Symmetry-Breaking Superconductor LaNiGa_2 , *Phys. Rev. B* **110**, 165115 (2024).

²³ J. R. Badger, Y. Quan, M. C. Staab, S. Sumita, A. Rossi, K. P. Devlin, K. Neubauer, D. S. Shulman, J. C. Fettinger, P. Klavins, S. M. Kauzlarich, D. Aoki, I. M. Vishik, W. E. Pickett, and V. Taufour, Dirac lines and loop at the Fermi level in the Time-Reversal Symmetry Breaking Superconductor LaNiGa_2 , *Commun. Phys.* **5**, 22 (2022).

²⁴ Y. Quan, V. Taufour, and W. E. Pickett, Nonsymmorphic Band Sticking in a Topological Superconductor, *Phys. Rev. B* **105**, 064517 (2022).

²⁵ P. Sherpa, I. Vinograd, Y. Shi, S. A. Sreedhar, C. Chaffey, T. Kissikov, M.-C. Jung, A. S. Botana, A. P. Dioguardi, R. Yamamoto, M. Hirata, G. Conti, S. Nemsak, J. R. Badger, P. Klavins, I. Vishik, V. Taufour, and N. J. Curro, Absence of strong magnetic fluctuations or interactions in the normal state of LaNiGa_2 , *Phys. Rev. B* **109**, 125113 (2024).

²⁶ S. Sundar, M. Yakovlev, N. Azari, M. Abedi, D. M. Broun, H. U. Ozdemir, S. R. Dunsiger, D. Zackaria, H. Bowman, P. Klavins, V. Taufour, J. E. Sonier, Gap structure of the non-symmorphic superconductor LaNiGa_2 probed by μSR , *Phys. Rev. B* **109**, 104517 (2024).

²⁷ S. Ghimire, K. R. Joshi, E. H. Krenkel, M. A. Tanatar, Y. Shi, M. Konczykowski, R. Grasset, V. Taufour, P. P. Orth, M. S. Scheurer, and R. Prozorov, Electron irradiation reveals robust fully gapped superconductivity in LaNiGa_2 , *Phys. Rev. B* **109**, 024515 (2024).

²⁸ A. Schenck, *Muon spin rotation spectroscopy: principles and applications in solid state physics*, (Adam Hilger Ltd., Bristol, U.K., 1985).

²⁹ C.P. Slichter, *Principles of Magnetic Resonance*, (Springer-Verlag, 1980).

³⁰ J.H. Brewer and P.W. Percival, eds., *Muon Spin Rotation II: Proceedings of 2nd Int. Topical Meeting on Muon Spin Rotation, Vancouver, 1980* (North-Holland, Amsterdam, 1981).

³¹ J.H. Brewer, R.F. Kiefl and P.W. Percival, eds., *Muon Spin Rotation VI: Proceedings of 6th Int. Topical Meeting on Muon Spin Rotation/Relaxation/Resonance, Wailea, Maui, 1993* (North-Holland, Amsterdam, 1994).

³² S. J. Blundell, Spin-polarized muons in condensed matter, *Contemp. Phys.* **40**, 175 (1999); <https://doi.org/10.1080/001075199181521>.

³³ S.L. Lee, S.H. Kilcoyne, and R. Cywinski, eds., “Muon Science: Muons in physics, chemistry and materials,” *Proceedings of the 51st Scottish Summer School in Physics, NATO Advanced Study Institute* (Institute of Physics Publishing, London 1999.)

³⁴ A. Yaouanc and P. Dalmas de Réotier, *Muon Spin Rotation, Relaxation, and Resonance: Applications to Condensed Matter*, Intl. Series of Monographs on Physics 147, 1-504 (Oxford University Press, 2011).

³⁵ S. J. Blundell, R. de Renzi, T. Lancaster, and F. L. Pratt, *Muon Spectroscopy – An Introduction* (Oxford University Press, Oxford, U.K., 2021).

³⁶ A. D. Hillier *et al.*, Muon spin spectroscopy, *Nat. Rev. Methods Primers* **2-4** (2022). <https://doi.org/10.1038/s43586-021-00089-0>

³⁷ S. J. Blundell and T. Lancaster, DFT plus μ : Density functional theory for muon site determination, *Appl. Phys. Rev.* **10**, 021316 (2023).

³⁸ B. M. Huddart, A. Hernandez-Melian, T. J. Hicken, M. Gomilsek, Z. Hawkhead, S. J. Clark, F. L. Pratt, T. Lancaster, MuFinder: A Program to determine and analyze muon stopping sites, *Comp. Phys. Commun.* **280**, 108488 (2022).

³⁹ M. Gomilsek, F. Pratt, S. Cottrell, S. Clark, and T. Lancaster, Many-body quantum muon effects and quadrupolar coupling in solids, *Commun. Phys.* **6**, 142 (2023).

⁴⁰ I. Errea, M. Calandra, and F. Mauri, First-Principles Theory of Anharmonicity and the Inverse Isotope Effect in Superconducting Palladium-Hydride Compounds, *Phys. Rev. Lett.* **111**, 177002 (2013).

⁴¹ L. Monacelli, R. Bianco, M. Cherubini, M. Calandra, I. Errea, and F. Mauri, The stochastic self-consistent harmonic approximation: calculating vibrational properties of materials with full quantum and anharmonic effects, *J. Phys.: Condens. Matter* **33**, 363001 (2021).

⁴² I. Errea, F. Belli, L. Monacelli, A. Sanna, T. Koretsune, T. Tadano, R. Bianco, M. Calandra, R. Arita, F. Mauri, and J. A. Flores-Livas, Quantum crystal structure in the 250-kelvin superconducting lanthanum hydride, *Nature* **578**, 66 (2020).

⁴³ I. Errea, M. Calandra, C. J. Pickard, J. R. Nelson, R. J. Needs, Y. Li, H. Liu, Y. Zhang, Y. Ma, and F. Mauri, Quantum hydrogen-bond symmetrization in the superconducting hydrogen sulfide system, *Nature* **532**, 81 (2016).

⁴⁴ I. J. Onuorah, P. Bonfà, R. De Renzi, L. Monacelli, F. Mauri, M. Calandra, and I. Errea, Quantum effects in muon spin spectroscopy within the stochastic self-consistent harmonic approximation, *Phys. Rev. Mater.* **3**, 073804 (2019).

⁴⁵ A. Balatsky, I. Vekhter, and J.-X. Zhu, Impurity-induced states in conventional and unconventional superconductors, *Rev. Mod. Phys.* **78**, 373 (2006).

⁴⁶ F. and H. London, The Electromagnetic Equations of a Supraconductor, *Proc. Roy. Soc. A* **149**, 71 (1935).

⁴⁷ J. Bardeen, L. N. Cooper, and J. R. Schrieffer, Theory of Superconductivity, *Phys. Rev.* **108**, 1175 (1957).

⁴⁸ V. L. Ginzburg and L. D. Landau, *Zh. Eksp. Teor. Fiz.* **20**, 1064 (1950). English translation in *L. D. Landau, Collected Papers* (Pergamon Press, Oxford, 1965).

⁴⁹ M. Sigrist, Broken time reversal symmetry in unconventional superconductors, *Physica* **341-348**, 695 (2000).

⁵⁰ B. M. Andersen, A. Kreisel, and P. J. Hirschfeld, Spontaneous time-reversal symmetry breaking by disorder in superconductors, [arXiv:2312.08099](https://arxiv.org/abs/2312.08099).

⁵¹ B. M. Huddart, I. J. Onuorah, M. M. Isah, P. Bonfà, S. J. Blundell, S. J. Clark, R. De Renzi, and T. Lancaster, Intrinsic Nature of Spontaneous Magnetic Fields in Superconductors with Time-Reversal Symmetry Breaking, *Phys. Rev. Lett.* **127**, 237002 (2021).

⁵² F. Bernardini, P. Bonfa, S. Massidda, and R. De Renzi, *Ab initio* strategy for muon site assignment in wide band gap fluorides, *Phys. Rev. B* **87**, 115148 (2013).

⁵³ P. Bonfa, F. Sartori, and R. De Renzi, Efficient and reliable strategy for identifying muon sites based on the double adiabatic approximation, *J. Phys. Chem. C* **199**, 4278 (2015).

⁵⁴ S. K. Ghosh, M. Smidman, T. Shang, J. F. Annett, A. D. Hillier, J. Quintanilla, and H. Yuan, Recent progress on superconductors with time-reversal symmetry breaking, *J. Phys.: Condens. Matt.* **33**, 033001 (2021).

⁵⁵ See 54, Sec. 5.4.b.

⁵⁶ M. Sato and Y. Ando, Topological Superconductors: A Review, *Rep. Prog. Phys.* **80**, 076501 (2017).

⁵⁷ S. Sautbekov, The vector potential of a magnetic dipole, *J. Magn. Magn. Matls.* **484**, 403 (2019).

⁵⁸ J. D. Jackson, The Nature of Intrinsic Magnetic Dipole Moments, CERN document 77-17 (1977).

⁵⁹ A. I. Duff and J. F. Annett, Variational QMC of a hydrogen atom in jellium with comparison to LSDA and self-interaction corrected LSDA solutions, *Phys. Rev. B* **76**, 115113 (2007).

⁶⁰ J. F. Janak, Uniform susceptibilities of metallic elements, *Phys. Rev. B* **16**, 255 (1977).

⁶¹ R. M. Martin, *Electronic Structure Basic Theory and Practical Methods* (Cambridge University Press, 2004).

⁶² P.B. Allen, W.E. Pickett, and H. Krakauer, Anisotropic Normal State Transport Properties Predicted and Analyzed for High T_c Oxide Superconductors, *Phys. Rev. B* **37**, 7482 (1988).

⁶³ C. P. Slichter, *Principles of Magnetic Resonance*, 3rd Ed., (Harper & Row, New York, 1996).

⁶⁴ A. Abragam and B. Bleaney, *Electron paramagnetic resonance of transition ions*, (Oxford University Press, Oxford U.K., 2012).

⁶⁵ J. Autschbach, Perspective: Relativistic Effects, *J. Chem. Phys.* **136**, 150902 (2012).

⁶⁶ A. Meninno and I. Errea, *Ab initio* study of metastable occupation of tetrahedral sites in palladium hydrides and its impact on superconductivity, *Phys. Rev. B* **107**, 024504 (2023), and references therein.

⁶⁷ G. Ortiz, M. D. Jones, and D. M. Ceperley, Ground state of a hydrogen molecule in superstrong magnetic fields, *Phys. Rev. A* **52**, R3405 (1995).

⁶⁸ W. E. Pickett and J. Q. Broughton, Variational Monte Carlo study of the partially polarized electron gas, *Phys. Rev. B* **48**, 14859 (1993).

⁶⁹ G. Ortiz and P. Ballone, Correlation energy, structure factor, radial distribution function, and momentum distribution of the spin-polarized uniform electron gas, *Phys. Rev. B* **50**, 1391 (1994).

⁷⁰ G. G. Spink, R. J. Needs, and N. D. Drummond, Quantum Monte Carlo study of the three-dimensional spin-polarized homogeneous electron gas, *Phys. Rev. B* **88**, 085121 (2013).

⁷¹ W. E. Pickett, Superfluid Density, Penetration Depth, Condensate Density, arXiv:2601.10578.

⁷² J. Ashcroft and S. Krusch, Vortices and magnetic impurities, *Phys. Rev. D* **101**, 025004 (2020).

⁷³ F. Küster, A. M. Montero, F. S. M. Guimaraes, S. Brinker, S. Lounis, S. S. P. Parkin, and P. Sessi, Correlating Josephson supercurrents and Shiba states in quantum spins unconventionally coupled to superconductors, *Nat. Comm.* **12**, 1108 (2021).

⁷⁴ E. Pechenik, B. Rosenstein, B. Ya. Shapiro, and I. Shapiro, Unconventional vortices in multicomponent Ginzburg-Landau theory, *Phys. Rev. B*, **65**, 214532 (2002). This study focuses on the difference between triplet vector vortices and singlet Abrikosov vortices.

⁷⁵ B. Rosenstein, B. Ya. Shapiro, and I. Shapiro, Collective modes, ac response, and magnetic properties of the three-dimensional Dirac semimetal in the triplet superconducting state, *Phys. Rev. B* **92**, 054503 (2015). For their model, they find that transverse and longitudinal coherence lengths and penetration depths can differ by a factor of order 30.

⁷⁶ Y. Aoki, A. Tsuchiya, T. Kanayama, S. R. Saha, H. Sugawara, H. Sato, W. Higemoto, A. Koda, K. Ohishi, K. Nishiyama, and R. Kadono, Time-Reversal Symmetry-Breaking Superconductivity in Heavy-Fermion in $\text{PrSb}_4\text{O}_{12}$ Detected by Muon-Spin Relaxation, *Phys. Rev. Lett.* **91**, 067003 (2003).

⁷⁷ R. P. Singh, A. D. Hillier, B. Mazidian, J. Quintanilla, J. F. Annett, D. McK. Paul, G. Balakrishnan, and M. R. Lees, Detection of Time-Reversal Symmetry Breaking in the Noncentrosymmetric Superconductor Re_6Zr Using Muon-Spin Spectroscopy, *Phys. Rev. Lett.* **112**, 107002 (2014).

⁷⁸ A. D. Hillier, J. Quintanilla, and R. Cywinski, Evidence for Time-Reversal Symmetry Breaking in the Noncentrosymmetric Superconductor LaNiC_2 , *Phys. Rev. Lett.* **102**, 117007 (2009); *erratum*, **105**, 229901 (2010).

⁷⁹ J. Quintanilla, A. D. Hillier, J. F. Annett, and R. Cywinski, Relativistic analysis of the pairing symmetry of the noncentrosymmetric superconductor LaNiC_2 , *Phys. Rev. B* **82**, 174511 (2010).

⁸⁰ A. Sumiyama, D. Kawakatsu, J. Gouchi, A. Yamaguchi, G. Motoyama, Y. Hirose, R. Settai, and Y. Onuki, Spontaneous magnetization of non-centrosymmetric superconductor LaNiC_2 , *J. Phys. Soc. Japan* **84**, 013702 (2015).

⁸¹ S. Sundar, S. R. Dunsiger, S. Gheidi, K. S. Akella, A. M. Côté, H. U. Özdemir, N. R. Lee-Hone, D. M. Broun, E. Mun, F. Honda, Y. J. Sato, T. Koizumi, R. Settai, Y. Hirose, I. Bonalde, and J. E. Sonier, Two-gap time reversal symmetry breaking superconductivity in noncentrosymmetric LaNiC_2 , *Phys. Rev. B* **103**, 014511 (2021).

⁸² S. K. Ghosh, P. K. Biswas, C. Xu, B. Li, J. Z. Zhao, A. D. Hillier, and X. Xu, Time-reversal symmetry breaking superconductivity in three-dimensional Dirac semimetallic silicides, *Phys. Rev. Research* **4**, L012031 (2022).

⁸³ R. F. Kiefl, J. H. Brewer, I. Affleck, J. F. Carolan, P. Dosanjh, W. N. Hardy, T. Hsu, R. Kadono, J. R. Kempston, S. R. Kreitzman, Q. Li, A. H. O'Reilly, T. M. Riseman, P. Schleger, P. C. E. Stamp, H. Zhou, L. P. Le, G. M. Luke, B. Sternlieb, Y. J. Uemura, H. R. Hart, and K. W. Lay, Search for Anomalous Internal Magnetic Fields in High- T_c Superconductors as Evidence for Broken Time-Reversal Symmetry, *Phys. Rev. Lett.* **64**, 2082 (1990).

⁸⁴ A. Kataria, J. A. T. Verezak, O. Prakash, R. K. Kushwaha, A. Thamizhavel, S. Ramakrishnan, M. S. Scheurer, A. D. Hillier, and R. P. Singh, Time-reversal symmetry breaking in the superconducting low carrier density quasikutterudite $\text{Lu}_3\text{Os}_4\text{Ge}_{13}$, *Phys. Rev. B* **107**, L100506 (2023).

⁸⁵ M. Mandal, A. Kataria, C. Patra, D. Singh, P. K. Biswas, A. D. Hillier, T. Das, and R. P. Singh, Time-reversal symmetry breaking in frustrated superconductor Re_2Hf , *Phys. Rev. B* **105**, 094513 (2022).

⁸⁶ D. A. Mayoh, A. D. Hillier, B. Balakrishnam, and M. R. Lees, Evidence for the coexistence of time-reversal symmetry breaking and Bardeen-Cooper-Schrieffer-like superconductivity in La_7Pd_3 , *Phys. Rev. B* **103**, 024507 (2021).

⁸⁷ Arushi, R. K. Kushwaha, D. Singh, A. D. Hillier, M. S. Scheurer, and R. P. Singh, Time-reversal symmetry breaking in the superconducting state of ScS , *Phys. Rev. B* **106**, L020504 (2022).

⁸⁸ J. Xia, Y. Maeno, P. T. Beyersdorf, M. M. Fejer, and A. Kapitulnik, High Resolution Polar Kerr Effect Measurements of Sr_2RuO_4 : Evidence for Broken Time-Reversal Symmetry in the Superconducting State, *Phys. Rev. Lett.* **97**, 167002 (2006).

⁸⁹ E. M. Levenson-Falk, E. R. Schemm, Y. Aoki, M. B. Maple, and A. Kapitulnik, Polar Kerr Effect from Time-Reversal Symmetry Breaking in the Heavy-Fermion Superconductor $\text{PrOs}_4\text{Sb}_{12}$, *Phys. Rev. Lett.* **120**, 187004 (2018).

⁹⁰ R. H. Heffner *et al.*, New Phase Diagram for $(\text{U},\text{Th})\text{Be}_{13}$: A Muon-Spin-Resonance and H_{c1} Study, *Phys. Rev. Lett.* **65**, 2816 (1990).

⁹¹ L. P. Gor'kov, Microscopic Derivation of the Ginzburg-Landau Equations in the Theory of Superconductivity, *Sov. Phys. JETP* **36**, 1364 (1959), and references therein.

⁹² K. D. Usadel, Generalized diffusion equation for superconducting alloys, *Phys. Rev. Lett.* **25**, 507 (1970).

⁹³ J. B. Ketterson and S. N. Sun, *Superconductivity* (Cambridge University Press, Cambridge, U.K., 1999).

⁹⁴ H. Koizumi and A. Ishikawa, Theory of supercurrent in superconductors, *Intl. J. Mod. Phys. B* **34**, 2030001 (2020).

⁹⁵ I. S. Gradshteyn and I. M. Ryzhik, *Table of Integrals, Series, and Products* (Academic Press, Harcourt Brace Jovanovich, New York, 1980), equation 2.125.1.

⁹⁶ J. Pinel, C. Lebeau, and J. Rosenblatt, Behaviour of a type I superconductor in the presence of magnetic dipoles, *Solid State Commun.* **9**, 725 (1971).

⁹⁷ J. Pinel and C. Lebeau, Effect of magnetic dipoles on order parameter of superconductor, *Phys. Lett. A* **58**, 477 (1976).

⁹⁸ S. N. Burmistrov and L. B. Dubovskii, Magnetic Dipole Interaction in an Anisotropic Type-II Superconductor, *J. Supercond.* **4**, 207 (1991).

⁹⁹ Z. J. Yang, Surface effect of a superconductor on a magnetic dipole, *Physica C* **234**, 263 (1994).

¹⁰⁰ U. Yaron, P. L. Gammel, A. P. Ramirez, D. A. Huse, D. J. Bishop, A. I. Goldman, C. Stassis, P. C. Canfield, K. Mortensen, and M. R. Eskildsen, Microscopic coexistence of magnetism and superconductivity in $\text{ErNi}_2\text{B}_2\text{C}$, *Na-*

ture **382**, 236 (1996).

¹⁰¹ K. Miyake and A. Tsuruta, Theory for Intrinsic Magnetic Field in Chiral Superconductor Measured by μ SR: Case of Sr_2RuO_4 , arXiv:1709.09388.

¹⁰² J. Zittartz and E. Müller-Hartmann, Theory of Magnetic Impurities in Superconductors I. Exact Solutions of the Nagaoka Equations, *Z. Physik* **232**, 11 (1970).

¹⁰³ S. Sykora and T. Meng, Renormalization approach to the superconducting Kondo model, arXiv:2109.11995 (2022).

¹⁰⁴ C. H. Choi and P. Muzikar, Impurity-induced magnetic fields in unconventional superconductors, *Phys. Rev. B* **39**, 9664 (1989).

¹⁰⁵ L. Yu, Bound state in superconductors with paramagnetic impurities, *Acta Phys. Sin.* **21**, 75 (1965).

¹⁰⁶ H. Shiba, Classical spins in superconductors, *Prog. Theor. Phys.* **40**, 435 (1965); *Prog. Theor. Phys.* **50**, 50 (1973).

¹⁰⁷ A. I. Rusinov, On the theory of gapless superconductivity in alloys containing paramagnetic impurities, *Zh. Eksp. Teor. Fiz. Pis'ma Red.* **9**, 146 (1968); [JETP Lett. **9**, 85 (1969)].

¹⁰⁸ A. I. Rusinov, Superconductivity near a paramagnetic impurity, *Zh. Eksp. Teor. Fiz.* **56**, 2047 (1969); [Sov. Phys. JETP **29**, 1101 (1969)].

¹⁰⁹ J. B. Goodenough, Theory of the Role of Covalence in the Perovskite-Type Manganites [La, M(II)] MnO_3 , *Phys. Rev.* **100**, 564 (1955).

¹¹⁰ J. Kanamori, Superexchange interaction and symmetry properties of electron orbitals, *J. Phys. Chem. Solids* **10**, 87 (1959).

¹¹¹ P. W. Anderson, Antiferromagnetism: Theory of Superexchange Interaction, *Phys. Rev.* **79**, 350 (1950).

¹¹² W. E. Pickett, M. L. Cohen, and C. Kittel, Theory of the hydrogen interstitial impurity in germanium, *Phys. Rev. B* **20**, 5050 (1979).

¹¹³ J. Senkpiel, C. Rubio-Verd'u, M. Etzkorn, R. Drost, L. M. Schoop, S. Dambach, C. Padurariu, B. Kubala, J. Ankerhold, C. R. Ast, and K. Kern, Robustness of Yu-Shiba-Rusinov resonances in presence of a complex superconducting order parameter, *Phys. Rev. B* **100**, 014502 (2019).

¹¹⁴ S. H. Ji, T. Zhang, Y. S. Fu, X. Chen, X. C. Ma, J. Li, W. H. Duan, J. F. Jia, and O. K. Xue, High-resolution scanning tunneling spectroscopy of magnetic impurity induced bound states in the superconducting gap of Pb thin films, *Phys. Rev. Lett.* **100**, 226801 (2008).

¹¹⁵ T. G. Saunderson, Z. Györgypál, J. F. Annett, G. Csire, B. Üjjfalussy, and M. Gradhand, Real-space multiple scattering theory for superconductors with impurities, *Phys. Rev. B* **102**, 245106 (2020).

¹¹⁶ William of Ockham, ca. 14th century, as quoted by others later. See the Wikipedia page for references.

¹¹⁷ N. N. Bogoliubov, V. V. Tolmachev, and D. V. Shirkov, *A New Method in the Theory of Superconductivity*, (1958) (translation: Consultants Bureau, Inc., New York, 1959).

¹¹⁸ P. Morel and P. W. Anderson, Calculation of the Superconducting State Parameters with Retarded Electron-Phonon Interaction, *Phys. Rev.* **125**, 1263 (1962).

¹¹⁹ A. Sanna, C. Pellegrini, and E. K. U. Gross, Combining Eliashberg theory with density functional theory for the accurate prediction of superconducting transition temperatures and gap functions, *Phys. Rev. Lett.* **125**, 057001 (2020).

¹²⁰ P. B. Allen and R. C. Dynes, Transition temperature of strong-coupled superconductors reanalyzed, *Phys. Rev. B* **12**, 905 (1975).

¹²¹ I. F. Foulkes and B. L. Györfi, *p*-wave pairing in metals, *Phys. Rev. B* **15**, 1395 (1977).

¹²² A. Subedi and D. J. Singh, Electron-phonon superconductivity in noncentrosymmetric LaNiC_2 : First-principles calculations, *Phys. Rev. B* **80**, 092506 (2009).

¹²³ X. Tütüncü and G. Srivastava, Origin of superconductivity in layered centrosymmetric LaNiGa_2 , *Appl. Phys. Lett.* **104**, 022603 (2014).

¹²⁴ I. Schnell, I. I. Mazin, and A. Y. Liu, Unconventional superconducting pairing symmetry induced by phonons, *Phys. Rev. B* **74**, 184503 (2006).

¹²⁵ P. M. R. Brydon, S. Das Sarma, H.-Y. Hui, and J. D. Sau, Odd-parity superconductivity from phonon-mediated pairing: Application to $\text{Cu}_x\text{Bi}_2\text{Se}_3$, *Phys. Rev. B* **90**, 184512 (2014).

¹²⁶ N. F. Berk and J. R. Schrieffer, Effect of Ferromagnetic Spin Correlations on Superconductivity, *Phys. Rev. Lett.* **17**, 433 (1966).

¹²⁷ A. Kreisel, Y. Quan, and P. J. Hirschfeld, Spin-triplet superconductivity driven by finite-momentum spin fluctuations, *Phys. Rev. B* **105**, 104507 (2022).

¹²⁸ S. K. Ghosh, J. F. Annett, and J. Quintanilla, Time-reversal symmetry breaking in superconductors through loop supercurrent order, *New. J. Phys.* **23**, 083018 (2021).

¹²⁹ C. M. Varma, Non-Fermi-liquid states and pairing instability of a general model of copper oxide metals, *Phys. Rev. B* **55**, 14554 (1997).

¹³⁰ C. Nayak, Density-wave states of nonzero angular momentum, *Phys. Rev. B* **62**, 4880 (2000).

¹³¹ S. Strässle, J. Roos, M. Mali, H. Keller, and T. Ohno, Lack of Evidence for Orbital-Current Effects in the High-Temperature $\text{Y}_2\text{Ba}_4\text{Cu}_7\text{O}_{15-\delta}$ Superconductor using ^{89}Y Nuclear Magnetic Resonance, *Phys. Rev. Lett.* **101**, 237001 (2008).

¹³² A. H. Castro Neto, F. Guinea, N. M. R. Peres, K. S. Novoselov, and A. K. Geim, The electronic properties of graphene, *Rev. Mod. Phys.* **81**, 109 (2009).

¹³³ G. M. Luke, A. Keren, L. P. Le, W. D. Wu, Y. J. Uemura, D. A. Bonn, L. Taillefer, and J. D. Garrett, Muon spin relaxation in UPt_3 , *Phys. Rev. Lett.* **71**, 1466 (1993).

¹³⁴ G. M. Luke, A. Keren, L.P. Le, W.D. Wu, Y.J. Uemura, D.A. Bonn, L. Taillefer, J.D. Garrett, Muon spin relaxation in the heavy fermion system UPt_3 , *Physica B* **186**, 264, (1993).

¹³⁵ E. R. Schemm, W. J. Gannon, C. M. Wishne, W. P. Halperin, and A. Kapitulnik, Observation of broken time-reversal symmetry in the heavy-fermion superconductor UPt_3 , *Science* **345**, 190 (2014).

¹³⁶ P. Dalmas de Reötier, A. Huxley, A. Yaouanc, J. Flouquet, P. Bonville, P. Imbert, P. Pari, P. C. M. Gubbens, and A.M. Mulders, Absence of zero field muon spin relaxation induced by superconductivity in the B phase of UPt_3 , *Phys. Lett. A* **205**, 239 (1995).

¹³⁷ W. Higemoto, K. Satoh, N. Nishida, A. Koda, K. Nagamine, Y. Haga, E. Yamamoto, N. Kimura, and Y. Onuki, Studies of superconductivity and magnetism in UPt_3 by $\mu^+\text{SR}$, *Physica B* **281** & **282**, 984 (2000).

¹³⁸ A. Hiess, R. H. Heffner, J. E. Sonier, G. H. Lander, J. L. Smith, and J. C. Cooley, Neutron elastic and inelastic scattering investigations of $\text{U}_{0.965}\text{Th}_{0.035}\text{Be}_{13}$, *Phys. Rev. B* **66**, 064531 (2002).

¹³⁹ G. R. Stewart, UBe_{13} and $\text{U}_{1-x}\text{Th}_x\text{Be}_{13}$ – Unconventional Superconductors, *J. Low Temp. Phys.* **191**, 1 (2019).

¹⁴⁰ P. Holmvall and A. M. Black-Schaffer, Coreless vortices as

direct signature of chiral d -wave superconductivity, Phys. Rev. B **108**, L100506 (2023).

¹⁴¹ G. Nakamine, S. Kitagawa, K. Ishida, Y. Tokunaga, H. Sakai, S. Kambe, A. Nakamura, Y. Shimizu, Y. Homma, D. Li, F. Honda, and D. Aoki, Superconducting properties of heavy fermion UTe₂ revealed by ¹²⁵Te-nuclear magnetic resonance, J. Phys. Soc. Jpn. **88**, 113703 (2019).

¹⁴² H. Fujibayashi, G. Nakamine, K. Kinjo, S. Kitagawa, K. Ishida, Y. Tokunaga, H. Sakai, S. Kambe, A. Nakamura, Y. Shimizu, Y. Homma, D. Li, F. Honda, and D. Aoki, Superconducting order parameter in UTe₂ determined by Knight shift measurement, J. Phys. Soc. Jpn. **91**, 043705 (2022).

¹⁴³ H. Matsumura, H. Fujibayashi, G. Nakamine, K. Kinjo, S. Kitagawa, K. Ishida, Y. Tokunaga, H. Sakai, S. Kambe, A. Nakamura, Y. Shimizu, Y. Homma, D. Li, F. Honda, and D. Aoki, Large reduction in the a -axis Knight shift on UTe₂ with $T_c \approx 2.1$ K, J. Phys. Soc. Jpn. **92**, 063701 (2023).

¹⁴⁴ I. M. Hayes, D. S. Wei, T. Metz, J. Zhang, Y. S. Eo, S. Ran, S. R. Saha, J. Collini, N. P. Butch, D. F. Agterberg, A. Kapitulnik, and J. Paglione, Multicomponent superconducting order parameter in UTe₂, Science **373**, 797 (2021).

¹⁴⁵ D. S. Wei, D. Saykin, O. Y. Miller, S. Ran, S. R. Saha, D. F. Agterberg, J. Schmalian, N. P. Butch, J. Paglione, and A. Kapitulnik, Interplay between magnetism and superconductivity in UTe₂, Phys. Rev. B **105**, 024521 (2022).

¹⁴⁶ M. O. Ajeesh, M. Bordelon, C. Girod, S. Mishra, F. Ronning, E. D. Bauer, B. Maiorov, J. D. Thompson, P. F. S. Rosa *et al.*, Fate of Time-Reversal Symmetry Breaking in UTe₂, Phys. Rev. X **13**, 041019 (2023).

¹⁴⁷ N. Azari, M. Yakovlev, N. Rye, S. R. Dunsiger, S. Sundar, M. M. Bordelon, S. M. Thomas, J. D. Thompson, P. F. S. Rosa, and J. E. Sonier, Absence of Spontaneous Magnetic Fields due to Time-Reversal Symmetry Breaking in Bulk Superconducting UTe₂, Phys. Rev. Lett. **131**, 226504 (2023).

¹⁴⁸ G. M. Luke, Y. Fudamoto, K. M. Kojima, M. I. Larkin, J. Merrin, B. Nachumi, Y. J. Uemura, Y. Maeno, Z. Q. Mao, Y. Mori, H. Nakamura, and M. Sigrist, Time-reversal symmetry-breaking superconductivity in Sr₂RuO₄, Nature **394**, 558 (1998).

¹⁴⁹ A. Kapitulnik, J. Xia, E. Schemm, and A. Palevski, Polar Kerr effect as probe for time-reversal symmetry breaking in unconventional superconductors, New J. Phys. **11**, 055060 (2009).

¹⁵⁰ V. Grinenko *et al.*, Unsplit superconducting and time reversal symmetry breaking transitions in Sr₂RuO₄ under hydrostatic pressure and disorder, Nat. Commun. (2021), <https://doi.org/10.1038/s41467-021-24176-8>.

¹⁵¹ V. Grinenko *et al.*, Split superconducting and time-reversal symmetry-breaking transitions in Sr₂RuO₄ under stress, Nat. Phys. **17**, 748 (2021).

¹⁵² K. Miyake, Theory of Pairing Assisted Spin Polarization in Spin-Triplet Equal Spin Pairing: Origin of Extra Magnetization in Sr₂RuO₄ in Superconducting State, J. Phys. Soc. Jpn **83**, 053701 (2014).

¹⁵³ S. A. Kivelson, A. C. Yuan, B. Ramshaw, and R. Thomale, A proposal for reconciling diverse experiments on the superconducting state in Sr₂RuO₄, npj Quantum Mater. **5**, 43 (2020).

¹⁵⁴ A. T. Romer, A. Kreisel, M. A. Müller, P. J. Hirschfeld, I. M. Eremin, and B. M. Andersen, Theory of strain-induced magnetic order and splitting of T_c and T_{TRSB} in Sr₂RuO₄, Phys. Rev. B **102**, 054506 (2020).

¹⁵⁵ S. Benhabib, C. Lupien, I. Paul, L. Berges, M. Dion, M. Nardone, A. Zitouni, Z. Q. Mao, Y. Maeno, A. Georges, L. Taillefer, and C. Proust, Ultrasound evidence for a two-component superconducting order parameter in Sr₂RuO₄, Nat. Phys. **17**, 194 (2021).

¹⁵⁶ V. Grinenko, S. Ghosh, R. Sarkar, J.-C. Orain, A. Nikitin, M. Elender, D. Das, Z. Guguchia, F. Brückner, M. E. Barber, J. Park, N. Kikugawa, D. A. Sokolov, J. S. Bobowski, T. Miyoshi, Y. Maeno, A. P. Mackenzie, H. Luetkens, C. W. Hicks, and H.-H. Klauss, Split superconducting and time-reversal symmetry-breaking transitions in Sr₂RuO₄ under stress, Nat. Phys. **17**, 748 (2021).

¹⁵⁷ A. J. Leggett and Y. Liu, Symmetry Properties of Superconducting Order Parameter in Sr₂RuO₄: A Brief Review, J Supercond. Nov. Magn. **34**, 1647 (2021).

¹⁵⁸ Y. Maeno, A. Ikeda, and G. Mattioni, Thirty years of puzzling superconductivity in Sr₂RuO₄, Nat. Phys. **20**, 1712 (2024).

¹⁵⁹ Y. Maeno, S. Yonezawa, and A. Ramires, Still Mystery after All These Years — Unconventional Superconductivity of Sr₂RuO₄, J. Phys. Soc. Jpn. **93**, 062001 (2024).

¹⁶⁰ A. P. Mackenzie and Y. Maeno, The superconductivity of Sr₂RuO₄ and the physics of spin-triplet pairing, Rev. Mod. Phys. **75**, 657 (2024).

¹⁶¹ I. I. Mazin, Inverse Occam's Razor, Nat. Phys. **18**, 367 (2022). <https://doi.org/10.1038/s41567-022-01575-2>.

¹⁶² G. Vignale, M. Rasolt, and D. J. W. Geldart, Magnetic Fields and Density Functional Theory, Adv. Quant. Chem **21**, 235 (1990).

¹⁶³ R. Bayes *et al.* (TWIST Collaboration), Experimental Constraints on Left-Right Symmetric Models from Muon Decay, Phys. Rev. Lett. **106**, 041804 (2011).

¹⁶⁴ L. Michel, Interaction between Four Half-Spin Particles and the Decay of the μ -Meson, Proc. Phys. Soc. London **A63**, 514 (1950); erratum: Proc. Phys. Soc. London **A63**, 1371 (1950).

¹⁶⁵ C. Bouchiat and L. Michel, Theory of μ -Meson Decay with the Hypothesis of Nonconservation of Parity, Phys. Rev. **106**, 170 (1957).

¹⁶⁶ A. Grossheim, Muon Decay Parameters (TWIST experiment at TRIUMF), *10th Intl. Workshop on Neutrino Factories, Super beams, and Beta beams*, Valencia, Spain (July 2008); Proc. of Science (Nufact08)108.

¹⁶⁷ J. D. Jackson, *Classical Electrodynamics* (John Wiley & Sons, New York, 1962).

¹⁶⁸ F. London, On the Problem of the Molecular Theory of Superconductivity, Phys. Rev. **74**, 562 (1948).

¹⁶⁹ B. S. Chandrasekhar and D. Einzel, The superconducting penetration depth from the semiclassical model, Ann. Physik **2**, 535 (1993).

¹⁷⁰ Y. Takada, R. Maezono, and K. Yoshizawa, Emergence of a Kondo singlet state with the Kondo temperature well beyond 1,000K in the proton-embedded electron gas: Novel route to high- T_c superconductivity, arXiv:1507.06432.

¹⁷¹ R. Kubo and T. Toyabe, *Magnetic resonance and relaxation*, ed. R. Blink, (North Holland, Amsterdam, 1967), p.810.

¹⁷² E. I. Kornilov and V. Yu. Pomjakushin, On a generalization of the Kubo-Toyabe formula, Phys. Lett. A **153**, 364 (1991).

¹⁷³ H. Takahashi and Y. Tanimura, Open Quantum Dynamics Theory of Spin Relaxation: Application to μ SR and Low-Field NMR Spectroscopies, J. Phys. Soc. Japan **89**,

064710 (2020); arXiv:2004.06994 (2020).

¹⁷⁴ K. Park, B. Nyari,, A. Laszloffy, L. Szunyogh, and B. Ujfaluassy, Spin-polarized zero-bias peak from a single magnetic impurity at an *s*-wave superconductor: first-principles study, arXiv:2109.05511 (2021).

¹⁷⁵ P. Rüssmann, 2 D. A. Silva, M. Hemmati, I. Klepetisanis, B. Trauzettel, P. Mavropoulos, and S. Blügel, Density-functional description of materials for topological qubits and superconducting spintronics, arXiv:2308.07383 (2023).

¹⁷⁶ C.-K. Chiu and Z. Wang, Yu-Shiba-Rusinov states in a superconductor with topological Z_2 bands, arXiv:2109.15227.

¹⁷⁷ D.-J. Choi, C. Rubio-Verdú, J. de Bruijckere, M. M. Ugeda, N. Lorente, and J. I. Pascual, Mapping the orbital structure of impurity bound states in a superconductor, Nat. Comm. **8**, 15175 (2017).

¹⁷⁸ F. von Oppen and K. J. Franke, Yu-Shiba-Rusinov states in real metals, Phys. Rev. B **103**, 205424 (2021).

¹⁷⁹ H.-N. Xia, E. Minamitani, R. Zitko, Z.-Y. Liu, X. Liao, M. Cai, Z.-H. Ling, W.-H. Zhang, S. Klyatskaya, M. Ruben, and Y.-S. Fu, Spin-orbital Yu-Shiba-Rusinov states in single Kondo molecular magnet, Nature Commun. **13**, 6388 (2022).

¹⁸⁰ T. G. Saunderson, J. F. Annett, G. Csire, and M. Gradhand, Full orbital decomposition of Yu-Shiba-Rusinov states based on first principles, Phys. Rev. B **105**, 014424 (2022).

¹⁸¹ A. B. Shick, V. Janis, V. Drchal, and W. E. Pickett, Spin and Orbital Magnetic State of UGe₂ Under Pressure, Phys. Rev. B **70**, 134506 (2004).

¹⁸² A. B. Shick, S.-I. Fujimori, and W. E. Pickett, UTe₂: a Nearly Insulating Half-filled $j = \frac{5}{2}$ 5f³ Heavy Fermion Metal, Phys. Rev. B **103**, 125136 (2021).

¹⁸³ Z.-Q. Bao, X. C. Xie, and Q.-F. Sun, Ginzburg-Landau-type theory of spin superconductivity, Nature Commun. **4**, 2951 (2013).

¹⁸⁴ J. Robbins, J. F. Annett, and M. Gradhand, Theory of the orbital moment in a superconductor, Phys. Rev. B **101**, 134505 (2020).